Aimee Powell

Public Comment: Tier II Analysis
To: Forest Practices Board
From: Aimee Powell, Generational Steward
Date: August 18, 2025

Subject: Public Comment on Tier II Analysis of Forest Practices Draft Rules

Thank you for the opportunity to submit comments on Ecology's Tier II Analysis. I strongly support expanding protections for Type Np streams to safeguard water quality, cool downstream fish habitats, and protect wildlife like amphibians, insects, and birds.

As climate change accelerates, it is imperative that Washington's forest practice rules evolve to protect the ecological integrity of our non-fish bearing (Type Np) streams. These headwater reaches are not only vital for downstream water quality but also for maintaining watershed resilience in the face of intensifying heatwaves, drought, and sediment pulses.

I endorse the Board's proposal of enhancing riparian protections for climate resilience but oppose the prescribed fixed-width methodology. Drawing on four centuries of Bavarian forestry heritage, where adapting practices to microsites not only safeguarded the forests but also fueled regional economic growth, I urge the Board to enhance Washington's adaptive management leadership by adopting the following:

Four Actionable Recommendations

1. Precision Buffers in High-Impact Zones

Focus initial implementation in degraded lowland watersheds where temperature risks and pollution converge, using collaborative vulnerability mapping. Prioritizing these areas maximizes cooling and filtration benefits per protected acre while advancing equitable ecological outcomes.

2. Climate-Resilient Canopy Standards

Transition from fixed-width buffers to site-specific multi-layered shade standards.

This approach:

- Effectively reduces peak stream temperatures through site-adapted canopy density (Garner et al., 2017);
- Stabilizes banks via diverse root systems to reduce erosion;
- Enhances biodiversity through native vegetation layers (canopy, understory, groundcover);
- Maintains flexibility for topography, soil, and wetland conditions while delivering measurable outcomes;

- Builds on Washington-based science (Quick et al., 2024; DeWalle, 2008) where light-thinning maintained soil carbon while accelerating structural complexity - a model for stabilizing riparian zones along Type Np streams.

3. Economic Equity via Carbon Markets

Integrate buffer conservation into Washington's Climate Commitment Act framework. Allow landowners to generate verified carbon credits for exceeding shade targets, sustaining family forests through ecological stewardship.

4. Adaptive Management Loop

Require 5-year monitoring cycles for temperature and bank stability, using:

- Temperature tracking in high-risk reaches;
- Community-involved data review processes;
- Science-guided adjustments.

Why This Works for Washington

- Cold Water Protected: Targeted shading meets temperature reduction goals.
- Ecosystem Enhanced: These buffers will directly protect the amphibians, insects, and birds that rely on Np streams - a critical step for biodiversity.
- Working Forests Sustained: Carbon revenue offsets harvest impacts without
- compromising timber viability.
- Accountability Built-In: Regular monitoring enables adaptive management.

Heritage Stewardship Informing Policy

Heritage stewardship teaches that diverse landscapes demand flexibility. These measures protect streams while honoring rural livelihoods, ensuring our forests remain ecologically resilient and economically vibrant for generations.

Thank you,

Aimee Powell
Generational Steward

Journal of Hydrology 553 (2017) 471–485

Contents lists available at ScienceDirect

Journal of Hydrology

journal homepage: www.elsevier.com/locate/jhydrol

Research papers

The role of riparian vegetation density, channel orientation and water velocity in determining river temperature dynamics

Grace Garner [a], Iain A. Malcolm [b], Jonathan P. Sadler [a], David M. Hannah [a,*]

[a] School of Geography, Earth and Environmental Sciences, University of Birmingham, Edgbaston, Birmingham B15 2TT, UK
[b] Marine Scotland Science, Freshwater Laboratory, Faskally, Pitlochry, Perthshire, PH16 5LB, UK

ARTICLE INFO

Article history:
Received 15 September 2015
Received in revised form 5 March 2017
Accepted 13 March 2017
Available online 15 March 2017
This manuscript was handled by K. Georgakakos, Editor-in-Chief, with the assistance of Marco Toffolon, Associate Editor

Keywords:
River temperature
Stream temperature
Energy budget
Riparian forest
Riparian vegetation
Landuse change

ABSTRACT

A simulation experiment was used to understand the importance of riparian vegetation density, channel orientation and flow velocity for stream energy budgets and river temperature dynamics. Water temperature and meteorological observations were obtained in addition to hemispherical photographs along a ~1 km reach of the Girnock Burn, a tributary of the Aberdeenshire Dee, Scotland. Data from nine hemispherical images (representing different uniform canopy density scenarios) were used to parameterise a deterministic net radiation model and simulate radiative fluxes. For each vegetation scenario, the effects of eight channel orientations were investigated by changing the position of north at 45° intervals in each hemispheric image. Simulated radiative fluxes and observed turbulent fluxes drove a high-resolution water temperature model of the reach. Simulations were performed under low and high water velocity scenarios. Both velocity scenarios yielded decreases in mean (≥1.6 °C) and maximum (≥3.0 °C) temperature as canopy density increased. Slow-flowing water resided longer within the reach, which enhanced heat accumulation and dissipation, and drove higher maximum and lower minimum temperatures. Intermediate levels of shade produced highly variable energy flux and water temperature dynamics depending on the channel orientation and thus the time of day when the channel was shaded. We demonstrate that in many reaches relatively sparse but strategically located vegetation could produce substantial reductions in maximum temperature and suggest that these criteria are used to inform future river management.

1. Introduction

It is anticipated that a changing climate will alter river temperature regimes. Elevated temperatures relative to historical baselines are expected for most watercourses (e.g. Beechie et al., 2013; van Vliet et al., 2013; MacDonald et al., 2014a; Hannah and Garner, 2015). Such changes, particularly increased maxima, may diminish the spatial and temporal extent of suitable cool-water habitat for temperature sensitive organisms with potential impacts on the composition and productivity of aquatic ecosystems (Wilby et al., 2010; Leach et al., 2012). Consequently, there is substantial interest in adaptation strategies that may ameliorate the effects of climate warming, including: riparian planting (e.g. Hannah et al., 2008; Brown et al., 2010; Imholt et al., 2013; Ryan et al., 2013; Garner et al., 2014), reconnecting rivers to their floodplains (e.g. Poole et al., 2008; Opperman et al., 2010), restoring or enhancing hyporheic exchange (Beechie et al., 2013; Kurylyk et al., 2014), reducing and retaining urban runoff (e.g. Booth and Leavitt, 1999) and reducing rates of water abstraction (Poole and Berman, 2001). However in upland streams, where catchment hydrology and geomorphology have not been altered significantly by human activities, fewer of these strategies may be implemented to protect aquatic ecosystems from thermal extremes (Beschta, 1997; Poole and Berman, 2001). Observational datasets, frequently in combination with deterministic modelling approaches, have demonstrated that the summer temperature of headwater streams is generally dominated by: (1) advected heat from upstream (2) heat exchange at the air–water column interface (e.g. Westhoff et al., 2011; Leach and Moore, 2014; MacDonald et al., 2014a; Garner et al., 2014), predominantly solar radiation gains (Hannah et al., 2008; Leach and Moore, 2010; MacDonald et al., 2014a), and at some locations (3) groundwater inflows (e.g. Westhoff et al., 2007). Recognising the important role of energy exchange between the atmosphere and the water column and in response to the increasing scientific literature, river managers (e.g. The River Dee Trust; Upper Dee riparian scheme) are increasingly advocating the use of riparian vegetation to reduce total energy inputs to the water column,

* Corresponding author.
E-mail addresses: g.garner@bham.ac.uk (G. Garner), i.a.malcolm@marlab.ac.uk (I.A. Malcolm), j.p.sadler@bham.ac.uk (J.P. Sadler), d.m.hannah@bham.ac.uk (D.M. Hannah).

http://dx.doi.org/10.1016/j.jhydrol.2017.03.024
0022-1694/

and thus thermal variability and extremes (e.g. Gomi et al., 2006; Johnson and Jones, 2000; Hannah et al., 2008; Imholt et al., 2011, 2013; Garner et al., 2015).

Although there is a clear requirement for understanding the effects of riparian cover on stream temperature, there have been relatively few robust process based studies that provide realistic predictions of the likely effects of land use change. Moore et al. (2014) discussed various methods for representing the effects of vegetation on radiative energy fluxes above streams. However, to date river temperature models (e.g. Rutherford et al., 1997; Watanabe et al., 2005; DeWalle, 2008; Roth et al., 2010; Lee et al., 2012) have not considered the importance of vegetation structure (i.e. leaves, trunks and branches) and location relative to the position of the sun and the receiving waterbodies. Therefore, they were unable to adequately account for the temporally variable influence of discontinuous vegetation on the radiation budget. Furthermore, vegetation also has a significant effect on riparian microclimatic variables such as wind speed, relative humidity and air temperature, resulting in large reductions in latent heat losses (e.g. 60–87% was observed by Garner et al., 2015) in comparison to open reaches (e.g. Hannah et al., 2008; Garner et al., 2015). However, most modelling studies (e.g. Rutherford et al., 1997; Watanabe et al., 2005; DeWalle, 2008; Lee et al., 2012) have not considered the effects of changing microclimate as a result of riparian landuse change and so likely over-estimated the effect of forest canopies on reducing net energy fluxes and thus water temperature. Consequently, attempts to simulate the effects of riparian landuse change on water temperature have lacked the necessary physical realism to produce accurate estimates of effect sizes.

This study aims to generate systematic, process-based information on the effects of: (1) channel shading, (2) channel orientation and (3) water velocity on river temperature. Previous modelling and observational studies suggest that these three variables play an important role in determining river temperature dynamics. Firstly, because water temperatures are lower when vegetation is present (e.g. Hannah et al., 2008; Hrachowitz et al., 2010; Roth et al., 2010; Garner et al., 2015) and instantaneous differences in temperature between forested and open locations are greatest at sites under the densest canopies (e.g. Roth et al., 2010; Broadmeadow et al., 2011; Groom et al., 2011; Imholt et al., 2013). Secondly, because the orientation of the channel (LeBlanc et al., 1997; DeWalle, 2008; Li et al., 2012) and therefore the location of vegetation relative to the path of the sun is important in controlling solar radiation inputs (Lee et al., 2012). Finally, because longitudinal temperature gradients are reduced in steeper, faster flowing reaches compared with flatter, slower flowing ones (e.g. Danehy et al., 2005; Subehi et al., 2009; Groom et al., 2011). Knowledge of these controls and their interactions is important to inform optimal tree planting strategies and to assess likely outcomes.

In this context, we simulate the effects of varying riparian vegetation density and channel orientation on the stream energy budget and quantify their influence on water temperature dynamics under scenarios of high and low water velocity. The effects of riparian vegetation on river temperature are modelled using hemispheric photographs of different riparian canopy densities under field observed conditions and local measurements of micro-climate, thereby providing improved realism to estimates of likely effect size while at the same time being sufficiently generalisable to provide useful information to inform riparian planting strategies.

2. Study area

We collected field data within a 1050 m study reach of Glen Girnock. This upland basin is located in north east Scotland and drains into the Aberdeenshire Dee (Fig. 1). The catchment upstream of the reach has an area of ~22 km^2 in which heather (*Calluna*) moorland dominated landuse. Riparian landuse along the reach transitioned from moorland to semi-natural forest composed of birch (*Betula*), Scots pine (*Pinus*), alder (*Alnus*) and willow (*Salix*) (Imholt et al., 2010). Basin soils are composed predominantly of peaty podsols with some peaty gleys. Basin geology is dominated by granite at higher elevations and schists at lower elevations and is thus relatively impermeable (Tetzlaff et al., 2007). Within the study reach the riverbed is composed primarily of cobble and boulder with gravel accumulation in localised patches. The reach is 280 m above sea level (asl) at the upstream reach boundary and 255 m asl at the downstream reach boundary. During field data collection the mean wetted width of the channel was 9.5 m. Previous work within the study reach demonstrated that there are no substantial groundwater inflows and consequently that groundwater does not significantly modify water temperature dynamics (Malcolm et al., 2005; Garner et al., 2014). Thus, the influence of canopy density, channel orientation and water velocity on water temperature could be investigated in the absence of confounding groundwater influences (e.g. Story et al., 2003; Westhoff et al., 2011).

The UK Meteorological Office record daily averages of air temperature and totals of precipitation at Balmoral (<10 km north west of the catchment). During the period 1950–2013 annual average air temperature was 6.6 °C, maximum temperatures occurred in June and July (daily averages 13.0 and 12.6 °C respectively) and minima occurred in December to February (daily averages 2.4, 2.2 and 1.6 °C respectively). Between 1950 and 2013 annual average precipitation totalled 846 mm, October to January were the wettest months (daily average totals ranged from 85.7 mm in December to 92.5 mm in October) and February to September were the driest (daily average totals ranged from 55.1 mm in April to 70.8 mm in August). River discharge is monitored continuously by the Scottish Environmental Protection Agency (SEPA) in a rated natural section of the Girnock at Littlemill (Fig. 1). Annual mean flow is 0.530 m^3 s^{-1} (1969–2013). Summer flows (i.e. June-August) are typically <0.100 m^3 s^{-1} but the flow regime is highly responsive to precipitation and so high flow events (e.g. $\geq Q_{10}$, 1.126 m^3 s^{-1}) occur year-round.

3. Methods

3.1. Experimental design

Spatially distributed field data were used to parameterise a simulation experiment that investigated the influence of: (1) riparian vegetation density, (2) channel orientation (and thus vegetation orientation relative to the sun's path), and (3) water velocity (a proxy for stream gradient) on heat exchange patterns and water temperature dynamics within a 1050 m reach of the Girnock Burn. A single time series of discharge was used for each velocity scenario thereby separating the effects of velocity and residence time from those of varying water volume. Consequently, the effects of each vegetation and channel orientation scenario were simulated for a low (i.e. slow velocity: 0.023 ms^{-1}) or high gradient (i.e. fast velocity: 0.155 ms^{-1}) river. We did not investigate the effects of changing discharge because we were primarily interested in the effects of riparian woodland on river temperature under summer low flow conditions, when the most extreme high water temperatures are expected to occur.

Firstly, a process-based water temperature model (herein referred to as the 'base model') driven by spatially distributed energy flux data temperature (Garner et al., 2014 after Bartholow, 2000; Boyd and Kasper, 2003; Rutherford et al., 2004; Westhoff et al., 2007, 2010; Leach and Moore, 2011; MacDonald et al., 2014a,b) was parameterised for observed conditions within the Girnock Burn. Previous work suggested that the base model

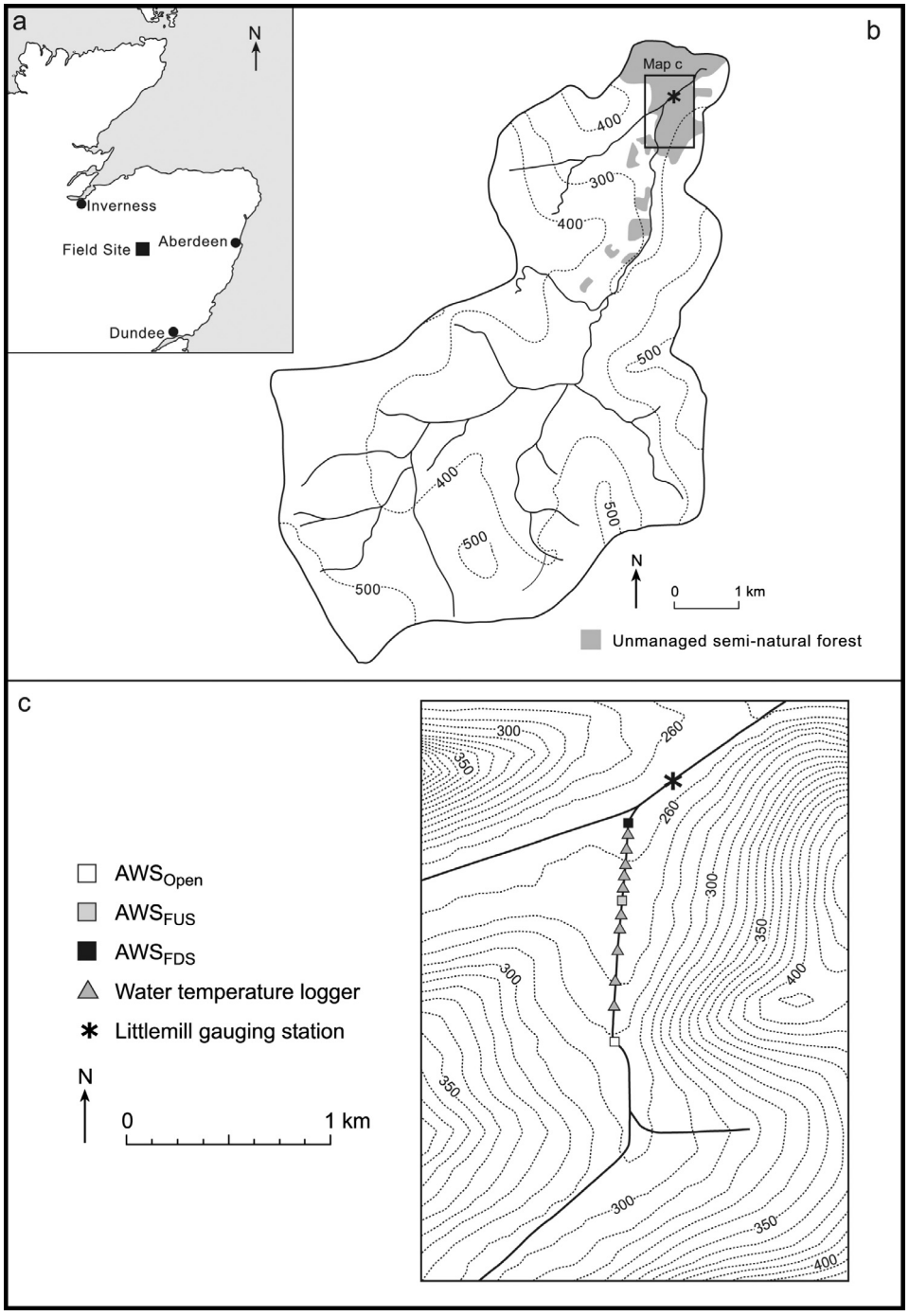

Fig. 1. Girnock Burn (a) location within Scotland (b) catchment map (c) locations of field data collection sites.

adequately described spatio-temporal variability in river temperature (Garner et al., 2014), and thus is capable of providing realistic assessments of the effects of interest. Secondly, simulations representative of varying vegetation density, channel orientation and water velocity scenarios were performed by adjusting selected parameters (see sections '3.2 Data' and '3.3 Estimation of stream energy budget components') in the base model (herein referred to as the 'simulation experiments').

For the simulation experiments, nine hemispherical images obtained in the field (Fig. 2; termed 'vegetation scenarios' herein) were used to represent different canopy densities (i.e. 10–90% in 10% increments). The images were used to parameterise a deterministic net radiation model (Leach and Moore, 2010) and simulate radiative fluxes at 1 m intervals indicative of uniform forestation of the entire reach. The effect of channel orientation on energy exchanges and water temperature was investigated for each vegetation scenario by changing the location of north and thus the path of the sun relative to the position of vegetation in each hemispherical image at 45-degree intervals (see sun-paths on Fig. 2). Thereby, we simulated the effects of each vegetation scenario on north-south (N-S), northeast-southwest (NE-SW), east-west (E-W), southeast-northwest (SE-NW), south-north (S-N), southwest-northeast (SW-NE), west-east (W-E) and northwest-southeast (NW-SE) flowing streams. Modelled radiative fluxes were com-

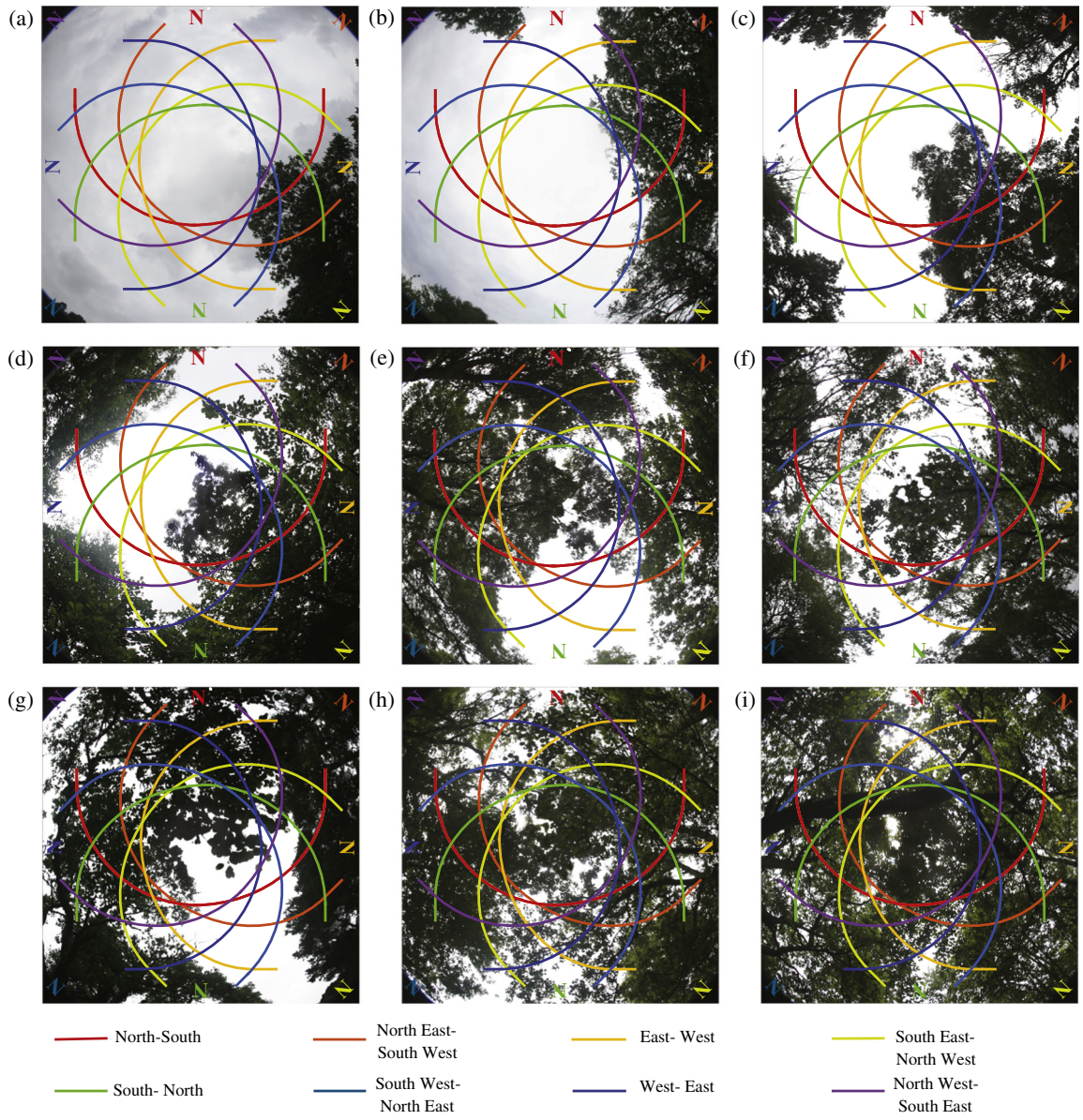

Fig. 2. Hemispherical images used to represent (a) 10% (b) 20% (c) 30% (d) 40% (e) 50% (f) 60% (g) 70% (h) 80% (i) 90% riparian canopy density scenarios. Eight coloured lines in each image represent the path of the sun across the sky relative to changing north in each image at 45-degree increments.

bined with linearly interpolated turbulent fluxes (i.e. sensible and latent heat) calculated from measured micro-meteorological variables at the three automatic weather stations (Fig. 1, see below for further details) to drive the water temperature model for each scenario. Stream temperature was predicted along the reach at a resolution of 50 m.

3.2. Data

Field data were collected between October 2011 and July 2013 (from Garner et al., 2014); hydrometeorological data collected on 6 July 2013 (Fig. 3) were chosen to meet the aim of the present study. On this day, measured water temperatures (Fig. 3a) and solar radiation gains to the water column (Fig. 3b) at an automatic weather station (AWS) sited within the reach on open moorland ($AWS_{open;}$ Fig. 1) were high, while discharge was very low. Consequently, the effects of vegetation density, channel orientation and water velocity on water temperature were evaluated under a 'worst-case scenario' of high energy inputs and low flows (after Garner et al., 2014).

3.2.1. Micrometeorological measurements

Three AWSs (automatic weather stations) were installed within the reach (Fig. 1) to characterise spatio-temporal variability in energy fluxes: the first was located in open moorland at the upstream reach boundary (AWS_{open}), the second was located in semi-natural forest 190 m downstream of the upstream boundary (named "AWS forest upstream" or AWS_{FUS}) and the third was located in semi-natural forest 685 m downstream of the upstream boundary (named "AWS forest downstream" or AWS_{FDS}). Hydrometeorological variables measured by each AWS were: air temperature (°C), relative humidity (%), wind speed (ms^{-1}), incoming solar radiation, net radiation and bed heat flux (all Wm^{-2}). The instruments deployed on the AWSs are detailed in Hannah et al. (2008). AWSs measured meteorological variables ~2 m above the stream surface. Bed heat flux measurements were made using heat

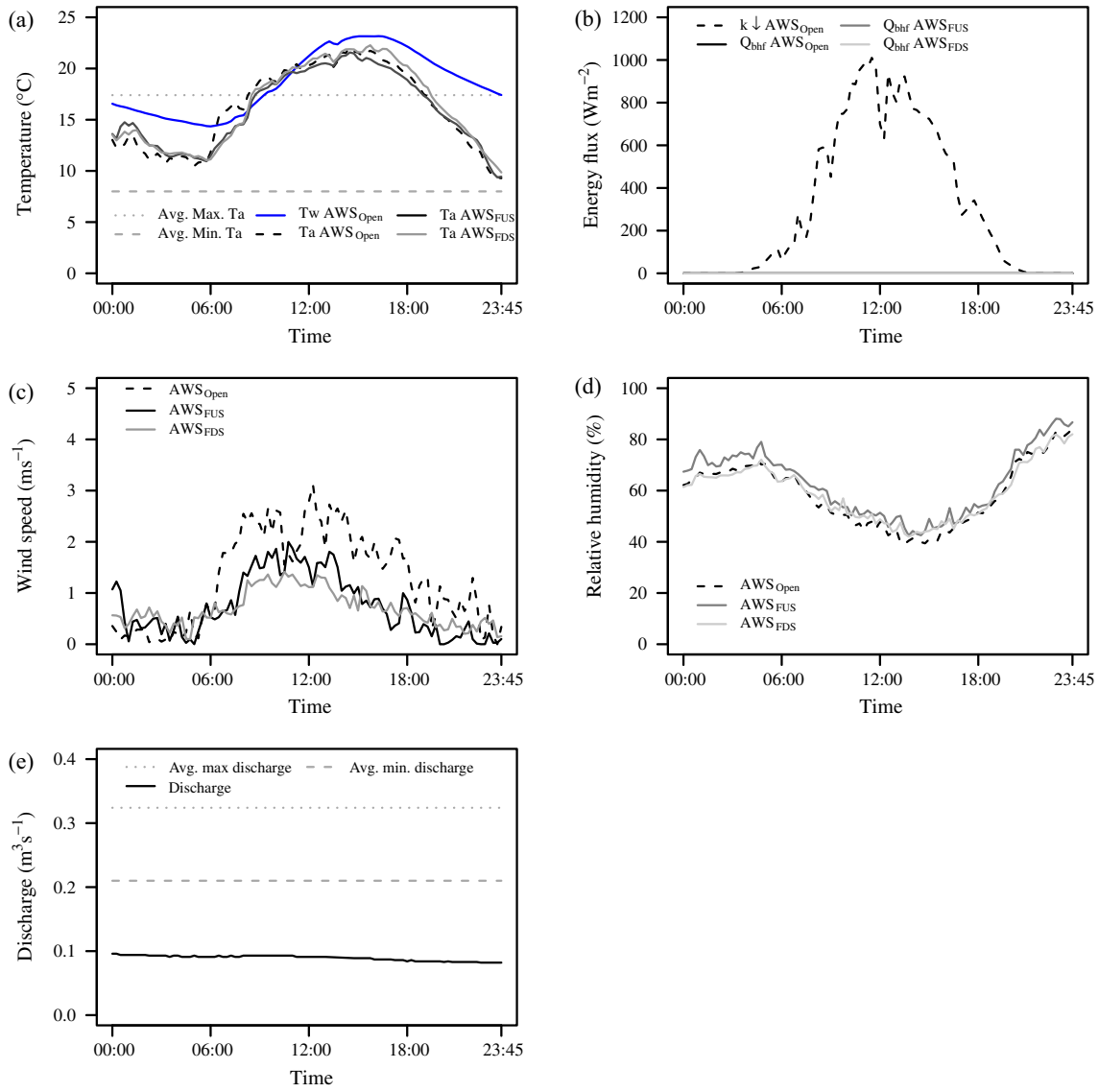

Fig. 3. Model input data for 6 July 2013 (a) air and water temperatures (b) solar radiation (c) wind speed (d) relative humidity (e) discharge.

flux plates buried (to avoid radiative and convective errors) at 0.05 m depth within the riverbed below each AWS. Heat flux plates provided aggregated measurements of convective, conductive, advective and radiative heat exchanges between the atmosphere and the riverbed and the riverbed and the water column (after Evans et al., 1998; Hannah et al., 2008; Garner et al., 2014). All AWS sensors were sampled at 10-s intervals and averages were logged every 15-min.

3.2.2. Stream temperature measurements

Stream temperature measurements were used to evaluate the performance of the base model under observed conditions (i.e. Garner et al., 2014) and provided initial conditions at the upstream reach boundary. Water temperature was measured at 15-min intervals using ten water temperature TinyTag Aquatic 2 dataloggers (manufacturer stated accuracy of ±0.5 °C) and three Campbell 107 thermistors (manufacturer stated accuracy ±0.1 °C) connected to AWSs and installed at 0 (AWS_{Open}), 190, 315, 460, 565, 630, 685 (AWS_{FUS}), 760, 815, 865, 940 1015 and 1050 (AWS_{FDS}) m downstream of the upstream reach boundary (Fig. 1). Prior to installation the sensors were compared (following Hannah et al., 2009) over the range 0–30 °C and were in agreement by <±0.1 °C. Sensors were deployed within white plastic PVC tubes to shield them from direct solar radiation.

3.2.3. Hydrology and stream geometry

Discharge ($m^3\ s^{-1}$) was obtained from a Scottish Environmental Protection Agency (SEPA) gauging station at Littlemill (Fig. 1). Discharge was required as input to the water temperature model (see "3.4 Modelling approach"). The time series of discharge from 6th July 2013 (Fig. 3e) was used as input to the base model run and for the simulation experiment model runs; values were very low (average 0.089 $m^3\ s^{-1}$, which is equal to Q_{96} calculated for June-August during the period 1983–2013), stable (0.082–0.096 $m^3\ s^{-1}$) and exhibited no sudden changes. Water velocity (ms^{-1}) for the base model was calculated from discharge using a discharge- mean velocity function for Littlemill derived by Tetzlaff et al. (2005) and was used to route discrete parcels of water through the reach in order to drive the flow-routing component of the water temperature model (see '3.4 Modelling approach'). For evaluation of the base model velocity was allowed to vary temporally (at hourly intervals) in response to changing

discharge. For the simulation experiments constant values of high (0.155 ms^{-1}) and low velocity (0.023 ms^{-1}) were used at all locations and time steps. Wetted width was required as input to the water temperature model. Spatially varying values measured at 50 m intervals along the reach were used for the base model evaluation, but a fixed value of 9.5 m (the mean wetted width) was used for the simulation experiments.

3.2.4. Hemispherical images

Hemispherical images were taken at 5 m intervals along the stream centreline using a Canon EOS-10D 6.3 megapixel digital camera with Sigma 8 mm fisheye lens. Prior to taking each image the camera was orientated to north and levelled ~20 cm above the stream surface (after Leach and Moore, 2010). All images were used to parameterise the radiation component of the base model and thus represent the baseline (current) riparian vegetation condition in the reach (i.e. Garner et al., 2014) for the model validation. Data derived from nine of these images (each representative of 10–90% canopy density at 10% increments; Fig. 2) were used to parameterise the vegetation scenarios.

3.3. Estimation of stream energy budget components

3.3.1. Net energy

Net energy (Q_n, Wm^{-2}) available to heat or cool the water column was calculated as:

$$Q_n = Q^* + Q_e + Q_h + Q_{bhf} \quad (1)$$

where Q_n is net energy, Q^* is net radiation, Q_e is latent heat, Q_h is sensible heat and Q_{bhf} is bed heat flux (all Wm^{-2}). Heat from fluid friction was omitted because it makes a negligible contribution to the energy budget in this reach (after Garner et al., 2015). Herein, positive energy fluxes represent gains to the water column while negative energy fluxes represent losses.

3.3.2. Net radiation

A deterministic model developed by Moore et al. (2005) and then extended and evaluated by Leach and Moore (2010) was used to compute net radiation (Q^*) at the location of each hemispherical image. At each location net radiation was calculated as:

$$Q^* = K^* + L^* \quad (2)$$

where K^* (Wm^{-2}) is net shortwave radiation (Eq. (3)) and L^* (Wm^{-2}) is net longwave radiation (Eq. (4)).

$$K^* = (1-\alpha)[D(t)g(t) + s(t)f_v] \quad (3)$$

$$L^* = [f_v\varepsilon_a + (1-f_v)\varepsilon_{vt}]\sigma(T_a + 273.2)^4 - \varepsilon_w\sigma(T_w + 273.2)^4 \quad (4)$$

where α is the stream albedo, $D(t)$ is the direct component of incident solar radiation at time t (Wm^{-2}), $g(t)$ is the canopy gap fraction at the position of the sun in the sky at time t, $s(t)$ is the diffuse component of solar radiation (Wm^{-2}), f_v is the sky view factor, ε_a, ε_{vt} and ε_w are the emissivity of the temperatures of the air, vegetation and water respectively (all °C), σ is the Stefan-Boltzmann constant (5.67×10^{-8} Wm^{-2} K^{-4}), and T_a and T_w are air and water temperature respectively (both °C).

Values for atmospheric emissivity were calculated for clear-sky day and night conditions using the equation presented in Prata (1996); (used also by Leach and Moore, 2010; Garner et al., 2014) and were subsequently adjusted for cloud cover using equations in Leach and Moore (2010). The emissivity and albedo were taken to be 0.95 and 0.05 for water, and 0.97 and 0.03 for vegetation respectively (after Moore et al., 2005 and used subsequently by Garner et al., 2014).

Gap fractions (g_*) were computed as a function of solar zenith angle (θ, °) and solar azimuth (ψ, °), $g_*(\theta, \psi)$, which were derived at 5° intervals from analysis of the hemispherical photographs with Gap Light Analyser software (Frazer et al., 1999). Hemispherical photographs were converted to binary images by setting a threshold that determines whether a pixel should be classified as sky (white) or another object (black) such as river banks, tree trunks, leaves or branches. An optimum threshold value of 130 was selected from candidate values of 120–190 at 10 unit increments. This threshold value minimised RMSE between observed and modelled incoming solar radiation at AWS_{FUS} during 1 and 7 July 2013 (see Garner et al., 2014). The solar zenith and azimuth angles were computed as a function of time (t, minutes) using equations in Iqbal (1983) so that the canopy gap at the location of the sun could be derived from $g*(\theta,\psi)$ as a function of time, $g(t)$. Sky view factor was computed as:

$$f_v = \frac{1}{\pi}\int_0^{2\pi}\int_0^{\pi/2} g_*(\theta,\psi)\cos\theta\sin\theta * d\theta * d\psi \quad (5)$$

Solar radiation measured at AWS_{open} was used to drive the solar radiation model for evaluation of the base model and the simulation experiments in order to simulate this energy flux at 1 m intervals along the reach centreline. For the simulation experiments, time series of air temperature (used to calculate net longwave radiation) were generated by linear interpolation between the two nearest AWSs to the point along the stream centreline at which the hemispherical photograph representative of the vegetation scenario was taken. Net longwave radiation is a function of water temperature; therefore initial values for this flux at the upstream reach boundary were calculated using observed water temperature at AWS_{Open}.

3.3.3. Latent and sensible heat fluxes

To compute heat lost by evaporation or gained by condensation, latent heat was estimated after Webb and Zhang (1997) (Eq. (6)).

$$Q_e = 285.9(0.132 + 0.143 * U)(e_a - e_w) \quad (6)$$

where U is wind speed (ms^{-1}) and e_a and e_w are vapour pressures of air and water (both kPa), respectively. Saturation vapour pressure (e_{sat}) was calculated as a function of air or water temperature, T (K), after Stull (2000) (Eq. (7)).

$$e_{sat}(T) = 0.611 * exp\left[\frac{2.5 * 10^6}{461} * \left(\frac{1}{273.2} - \frac{1}{T}\right)\right] \quad (7)$$

Vapour pressure of water (e_w) was assumed to be equal to $e_{sat}(T_w)$. Vapour pressure of air (e_a) was calculated using Eq. (8).

$$e_a = \frac{RH}{100}e_{sat}(T_a) \quad (8)$$

Sensible heat (Eq. (9)) was calculated as a function of Q_e (Eq. (6)) and Bowen ratio (β) (Eq. (10)), where P is air pressure (kPa).

$$Q_h = Q_e * \beta \quad (9)$$

$$\beta = 0.66 * \left(\frac{P}{1000}\right) * [(T_w - T_a)/(e_a - e_w)] \quad (10)$$

For the simulation experiments, time series of meteorological variables (i.e. air temperature, wind speed and relative humidity) required to calculate turbulent fluxes were generated for each vegetation scenario by linear interpolation between the two nearest AWSs to the point along the stream centerline at which the hemispherical photograph representative of the scenario was taken. Turbulent fluxes are a function of water temperature; therefore initial values at the upstream boundary were calculated using observed water temperature at AWS_{Open}.

3.4. Modelling approach

A Lagrangian modelling approach was used to simulate river water temperature (after Garner et al., 2014) in which the trajectory of discrete parcels of water is followed through the reach in order to determine the energy exchange conditions the parcels are exposed to and thus calculate changes in their temperature as they flow downstream and time elapses.

The reach was divided into a series of 1 m segments (s) bounded by nodes (x). At hourly intervals a discrete parcel of water (i) with an initial temperature was released from the upstream boundary at AWS_{Open} and routed through the reach using the discharge-mean velocity function (Tetzlaff et al., 2005). The distance travelled by each water parcel from its location (x) at time t to its next location ($x+1$) at time $t+\Delta t$ was calculated as the product of the length of each 15-min time step (Δt, i.e. 900 s) and either: (1) for evaluation of the base model, the average velocity of the parcel at times t and $t+\Delta t$ or (2) for the simulation experiments, 0.023 or 0.155 ms^{-1} for the low and high velocity scenarios, respectively. As the water parcel travelled downstream from x towards $x+1$ the model determined the mean of each of the meteorological variables the parcel was exposed to along its trajectory through the segments at times t and $t+1$. This information was used to calculate the water temperature of each parcel at 50 m intervals by integration of Eq. (11) in the deSolve package (Soetaert et al., 2010) for R (Version 3.0.2, R Group for Statistical Computing, 2013).

$$\frac{\partial T_{w(i)}}{\partial x} = \frac{[[w_{\bar{s}}(Q_{n(\bar{s},t)}) + w_{\bar{s}}(Q_{n(\bar{s},t+\Delta t)})]/2]}{C[(F_{(\bar{s},t)} + F_{(\bar{s},t+\Delta t)})/2]} \quad (11)$$

where $w_{\bar{s}}$ is the mean wetted width of the stream surface (m) within segments $\bar{s}$, $K^*_{(\bar{s},t/t+\Delta t)}$, $L^*_{(\bar{s},t/t+\Delta t)}$, $Q_{e(\bar{s},t/t+\Delta t)}$, $Q_{h(\bar{s},t/t+\Delta t)}$ and $Q_{bhf(\bar{s},t/t+\Delta t)}$ are the mean net shortwave, net longwave, latent, sensible and bed heat fluxes within segments $\bar{s}$ at time t or $t+\Delta t$. C is the specific heat capacity of water (4.18×10^6 Jm^{-3} $°C^{-1}$) and $F_{(\bar{s},t/t+\Delta t)}$ is the discharge [m^3 s^{-1}; scaled linearly by catchment area after Garner et al., 2014] within segments $\bar{s}$ at time t or $t+\Delta t$. In 'Supplement 1' we discuss the principles of Eq. (11) and demonstrate how continuity of mass was satisfied in the high and low velocity scenarios without changing wetted width or the time series of discharge used in all simulations.

Energy exchange due to bed heat flux, which accounted for <1% of the stream energy budget (Garner et al., 2014), was retained within the model structure for evaluation of the performance of the base model but omitted for the simulation experiments so as to investigate the influence of vegetation scenarios on water temperature dynamics driven by energy exchanges between the atmosphere and the water column only.

4. Results

4.1. Stream energy budget

4.1.1. Net solar radiation

For each vegetation scenario and channel orientation, simulated daily total net solar radiation flux is demonstrated in Fig. 4a while the underlying diurnal patterns are demonstrated in Fig. 5. Total net energy flux typically decreased as vegetation density increased (Fig. 4a). The orientation of the channel had a limited impact on total daily net solar radiation gains under: (1) the densest canopies (i.e. 70–90% density; Fig. 4a), when limited portions of the stream remained unshaded (Fig. 2d–g) and (2) under the sparsest canopies (i.e. ≤20%; Fig. 4a), when vegetation did not overhang the stream, cast minimal shade regardless of channel orientation (Fig. 2a and b) and diurnal patterns were similar regardless of channel orientation (scenarios of 10 and 20% canopy density on Fig. 5). However, the orientation of the channel influenced net solar radiation gains substantially under scenarios of 30–60% canopy density (termed intermediate scenarios herein) (Fig. 4a). We compare two channel orientations under a 30% canopy density in order to demonstrate the drivers of this variability (Fig. 6). In the first scenario the channel was orientated SE-NW and the position of the vegetation did not provide shade from net solar radiation, as demonstrated by minimal overlap between the sun-path and the vegetation on Fig. 6a. Consequently, the magnitude and diurnal pattern of modelled net solar radiation (Fig. 6b) was similar to those under sparse canopies (e.g. scenarios of 10 and 20% density on Fig. 5). In the second scenario the channel was orientated NW-SE and vegetation was located so that it shaded the channel when the sun was between south-easterly and south-westerly sky-positions, as demonstrated by the apex of the sun-path overlapping vegetation on Fig. 6d. Consequently, the channel was shaded when potential net solar radiation gains were greatest (i.e. around mid-day) and so simulated values were low (Fig. 6e). For all intermediate vegetation scenarios, large portions of the sky remained unshaded (Fig. 2c–f) so that large net solar radiation gains were simulated when vegetation did not provide shade from the strongest gains whereas low net solar radiation gains occurred when vegetation provided shade during these times (scenarios of 30–60% density on Fig. 5).

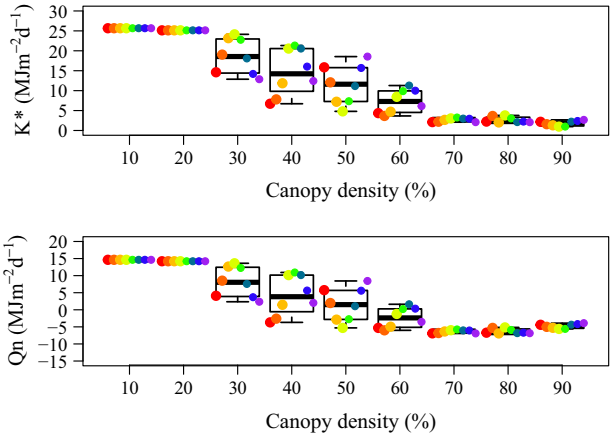

Fig. 4. Simulated daily total (a) net solar radiation (b) net energy flux at the upstream reach boundary under each vegetation scenario and channel orientation. Eight coloured points in each plot represent the path of the sun across the sky relative to changing north in each image at 45-degree increments.

4.1.2. Net energy

For each vegetation scenario and channel orientation, simulated daily total net energy flux is demonstrated in Fig. 4b while the underlying diurnal patterns are demonstrated in Fig. 7. Net energy flux was calculated in part as the sum of net longwave radiation, latent and sensible heat fluxes, which are dependent on water temperature. At each time step water temperature was not uniform throughout the reach, therefore modelled net energy at the upstream reach boundary is described in order to compare broad differences in energy loss from and gain to the water column between vegetation scenarios. Net energy exchange typically decreased as canopy density increased (Fig. 4b). Beneath the sparsest canopies, the water column gained energy during daylight hours and lost energy overnight regardless of channel orientation (scenarios of 10 and 20% on Fig. 7); this resulted in high daily total net energy gains to the water column under all channel orientations (Fig. 4b). Channel orientation also had limited impact on net energy fluxes beneath the densest canopies where energy losses typically occurred during the day and overnight (scenarios

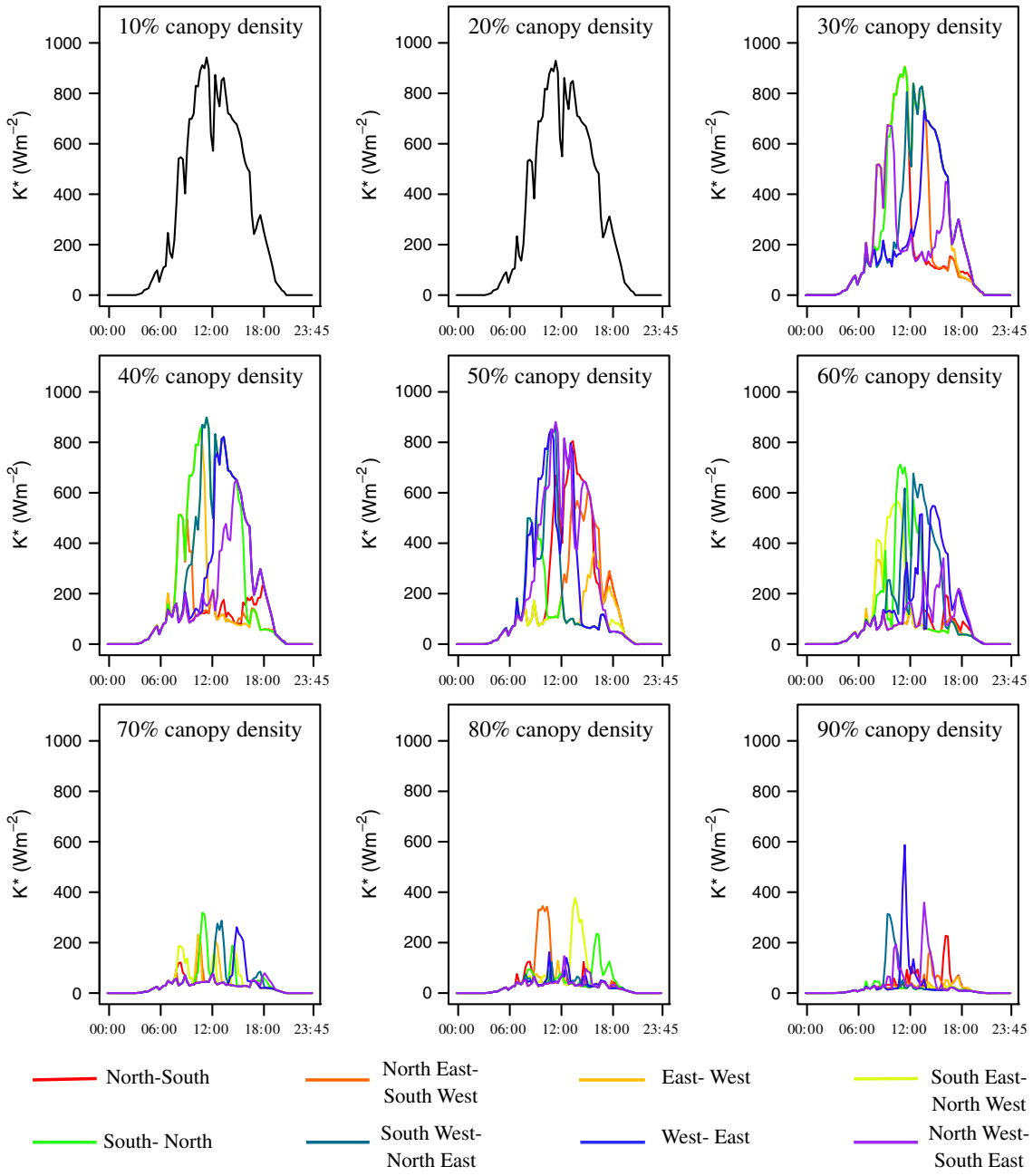

Fig. 5. Simulated net solar radiation at the upstream reach boundary under each vegetation scenario and channel orientation. Eight coloured lines in each image represent the path of the sun across the sky relative to changing north in each plot at 45-degree increments. [solar radiation receipt varied indiscernibly with channel orientation under scenarios of 10 and 20% canopy density and are therefore illustrated by a single black line].

of 70–90% density on Fig. 7), generating daily total net energy losses from the water column (Fig. 4b). However, daily total net energy exchange was highly variable under intermediate vegetation scenarios of 30–60% canopy density (Fig. 4b); the magnitude of energy gains or losses depended on channel orientation. We demonstrate the causes of this variability using the SE-NW (exposed to the greatest solar radiation gains) and NW-SE (shaded from the greatest solar radiation gains) orientated channels under a 30% canopy density. The diurnal pattern and magnitude of net energy flux to the SE-NW orientated channel (Fig. 6c) was similar to those under sparse canopies (e.g. scenarios of 10 and 20% density on Fig. 7) because vegetation did not shade the channel from the sun around mid-day (Fig. 5a). In contrast, the NW-SE orientated channel was shaded from the sun by vegetation when net solar radiation inputs were greatest (Fig. 6d and e) and small net energy losses or gains were simulated at these times (Fig. 6f). For all intermediate vegetation scenarios (Fig. 2d–g), large net energy gains were simulated when vegetation did not provide shade from the strongest net radiation gains; small net energy gains or losses were simulated when channels were shaded during these times (scenarios of 30–60% canopy density on Fig. 7).

4.2. Water temperature

4.2.1. Base water temperature model evaluation

The performance of the base water temperature model was evaluated previously by Garner et al. (2014) for a limited number of time steps between 1st and 7th July 2013 and deemed to be

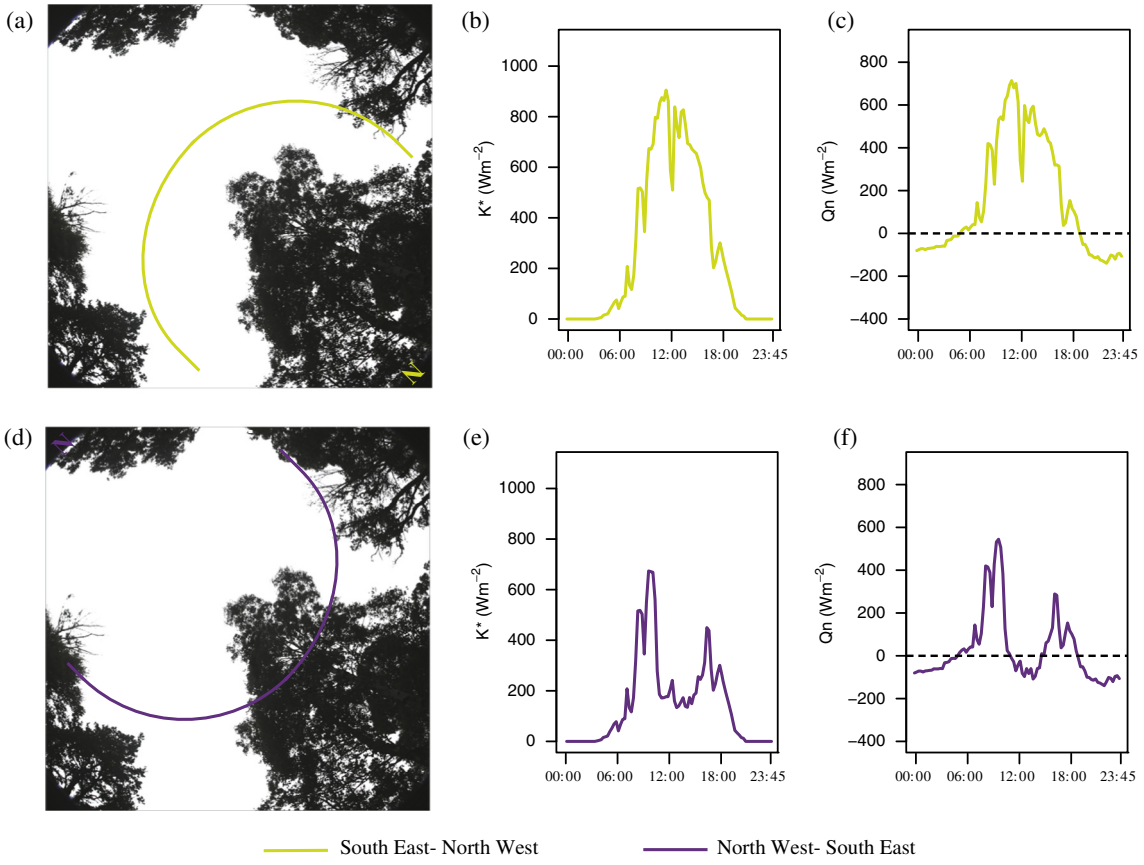

Fig. 6. (a) Hemispherical image and sun-path (b) net solar radiation (c) net energy under 30% canopy density and channel SE-NW orientation. (d) Hemispherical image and sun-path (e) net solar radiation (f) net energy under 30% canopy density and NW-SE channel orientation.

good. We calculated model evaluation statistics for the temperature of all water parcels released from AWS_{Open} on 6th July 2013 (i.e. statistics calculated from 23 time steps at 50 m intervals throughout the reach, thus n = 483 modelled values). Nash-Sutcliffe efficiency (0.97), percent-bias (−1.1%), and mean error (−0.2 °C) were well-within limits proposed for watershed simulations of flow and constituent processes by Moriasi et al. (2007). Furthermore, error (simulated minus observed values) in daily maximum (−0.6 °C), mean (−0.2 °C) and minimum (0.3 °C) water temperatures simulated throughout the reach demonstrated that temperatures were reproduced with high levels of accuracy.

4.2.2. Vegetation density and channel orientation effects on simulated water temperature dynamics

Water temperature metrics were derived from all values simulated throughout the reach (i.e. n = 483 temperatures). Typically, mean and maximum water temperatures decreased as vegetation density increased but minimum temperatures were not affected (Fig. 8). Channel orientation had little effect on simulated water temperature dynamics under the sparsest (i.e. ≤20%) and densest (i.e. ≥70%) vegetation scenarios, as indicated in Fig. 8 by little spread in the distribution of temperatures for these scenarios. Furthermore, under the densest canopies maximum temperatures simulated throughout the reach did not exceed the maximum inflow temperature at the upstream reach boundary (23.1 °C). Under canopies of intermediate density (i.e. 30–60%), varying channel orientation was associated with large variability in maximum and mean temperatures simulated throughout the reach (Fig. 8). For example under the 30% canopy density scenario and low flow velocity, the highest maximum (27.9 °C) and mean (18.8 °C) temperatures were simulated for the SE-NW (exposed to the strongest solar radiation gains) orientated channel while the lowest maximum (23.6 °C) and mean temperatures (16.1 °C) were simulated for the NW-SE (shaded from the strongest solar radiation gains) orientated channel.

Spatio-temporal variability in temperature was also varied for intermediate canopy density scenarios. As an example we compare the SE-NW (exposed to the strongest solar radiation gains) and NW-SE (shaded from the strongest solar radiation gains) channel orientations under a 30% canopy density. In comparison with the SE-NW orientated channel, the NW-SE orientated channel reduced water temperatures throughout the reach between around 11:00 and 17:00. The magnitude of the reduction increased in the downstream direction and greater reductions were observed under the low velocity condition (Fig. 9c and f). For example at noon (when the effect was particularly prominent) under the high velocity condition and NW-SE orientation water temperatures were reduced by 0.3 °C at 50 m and 6.5 °C at 1050 m (Fig. 9c). Under the low velocity condition and NW-SE orientation water temperatures were reduced by 2.8 °C at 50 m and 7.5 °C at 1050 m (Fig. 9f). Furthermore, maximum temperatures occurred later in the day under the NW-SE orientation, around 18:00 versus around 12:00 under the SE-NW orientation.

4.2.3. Effects of water velocity on simulated water temperature dynamics

The velocity under which simulations were performed determined the residence time of water parcels within the reach. The high velocity scenario resulted in shorter residence time (cf. low). For example the parcel of water released from AWS_{Open} under

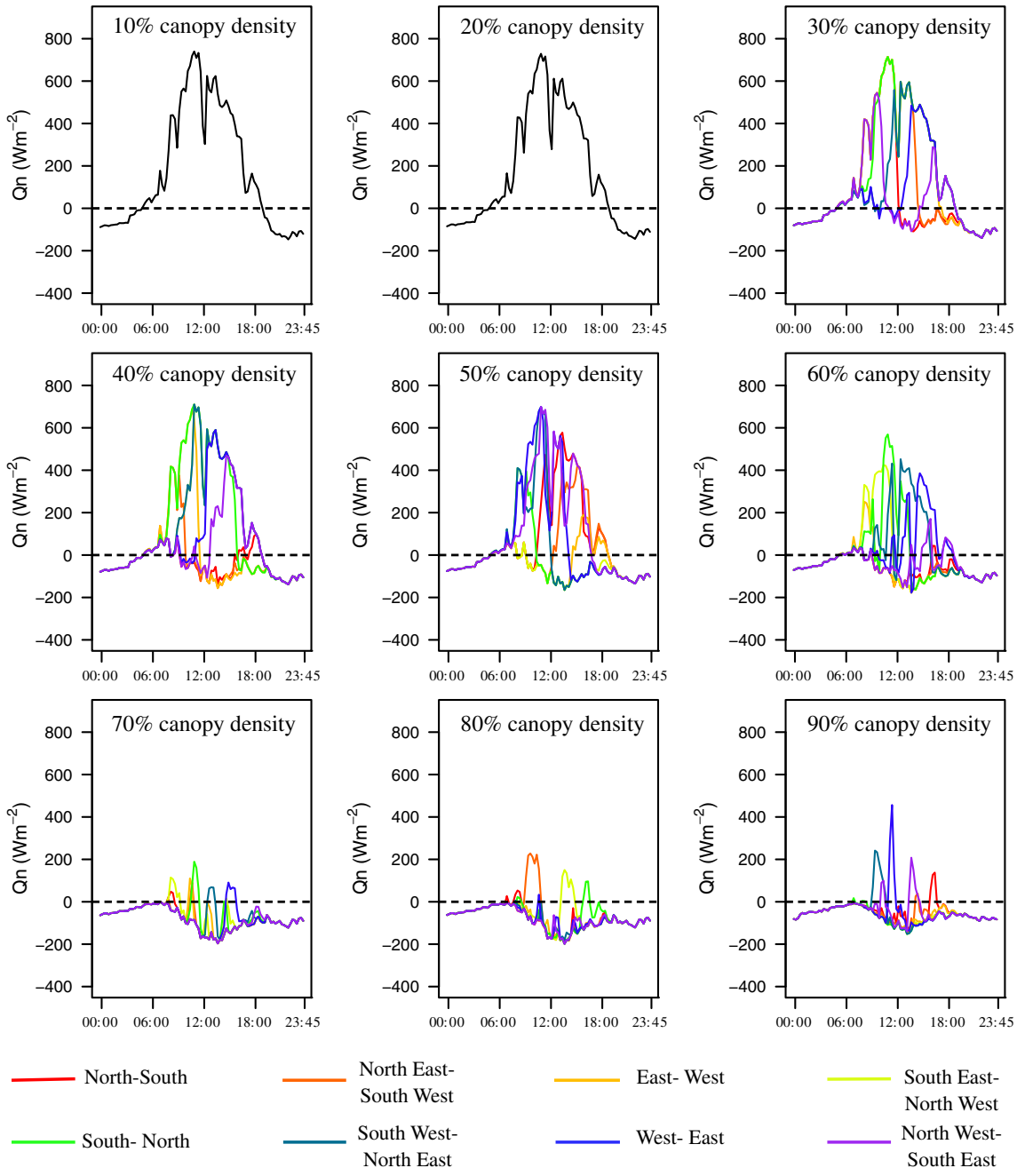

Fig. 7. Simulated net energy flux at the upstream reach boundary under each vegetation scenario and channel orientation. Eight coloured lines in each plot represent the path of the sun across the sky relative to changing north in each image at 45-degree increments. [net energy flux varied indiscernibly with channel orientation under scenarios of 10 and 20% canopy density and are therefore illustrated by a single black line].

the high velocity scenario at 23:00 on 23 July left the reach around 00:45 on 24 July (Fig. 9a and b) whereas under the low velocity scenario the water parcel did not leave the reach until around 11:30 on 24 July (Fig. 9d and e).

Shorter (longer) residence times resulted in less (greater) heating and cooling of water. Consequently, simulations under the low velocity resulted in greater differences in temperatures between vegetation scenarios. Increasing vegetation density from 10 to 90% decreased mean temperatures by up to 5.4 °C (SE-NW orientation) for the low velocity scenario and 1.6 °C (NE-SW, E-W, SE-NW, S-N orientations) for the high velocity scenario (Fig. 8a and d). Maximum temperatures decreased by 4.9 °C (all orientations) for the low velocity scenario and up to 3.0 °C (NE-SW, E-W, SW-NE, W-E, NW-SE orientations) for the high velocity scenario (Fig. 8b and e). While minimum temperatures were reduced by up to 0.3 °C (E-W, SE-NW orientations) for the low velocity scenario and up to 0.5 °C (NE-SW, E-W, SE-NW, W-E orientations) for the high velocity scenario (Fig. 8c and f). Furthermore, for each intermediate vegetation scenario (i.e. 30–60% density) the lower velocity enhanced differences in simulated temperatures between channel orientation scenarios. For example, under the high flow scenario and 30% vegetation density temperatures varied by up to 0.8 °C for mean and 2.7 °C for maximum. Under the same vegetation scenario with a low velocity temperatures varied by 2.7 °C for mean and 4.3 °C for maximum (Fig. 8). The effect of changing velocity was not confined to metrics; temperatures were modified

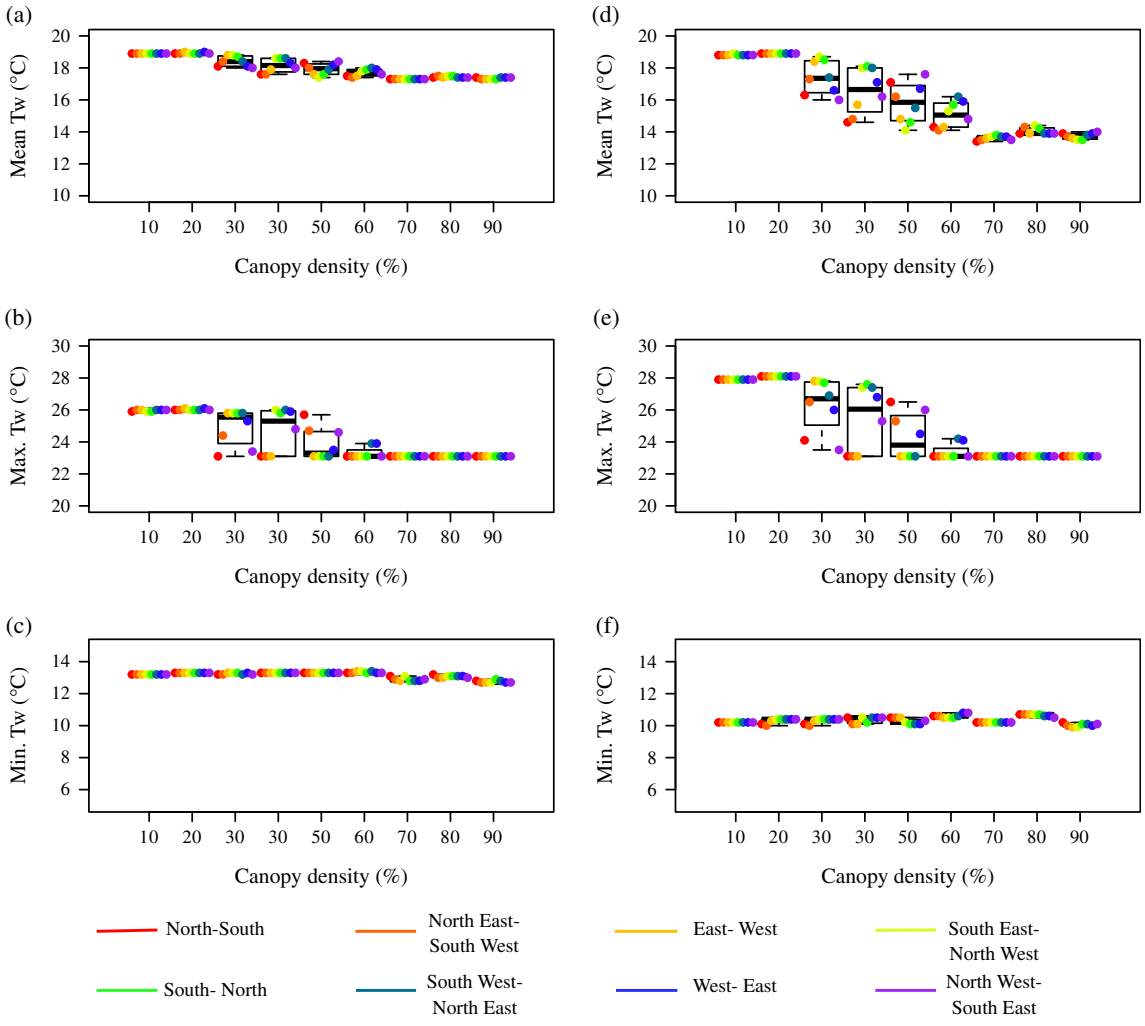

Fig. 8. Simulated mean (a, d), maximum (b, e) and minimum (c, f) water temperatures for (a–c) high flow velocity and (d–f) low flow velocity scenarios. Eight coloured points in each plot represent the path of the sun across the sky relative to changing north in each image at 45-degree increments.

throughout the reach at most time steps. Spatio-temporal differences between high and low velocity conditions are demonstrated in Fig. 9g and h for a scenario of 30% canopy density in which the channel was orientated SE-NW (i.e. exposed to the strongest solar radiation gains) and a scenario of 30% canopy density in which the channel was orientated NW-SE (i.e. shaded from the strongest solar radiation gains) respectively. Most notably, when the channel was exposed under the low velocity condition the highest temperatures (>25.0 °C) occurred throughout most of the reach and persisted for longer (Fig. 9g). When the channel was shaded under the low velocity condition the lowest daytime temperatures (<20.0 °C) occurred throughout the reach and persisted for longer (Fig. 9h).

5. Discussion

This study quantified the influence of riparian vegetation density on energy exchange and water temperature dynamics in channels of varying orientation and with varying water velocity. The latter is a control of hydraulic retention time within the reach, which increases for lower gradient streams if wetted width and discharge are unchanged. The following discussion considers the effects of: (1) interactions between vegetation density and channel orientation on stream heating and cooling processes and (2) water velocity, and we identify the limitations of our approach. The implications of the findings are discussed in the context of river management in a changing climate.

5.1. Vegetation density, channel orientation and effects on stream heating and cooling

Riparian vegetation reduces solar radiation inputs and consequently net energy available to heat the water column (Hannah et al., 2004, 2008; Leach and Moore, 2010; Garner et al., 2014, 2015). During the study period (Northern Hemisphere summer) at this relatively high latitude site (57°02′N) riparian vegetation had the greatest effect on net solar radiation and net energy inputs when it overhung the stream centreline and therefore shaded the stream from the greatest solar radiation inputs. Consequently during summer, when river flows are lowest and water temperature highest, riparian planting is only likely to be effective in reaches where river width is sufficiently narrow and/ or trees are sufficiently tall.

Around half of riparian vegetation scenarios did not typically reduce solar radiation sufficiently to produce net energy losses and therefore drive cooling of water as it travelled downstream. Previous research has demonstrated that under circumstances of net energy gain beneath a forested canopy, downstream reductions in instantaneous temperatures are generated when cool water that flows through exposed reaches overnight and during the early

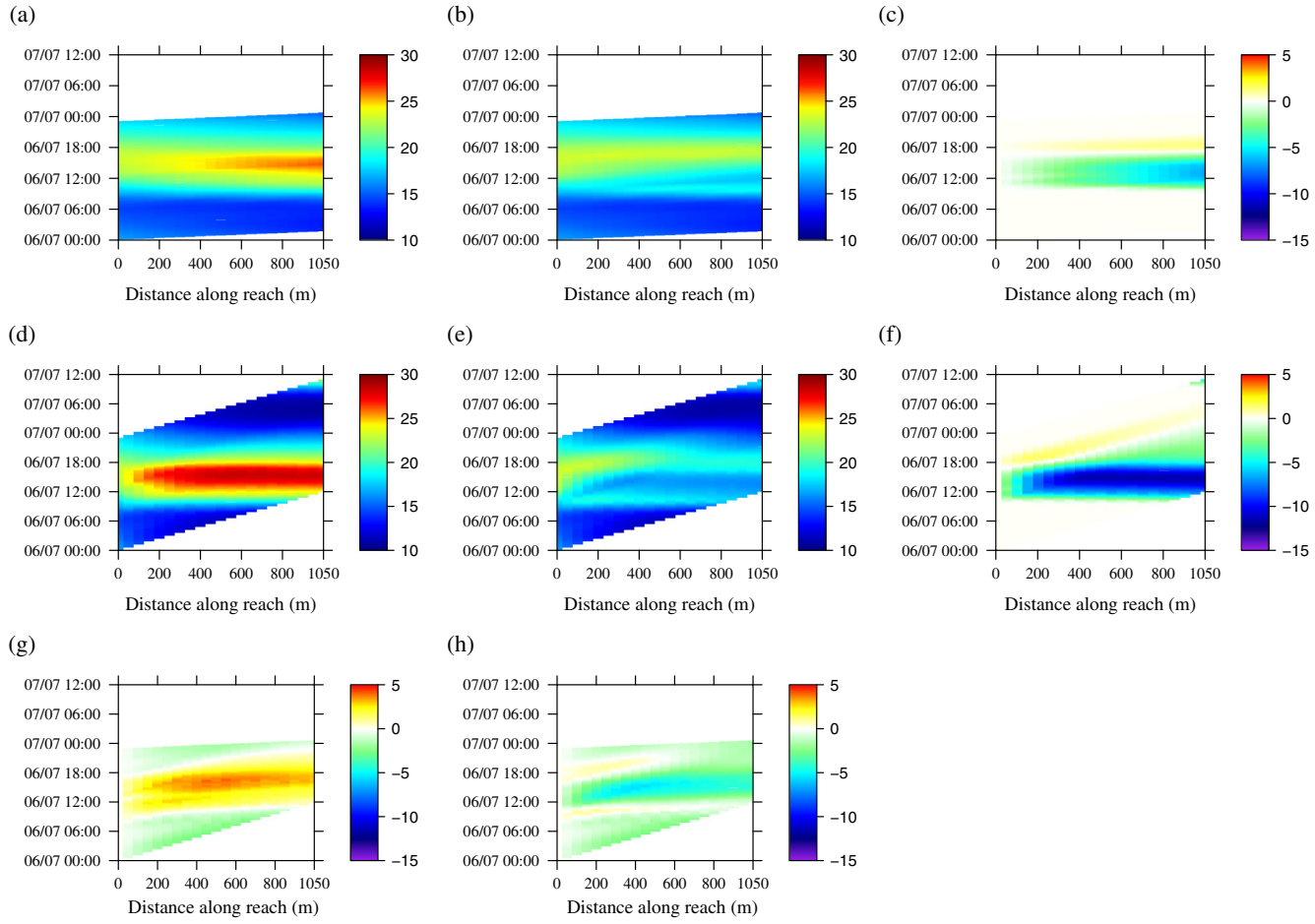

Fig. 9. Water temperatures (z-axis, °C) simulated throughout the reach under the scenario of 30% canopy density (a) southerly sky-positions exposed and high flow velocity (b) southerly sky-positions shaded and high flow velocity (c) effect of shading [b minus a] under high velocity (d) southerly sky-positions exposed and low flow velocity (e) southerly sky positions shaded and low flow velocity (f) effect of shading [e minus d] under low velocity (g) effects of velocity under high exposure [d minus a] (h) effects of velocity under low exposure [f minus c].

morning is advected through a forested reach and warms slowly due to greatly reduced net energy gains (*cf.* open reaches in which energy gains and thus rates of heating are greater) (see Garner et al., 2014). The present study supports these observations; considerably lower maximum and mean temperatures were simulated when riparian canopies reduced net energy gains to the water column. However, net energy losses were simulated under the densest canopies (i.e. 70–90%) and some channel orientations under scenarios of intermediate (i.e. 40–60%) canopy density so that maximum water temperatures within the reach did not exceed those at the upstream boundary. This suggests that under (1) very dense riparian canopies and (2) sparser canopies that provide shade when solar radiation inputs are greatest this energy flux may be blocked to such an extent that net energy losses occur and so water cools as it travels downstream. Scenarios of water cooling as it travelled downstream were not observed in an earlier study of the current riparian vegetation condition in the reach (Garner et al., 2014) and so we recommend field investigation of these processes.

Previous studies have demonstrated that summary daily water temperature metrics (especially maxima) are reduced under the densest riparian canopies (Broadmeadow et al., 2011; Groom et al., 2011; Imholt et al., 2013) and that the orientation of vegetation relative to the path of the sun is important in determining the magnitude of this reduction (Lee et al., 2012). Our study demonstrated that for intermediate canopy densities, the effect of riparian vegetation on maximum and mean temperatures is strongly dependent on channel orientation and thus the location of vegetation relative to the path of the sun. A canopy of 30% density could be as effective at reducing maximum and mean temperatures as a canopy of 60% density, provided that it shaded the water column when potential solar radiation gains were greatest (i.e. when the sun was between south-easterly and south-westerly sky positions in the Northern Hemisphere), while a canopy cover of up to 60% could have little effect in reducing maximum and mean temperatures if it did not shade the channel while the sun was in these sky-positions.

River managers are increasingly searching for ways to reduce deleterious maximum temperatures. re-introduction of riparian shading offers one of the most promising management approaches. Nevertheless, river managers must work within a broader social and economic context, where riparian planting (and associated fencing) comes with significant financial costs and has the potential to conflict with other landuses, which in the uplands of Scotland includes deer stalking and grouse shooting. Our study suggests that the channel must be shaded almost entirely to generate the greatest reductions in mean and maximum temperatures, so this is an 'expensive' and potentially unachievable way to create thermal refugia. Such dramatic reductions may be desirable at locations where water temperatures are near, or anticipated to exceed, lethal or sub-lethal thresholds for an organism of interest (Beechie et al., 2013). However extensive, dense shading can also

have environmentally deleterious effects, such as: (1) reducing light levels, consequently primary production, macroinvertebrate consumers, and thus food availability for fish (O'Grady, 1993; Kiffney et al., 2003) and (2) increased surface roughness, filtration of airborne sulphur and nitrogen compounds and thus acidified waters (Fowler et al., 1989; Malcolm et al., 2014). Consequently, the introduction of minimal shade targeted to appropriate headwater reaches may be the most cost-effective and ecologically beneficial method to generate cool-water refugia. Based on our results for Northern Hemisphere streams, optimal planting would take place on the most southerly bank of channels flowing east-west, northeast-southwest, or northwest-southeast, and *vice versa*. These planting locations could achieve considerable reductions in mean and maximum temperatures at minimal cost while minimising potential negative ecological consequences associated with dense shading. Channels that are orientated north-south, and *vice versa*, and thus do not have abundant southerly banks would require denser vegetation on their west and east banks to shade the water column from the highest solar radiation gains and thus yield reductions in water temperature. As such, they are likely to be a lower priority for targeted riparian planting schemes when reductions in stream temperature are a stated objective.

5.2. Effects of water velocity on stream heating and cooling

Mean and maximum water temperatures were increased and (to a lesser extent) minimum temperatures were decreased when water travelled at a low velocity (*cf.* high velocity) due to a longer residence time within the reach and thus greater accumulation/dissipation of heat (Subehi et al., 2009; Danehy et al., 2005; Groom et al., 2011). Consequently, our results suggest that riparian planting should be targeted in slow-flowing reaches, where retention times are longer and heat accumulation, and thus water temperatures, can be minimised most efficiently.

5.3. Limitations

Models are always simplifications of reality; therefore they must incorporate assumptions (Westhoff et al., 2011). Garner et al. (2014) discuss in full the assumptions and consequent limitations of the base model. Here we identify the assumptions made in conducting the simulation experiments and make suggestions for improvements in future model applications.

In the experiments presented herein we sought to represent spatial variability in micro-climate through linear interpolation between relatively closely spaced AWS_s. The effects of spatially variable micro-climate have been often ignored in previous studies (e.g. Rutherford et al., 1997; Watanabe et al., *2005*; DeWalle, 2008; Lee et al., 2012) but can modify turbulent fluxes and thus the energy budget significantly (e.g. Hannah et al., 2008; Garner et al., 2015). We considered this approach to be reasonable for the base scenario and the good evaluation statistics suggest that this simple method was reasonable and appropriate.

Unfortunately, with only three AWS sites, it was not possible to separate the influence of riparian landuse from wider landscape effects on micro-climate. Consequently, we were unable to scale turbulent fluxes appropriately for the different landuse scenarios where this resulted in a spatial distribution of vegetation or channel orientation characteristics that differed from the base model. Garner et al. (2014) observed no clear relationship between the canopy densities and micrometeorological measurements at the three AWS locations used in this study hypothesising that micrometeorological measurements were therefore probably determined by a complex combination of landuse, riparian canopy density and interactions with surrounding topography, altitude and aspect. Consequently, changing the orientation of the channel and thus the location of vegetation (as in the simulation experiments) could modify micrometeorology in ways that would not be represented by our models where turbulent fluxes were effectively fixed from the base model. For example, vegetation located on a bank orientated into prevailing winds could provide more shelter and thus reduce wind speeds, latent heat and net energy exchange more than vegetation located on the opposite bank. Such processes were not represented here and we recognise that failure to counter balance changes in radiative fluxes with changes in evaporative fluxes under different vegetation scenarios could lead to biased model predictions of the effects of varying landuse and channel orientation on river temperature. Future work should therefore seek to generate an evidence base for improving the spatial representation of micrometeorological conditions beneath forest canopies of varying characteristics, thereby allowing for appropriate scaling of fluxes and incorporation into modelling studies such as this one.

Finally, we investigated the effects of changing velocity on water temperature but did not investigate the potential effects of spatially or temporally varying discharge and did not consider the effects of changing velocity (for a fixed discharge) on wetted width. A full investigation of the effects of velocity, wetted width and discharge on river temperature could be conducted in future using channel geometry data in combination with hydraulic and hydrological models.

6. Conclusions

This study used field data from an upland Scottish salmon stream to underpin simulation experiments and provide systematic, mechanistic understanding of the effects of riparian shading scenarios, channel orientation and velocity on water temperature dynamics. The information gained from the novel modelling approach allows scientists and river managers to make better-informed decisions on optimal riparian tree planting strategies, through improved understanding of the inter-relationships between channel orientation and vegetation density that influence the effectiveness of riparian vegetation as a strategy for mitigating thermal extremes. The magnitude of reductions in water temperature under a given canopy density will depend on local conditions (Ryan et al., 2013) including the magnitude of net energy exchange (linked to meteorological conditions but also vegetation cover density and channel orientation), water velocity and hydrology. The experiments presented here demonstrate that where southerly banks (in the Northern Hemisphere) may be afforested then relatively sparse, overhanging vegetation is able to produce spatially and temporally extensive cool-water refugia when thermal extremes occur. Only in reaches where a southerly bank cannot be afforested is dense, overhanging vegetation required, and potentially deleterious effects should be considered in these circumstances. Additionally, planting should be targeted in slow-flowing (e.g. low gradient) reaches where flow retention times are longer and within which large heat loads can accumulate in the absence of shade.

Scientists and river managers can use models such as those presented here to quantify potential changes in river thermal conditions associated with riparian planting schemes under both present and future climates at relatively small spatial scales. However these models require large observational datasets that are rarely available, and are logistically and financially unfeasible to collect in many circumstances. Consequently, future research should also seek to upscale the information yielded in this study to identify readily defined proxies for sensitivity (e.g. channel orientation and gradient) that can be combined with rapid riparian canopy density assessments (e.g. Imholt et al., 2013) in statistical models capable of predicting water temperatures at large spatial scales (e.g. Hrachowitz et al., 2010; Jackson et al., 2017).

Acknowledgements

Grace Garner was funded by UK Natural Environment Research Council studentship NE/1528226/1. Anne Anckorn is thanked for cartographic assistance. Jason Leach and Dan Moore are thanked for generously sharing their net radiation model script. Marine Scotland Science Freshwater Laboratory staff provided field and technical assistance and maintained and downloaded weather stations. SEPA provided discharge data. We thank Xiaoming Cai for his assistance with Supplement 1. R was used for modelling and graphics. We are grateful to three anonymous reviewers for their constructive comments.

Appendix A. Supplementary data

Supplementary data associated with this article can be found, in the online version, at http://dx.doi.org/10.1016/j.jhydrol.2017.03.024.

References

Bartholow, J.M., 2000. The Stream Segment and Stream Network Temperature Models: A Self-Study Course. US Dept. of the Interior, US Geological Survey, Open-File Report 99-112.

Beechie, T., Imaki, H., Greene, J., Wade, A., Wu, H., Pess, G., Roni, P., Kimball, J., Stanford, J., Kiffney, P., Mantua, N., 2013. Restoring salmon habitat for a changing climate. River Res. Appl. 29 (8), 939–960. http://dx.doi.org/10.1002/rra.2590.

Beschta, R.L., 1997. Riparian shade and stream temperature: an alternative perspective. Rangelands 19 (2), 25–28.

Booth, D.B., Leavitt, J.L., 1999. Field evaluation of permeable pavement systems for improved stormwater management. J. Am. Plann. Assoc. 38 (3), 835–845. http://dx.doi.org/10.1080/01944369908976060.

Boyd, M., Kasper, B.V., 2003. Analytical methods for dynamic open channel heat and mass transfer: Methodology for heat source model Version 7.0, Oregon Department of Environmental Quality, Portland, OR, USA.

Broadmeadow, S.B., Jones, J.G., Langford, T.E.L., Shaw, P.J., Nisbet, T.R., 2011. The influence of riparian shade on lowland stream water temperatures in southern England and their viability for brown trout. River Res. Appl. 27 (2), 226–237. http://dx.doi.org/10.1002/rra.1354.

Brown, L.E., Cooper, L., Holden, J., Ramchunder, S.J., 2010. A comparison of stream water temperature regimes from open and afforested moorland, Yorkshire Dales, northern England. Hydrol. Process. 24 (22), 3206–3218. http://dx.doi.org/10.1002/hyp.7746.

Danehy, R.J., Colson, C.G., Parrett, K.B., Duke, S.D., 2005. Patterns and sources of thermal heterogeneity in small mountain streams within a forested setting. For. Ecol. Manage. 208 (1–3), 287–302. http://dx.doi.org/10.1016/j.foreco.2004.12.006.

DeWalle, D.R., 2008. Guidelines for riparian vegetative shade restoration based upon a theoretical shaded-stream model. J. Am. Water Resour. Assoc. 44 (6), 1373–1387. http://dx.doi.org/10.1111/j.1752-1688.2008.00230.x.

Evans, E.C., McGregor, G.R., Petts, G.E., 1998. River energy budgets with special reference to river bed processes. Hydrol. Process. 12 (4), 575–595. http://dx.doi.org/10.1002/(SICI)1099-1085(19980330)12:4<575::AID-HYP595>3.0.CO;2-Y.

Fowler, D., Cape, J.N., 1989. Deposition of atmospheric pollutants on forests. Philos. Trans. R. Soc. London Series B 324 (1223), 247–265. http://dx.doi.org/10.1098/rstb.1989.0047. M.H., and Unsworth,.

Frazer, G.W., Canham, C.D., Lertzman, K.P., 1999. Gap Light Analyzer (GLA), Version 2: Imaging Software to Extract Canopy Structure and Light Transmission Indices from True-Colour Fisheye Photographs, User's Manual and Program Documentation, Simon Frazer University and Institute of Ecosystem Studies, Millbrook, NY.

Garner, G., Malcolm, I.A., Sadler, J.P., Hannah, D.M., 2014. What causes cooling water temperature graidents in a forested stream reach? Hydrol. Earth Syst. Sci. 18 (12), 5361–5376. http://dx.doi.org/10.5194/hess-18-5361-2014.

Garner, G., Malcolm, I.A., Sadler, J.P., Millar, C.P., Hannah, D.M., 2015. Inter-annual variability in the effects of riparian woodland on micro-climate, energy exchanges and water temperature of an upland Scottish stream. Hydrol. Process. 29 (6), 1080–1095. http://dx.doi.org/10.1002/hp.10.223.

Gomi, T., Moore, R.D., Dhakal, A.S., 2006. Headwater stream temperature response to clear-cut harvesting with different riparian treatments coastal British Columbia Canada. Water Resour. Res. 42 (8), W08437. http://dx.doi.org/10.1029/2005WR004162.

Groom, J.D., Dent, L., Madesn, L.J., Fleuret, J., 2011. Response of western Oregon (USA) stream temperature to contemporary forest management. For. Ecol. Manage. 262 (8), 1618–1629. http://dx.doi.org/10.1016/j.foreco.2011.07.012.

Hannah, D.M., Garner, G., 2015. River water temperature in the United Kingdom: changes over the 20th century and possible changes over the 21st century. Prog. Phys. Geogr. 39 (1), 68–92. http://dx.doi.org/10.1177/0309133314550669.

Hannah, D.M., Malcolm, I.A., Soulsby, C., Youngson, A.F., 2004. Heat exchanges and temperatures within a salmon spawning stream in the Cairngorms, Scotland: seasonal and sub-seasonal dynamics. River Res. Appl. 20 (6), 635–652. http://dx.doi.org/10.1002/rra.771.

Hannah, D.M., Malcolm, I.A., Soulsby, C., Youngson, A.F., 2008. A comparison of forest and moorland stream microclimate, heat exchanges and thermal dynamics. Hydrol. Process. 22 (7), 919–940. http://dx.doi.org/10.1002/hyp.7003.

Hannah, D.M., Malcolm, I.A., Bradley, C., 2009. Seasonal hyporheic temperature dynamics over riffle bedforms. Hydrol. Process. 23 (15), 2178–2194. http://dx.doi.org/10.1002/hyp.7256.

Hrachowitz, M., Soulsby, C., Imholt, C., Malcolm, I.A., Tetzlaff, D., 2010. Thermal regimes in a large upland salmon river: a simple model to identify the influence of landscape controls and climate change on maximum temperatures. Hydrol. Process. 24 (23), 3374–3391. http://dx.doi.org/10.1002/hyp.7756.

Imholt, C., Gibbins, C.N., Malcolm, I.A., Langan, S., Soulsby, C., 2010. Influence of riparian tree cover on stream temperatures and the growth of the mayfly Baetis rhodani in an upland stream. Aquat. Ecol. 44 (4), 669–678. http://dx.doi.org/10.1007/s10452-009-9305-0.

Imholt, C., Soulsby, C., Malcolm, I.A., Gibbins, C.N., 2011. Influence of contrasting riparian forest cover on stream temperature dynamics in salmonid spawning and nursery streams. Ecohydrology 6 (3), 380–392. http://dx.doi.org/10.1002/eco.1291.

Imholt, C., Soulsby, C., Malcolm, I.A., Hrachowitz, M., Gibbins, C.N., Langan, S., Tetzlaff, D., 2013. Influence of scale on thermal characteristics in a large montane river basin. Ecohydrology 29 (4), 403–419. http://dx.doi.org/10.1002/rra.1608.

Iqbal, M., 1983. An Introduction to Solar Radiation. Academic Press, Toronto.

Jackson, F.L., Hannah, D.M., Fryer, R.J., Millar, C.P., Malcolm, I.A., 2017. Development of spatial regression models for predicting summer river temperatures from landscape characteristics: Implications for land and fisheries management. Hydrol. Process. 31, 1225–1238. http://dx.doi.org/10.1002/hyp.11087.

Johnson, S.L., Jones, J.A., 2000. Stream temperature responses to forest harvest and debris flows in Western Cascades, Oregon. Can. J. Fish. Aquat. Sci. 57 (2), 30–39. http://dx.doi.org/10.1139/f00-109.

Kiffney, P.M., Richardson, J.S., Bull, J.P., 2003. Responses of periphyton and insects to experimental manipulation of riparian buffer width along forest streams. J. Appl. Ecol. 40 (6), 1060–1076. http://dx.doi.org/10.1111/j.1365-2664.2003.00855.x.

Kurylyk, B.L., MacQuarrie, K.T.B., Linnansaari, T., Cunjak, R.A., Curry, R.A., 2014. Preserving, augmenting, and creating thermal refugia in rivers concepts derived from research on the Miramichi River, New Brunswick (Canada). Ecohydrology. http://dx.doi.org/10.1002/eco.1566.

Leach, J.A., Moore, R.D., 2010. Above stream microclimate and stream surface exchanges in a wildfire-disturbed riparian zone. Hydrol. Process. 24 (17), 2369–2381. http://dx.doi.org/10.1002/hyp.7639.

Leach, J.A., Moore, R.D., 2011. Stream temperature dynamics in two hydrogeomorphically distinct reaches. Hydrol. Process. 25 (5), 679–690. http://dx.doi.org/10.1002/hyp.7854.

Leach, J.A., Moore, R.D., 2014. Winter stream temperature in the rain-on-snow zone of the Pacific Northwest: influences of hillslope runoff and transient snow cover. Hydrol. Earth Syst. Sci. 18 (2), 819–838. http://dx.doi.org/10.5194/hess-18-819-2014.

Leach, J.A., Moore, R.D., Hinch, S.G., Gomi, T., 2012. Estimation of forest harvesting-induced stream temperature changes and bioenergetics consequences for cutthroat trout in a coastal stream in British Columbia, Canada. Aquat. Sci. 74 (3), 427–441. http://dx.doi.org/10.1007/s00027-011-0238-z.

LeBlanc, R.T., Brown, R.D., FitzGibbon, J.E., 1997. Modelling the effects of land use change on water temperature in unregulated urban streams. J. Environ. Manage. 49 (4), 445–469. http://dx.doi.org/10.1006/jema.1996.0106.

Lee, T.Y., Huang, J.C., Kao, S.J., Liao, L.Y., Tzeng, C.S., Yang, C.H., Kalita, P.K., Tung, C.P., 2012. Modeling the effects of riparian planting strategies on stream temperature: Increasing suitable habitat for endangered Formosan Landlocked Salmon in Shei-Pa National Park, Taiwan. Hydrol. Process. 26 (24), 3635–3644. http://dx.doi.org/10.1002/hyp.8440.

Li, G., Jackson, C.R., Kraseki, K.A., 2012. Modeled riparian stream shading: agreement with field measurements and sensitivity to riparian conditions. J. Hydrol. 428–429, 142–151.

MacDonald, R.J., Boon, S., Byrne, J.M., Sillins, U., 2014a. A comparison of surface and subsurface controls on summer temperature in a headwater stream. Hydrol. Process. 28 (4), 2338–2347. http://dx.doi.org/10.1002/hyp.9756.

MacDonald, R.J., Boon, S., Byrne, J.M., Silins, U., 2014b. A process based stream temperature modelling approach for mountain regions. J. Hydrol. 511, 920–931. http://dx.doi.org/10.1016/j.jhdrol.2014.02.009.

Malcolm, I.A., Souslby, C., Youngson, A.F., Hannah, D.M., 2005. Catchment scale controls on groundwater-surface water interactions: implications for the performance of juvenile salmonids. River Res. Appl. 21, 9. http://dx.doi.org/10.1002/rra.861.

Malcolm, I.A., Gibbins, C.N., Fryer, R.J., Keay, J., Tetzlaff, D., Soulsby, C., 2014. The influence of forestry on acidification and recovery: insights from long-term hydrochemical and invertebrate data. Ecol. Ind. 37, B, 317–329. http://dx.doi.org/10.1016/j.ecolind.2011.12.011.

Moore, R.D., Sutherland, P., Gomi, T., Dakal, A., 2005. Thermal regime of a headwater stream within a clear-cut, coastal British Columbia. Hydrol. Process. 19 (13), 2591–2608. 1 0.1002/hyp.5733.

Moore, R.D., Leach, J.A., Knudson, J.M., 2014. Geometric calculation of view factors for stream surface radiation modelling in the presence of riparian forest. Hydrol. Process. 28 (6), 2975–2986. http://dx.doi.org/10.1002/hyp.9848.

Moriasi, D.N., Arnold, J.G., Liew, M.W.N., Harmel, R.D., Veith, T.L., 2007. Model evaluation guidelines for systematic quantification of accuracy in watershed simulations. Am. Soc. Agric. Biol. Eng. 50 (3), 885–900. http://dx.doi.org/10.13031/2013.23153.

O'Grady, M.F., 1993. Initial observations on the effects of varying levels of deciduous bankside vegetation on salmonid stocks in Irish waters. Aquat. Fish. Manage. 24 (4), 563–573. http://dx.doi.org/10.1111/j.1365-2109.1993.tb00631.x.

Opperman, J.J., Luster, R., McKenney, B.A., Roberts, M., Meadows, A.W., 2010. Ecologically functional floodplains: connectivity, flow regime, and scale. J. Am. Water Resour. Assoc. 46 (2), 211–226. http://dx.doi.org/10.1111/j.1752-1688.2010.00426.x.

Poole, G.C., Berman, C.H., 2001. An ecological perspective on in-stream temperature: natural heat dynamics and mechanisms of human-caused degradation. Environ. Manage. 27 (6), 787–802. http://dx.doi.org/10.1007/s002670010188.

Poole, G.C., O'Daniel, S.J., Jones, K.L., Woessner, W.W., Bernhardt, E.S., Helton, A.M., Stanford, J.A., Boer, B.R., Beechie, T., 2008. Hydrologic spiralling: the role of multiple interactive flow paths in stream ecosystems. River Res. Appl. 24 (7), 1018–1031. http://dx.doi.org/10.1002/rra.1099.

Prata, A.J., 1996. A new long-wave formula for estimating downward clear-sky radiation at the surface. Q. J. R. Meteorol. Soc. 122 (553), 1127–1151. http://dx.doi.org/10.1002/qj.49712253306.

R Core Team, R: A Language and Environment for Statistical Computing, R Foundation for Statistical Computing, Vienna, Austria, http://www.R-project.org, last access: 25 September 2013.

Roth, T.R., Westhoff, M.C., Huwald, H., Huff, J.A., Rubin, J.F., Barrenetxea, G., Vettereli, M., Parriaux, A., Selker, J.S., Parlange, M.B., 2010. Stream temperature response to three riparian vegetation scenarios by use of a distributed temperature validated model. Environ. Sci. Technol. 44 (6), 2072–2078. http://dx.doi.org/10.1021/es902654f.

Rutherford, J.C., Blackett, S., Blackett, C., Saito, L., Davies-Colley, R.J., 1997. Predicting the effects of shade on water temperature in small streams. NZ J. Mar. Freshwat. Res. 31 (5), 707–721. http://dx.doi.org/10.1080/00288330.1997.9516801.

Rutherford, J.C., Marsh, N.A., Davies, P.M., Bunn, S.E., 2004. Effects of patchy shade on stream water temperature: how quickly do small streams heat and cool? Mar. Freshw. Res. 55 (737–748), 2004. http://dx.doi.org/10.1071/MF04120.

Ryan, D.K., Yearsley, J.M., Kelly-Quinn, M., 2013. Quantifying the effect of semi-natural riparian cover on stream temperatures: implications for salmonid habitat management. Fish. Manage. Ecol. 20 (6), 494–507. http://dx.doi.org/10.1111/fme.12038.

Soetaert, K., Petzoldt, T., Woodrow Setzer, R., 2010. Solving differential equations in R: package deSolve. J. Stat. Softw. 33 (9), 1–25.

Story, A., Moore, R.D., Macdonald, J.S., 2003. Stream temperatures in two shaded reaches below cutblocks and logging roads: downstream cooling linked to subsurface hydrology. Can. J. For. Res. 33 (8), 1383–1396. http://dx.doi.org/10.1139/x03-087.

Stull, R.B., 2000. Meteorology for Scientists and Engineers. Brooks/Cole, Pacific Grove.

Subehi, L., Fukushima, T., Onda, Y., Mizugaki, S., Gomi, T., Terajima, T., Kosugi, K., Hiramatsu, S., Kitahara, H., Kuraji, K., Ozaki, N., 2009. Influences of forested watershed conditions on fluctuations in stream water temperature with special reference to watershed area and forest type. Limnology 10 (1), 33–45. http://dx.doi.org/10.1007/s10201-008-0258-0.

Tetzlaff, D., Soulsby, C., Gibbins, C., Bacon, P.J., Youngson, A.F., 2005. An approach to assessing hydrological influences on feeding opportunities of juvenile Atlantic salmon (Salmo salar): a case study of two contrasting years in a small, nursery stream. Hydrobiologia 549 (1), 65–77. http://dx.doi.org/10.1007/s10750-005-4166-6.

Tetzlaff, D., Soulsby, C., Waldron, S., Malcolm, I.A., Bacon, P.J., Dunn, S.M., Lilly, A., Youngson, A.F., 2007. Conceptualisation of runoff processes using a geographical information system and tracers in a nested mesoscale catchment. Hydrol. Process. 21 (10), 1289–1307. http://dx.doi.org/10.1002/hyp.6309.

Upper Dee riparian scheme, The River Dee Trust: http://www.theriverdeetrust.org.uk/information/ourwork.asp (last access: 14 January 2016), 2011.

Van vliet, M.T.H., Ludwig, F., Kabat, P., 2013. Global streamflow and thermal habitats of freshwater fishes under climate change. Clim. Change 121 (4), 739–754. http://dx.doi.org/10.1007/s10584-013-0976-0.

Watanabe, M., Adams, R.M., Wu, J., Bolte, J.P., Cox, M.M., Johnson, S.L., Liss, W.J., Boggess, W.G., Ebersole, J.L., 2005. Toward efficient riparian restoration: integrating economic, physical and biological models. Environ. Manage. 75 (2), 92–104. http://dx.doi.org/10.1016/j.jenvman.2004.11.005.

Webb, B.W., Zhang, Y., 1997. Spatial and seasonal variability in the components of the river heat budget. Hydrol. Process. 111, 79–101. http://dx.doi.org/10.1002/(SICI)1099-1085(199701)11:1<79::AID-HYP404>3.3.CO;2-E.

Westhoff, M.C., Savenije, H.H.G., Luxemburg, W.M.J., Stelling, G.S., van de Giesen, N.C., Selker, J.S., Pfister, L., Uhlenbrook, S., 2007. A distributed stream temperature model using high resolution temperature observations. Hydrol. Earth Syst. Sci. 11, 1469–1480. http://dx.doi.org/10.5194/hess-11-1469-2007.

Westhoff, M.C., Bogaard, T.A., Savenije, H.H.G., 2010. Quantifying the effect of in-stream rock clasts on the retardation of heat along a stream. Adv Water Resour 33 (11), 1417–1425. http://dx.doi.org/10.1016/j.advwatres.2010.02.006.

Westhoff, M.C., Gooseff, M.N., Bogaard, T.A., Savenije, H.H.G., 2011. Quantifying hyporheic exchange at high spatial resolution using natural temperature variations along a first-order stream. Water Resour. Res. 47 (10), W10508. http://dx.doi.org/10.1029/2010WR009767.

Wilby, R.L., Orr, H.G., Watts, G., Battarbee, R.W., Berry, P.M., Chadd, R., Dugdale, S.J., Dunbar, M.J., Elliott, J.A., Extence, C., Hannah, D.M., Holmes, N., Johnson, A.C., Knights, B., Milner, N.J., Ormerod, S.J., Solomon, D., Timlett, R., Whitehead, P.J., Wood, P.J., 2010. Evidence needed to manage freshwater ecosystems in a changing climate: turning adaptation principles into practice. Sci. Total Environ. 408 (19), 4150–4164. http://dx.doi.org/10.1016/j.scitotenv.2010.05.014.

forests

MDPI

Article

Forest Restoration Thinning Has Minimal Impacts on Surface Soil Carbon in a Second-Growth Temperate Rainforest

Steven A. Quick [1], Dylan G. Fischer [1,*] and Michael J. Case [2]

[1] Evergreen Ecosystem Ecology Laboratory, The Evergreen State College, Olympia, WA 98505, USA; steven.quick@wsu.edu
[2] The Nature Conservancy, Seattle, WA 22203-1606, USA; michael.case@tnc.org
* Correspondence: fischerd@evergreen.edu

Abstract: Forest restoration thinning may accelerate the development of structural complexity toward old-growth conditions faster than a natural forest, yet associated changes in forest carbon (C) are poorly understood. Old-growth forests are characterized by high levels of sequestered C in aboveground biomass and soil C pools, yet active management has well-recognized negative impacts on stored C. Effects of forest restoration thinning on forest C can be determined using longitudinal measurements and modeling based on stand conditions and tree growth. At Ellsworth Creek Preserve in Southwest Washington, forest restoration efforts in a second-growth temperate rainforest have been monitored using permanent plots since 2007. Here, we compare repeat measurements from 2020, modeled forest C, and measurements of O-horizon C pools from 2022 to determine C impacts of silvicultural treatments for old-growth restoration. We found good general agreement between empirical measurements and models of forest C using the Forest Vegetation Simulator (FVS). However, treatment alone was not a strong indicator for C conditions; rather, forest age and age–treatment interactions better predicted soil C responses to restoration treatments. These data may indicate that "light" forest restoration thinning can accelerate old-growth development with minimal effects on soil carbon—a win-win conservation strategy for old-growth forests and the climate.

Keywords: carbon; forest; FVS; modeling; old-growth; restoration; soil; thinning

Citation: Quick, S.A.; Fischer, D.G.; Case, M.J. Forest Restoration Thinning Has Minimal Impacts on Surface Soil Carbon in a Second-Growth Temperate Rainforest. *Forests* **2024**, *15*, 1758. https://doi.org/10.3390/f15101758

Academic Editor: Anne-Marie Farnet Da Silva

Received: 3 September 2024
Revised: 25 September 2024
Accepted: 4 October 2024
Published: 6 October 2024

1. Introduction

The need to understand forest soils and their importance for ecosystem functions like carbon (C) sequestration is becoming more important with the growing threat of climate change [1]. A review of negative emissions technologies suggested that afforestation and reforestation is the most cost-effective approach to mitigating the effects of global warming, although forest preservation may have the most significant potential impact [2]. In many temperate rainforest systems, less than 18% of the world's original primary old-growth forests remain [3]. Land-use changes and short-rotation forestry over the last century have resulted in a deficit of these late-successional forests, and wildfire and insect disturbances associated with climate change may reduce intact primary forests even more [4]. There is an increasing need to understand the long-term impacts of old-growth preservation and restoration on timber production and biodiversity [5,6] as well as for carbon storage [7–9], especially regarding soil C [1].

Ecological restoration activities offer significant promise in restoring many structural attributes of temperate old-growth forest ecosystems through selective harvests, small patch cuts, thinning from below, and targeted species removal and release thinning [10,11]. Nevertheless, it is less clear how such restoration treatments will intersect with forest carbon (C) storage and uptake, especially given the well-known effects of harvests on long-term carbon balance [12]. Further, long-term research has demonstrated predictable trends in soil organic matter following harvests where organic matter declines immediately

and then slowly recovers over time [13]. For example, in a 70-year-old white spruce forest in Fairbanks, Alaska [14], thinning had a negative relationship on soil C, influenced by microclimatic changes to decomposition rates. Soil respiration has been found to be higher than net primary productivity from regrowth in younger stands [15] due to high heterotrophic respiration. It is unclear how such trends might apply to the relatively light ecological forestry prescriptions typical of management designed to increase old-growth attributes in wet coastal forests of the highly productive Northwestern coast [16–19]. Showcase restoration projects, such as the silvicultural treatments in The Ellsworth Creek Preserve in Washington State, USA (hereafter referred to as Ellsworth), provide a unique opportunity to examine changes in soil C associated with ecological forestry in a temperate rainforest ecosystem [20,21]. Previous work in pacific coast temperate rainforests has addressed how aboveground structural attributes have responded to restoration treatments [9,21] and understory plant responses to restoration treatments [21,22], but responses of whole-ecosystem carbon storage and soil organic matter (OM) C have not been evaluated or modeled in detail. Quantifying the accuracy of modeled relationships for forest C over time, coincident with the comparison of C between managed and control stands, would help us understand how management decisions are impacting C pools and the predictability of their outcomes. Past studies have demonstrated the greatest proportion of C losses in the O-horizon soil layer (>30%) [23]. Although deeper layers are significant [24]), we chose to focus on aboveground carbon storage and potentially dynamic changes in the OM layer.

In this study, we (1) used measures of stand structure from 2007 and 2020 to model forest stand C and soil OM C at the Ellsworth site using the United States Forest Service's (USFS) Forest Vegetation Simulator (http://www.fs.fed.us/fvs/; FVS, accessed on 1 June 2022); (2) directly measured accumulated OM pools and OM C pools in treated and control stands more than a decade after restoration treatments; (3) compared modeled and empirical values for stand C, soil OM, and soil OM pools; and (4) evaluated differences in O-horizon soil C sequestration between treated and control (no treatment) plots. We hypothesized that treated plots would show a decrease in stand C and O-horizon soil C pools compared to control plots, driven by the removal of biomass and reductions in O-horizon C due to reduced litter inputs and increased heterotrophic respiration and decomposition [25].

2. Materials and Methods

2.1. Study Area and Experimental Design

The Ellsworth Creek Preserve (Ellsworth) covers approximately 2300 ha of forested and freshwater stream systems in the Willapa Hills region of Southwestern Washington, USA (Figure 1). The property was acquired by The Nature Conservancy (TNC) in the early 2000s and has an elevation range from 0 to 365 m and a mild, maritime climate characterized by cool, wet winters and relatively warm, dry summers (Western Regional Climate Data center, https://wrcc.dri.edu/, accessed on 21 September 2023). Ellsworth forests are typical of second-growth forests dominated by a mix of western hemlock (*Tsuga heterophylla*), Sitka spruce (*Picea sitchensis*), western redcedar (*Thuja plicata*), and red alder (*Alnus rubra*) [26]). Ellsworth was previously managed for timber production, and ages typically range from 20 to 80 years old. Structurally, most stands are in the competitive exclusion stage of stand development—a common result of systematic re-planting after clear-cut harvesting [5,27].

A science advisory committee composed of academic and management agency representatives assisted TNC in implementing a watershed-scale experiment designed to evaluate the effectiveness of forest restoration efforts at Ellsworth in the early 2000s. Restoration treatments were replicated across the study area. Control sites are represented by areas of forest where no management interventions were implemented. Treated sites, however, are areas where restoration treatments were implemented to stimulate forest growth, lower tree density, increase species diversity and abundance, and accelerate the development of forest structural complexity. Our analysis focused on forest structure and vegetation

plots within two treated sub-basins (C1 and N2) and two control sub-basins (C2 and N1). Each sub-basin contained 28 0.1 ha plots, for a total of 112 permanent plots, measured in 2007 (pre-treatment). Remeasurements took place in 2020 (post-treatment) and 60 plots were revisited for sampling. The plots consisted of 31 plots in control sub-basins and 29 in treated sub-basins. Among these, 16 young plots (15–30 years old) and 15 mature plots (60–71 years old) were in the control sub-basins, and 13 young and 16 mature plots were in the treatment sub-basins. Each permanent plot contained four subplots located 10 m from the plot center in each cardinal direction where soil carbon was measured. See Case et al. [21] for more information.

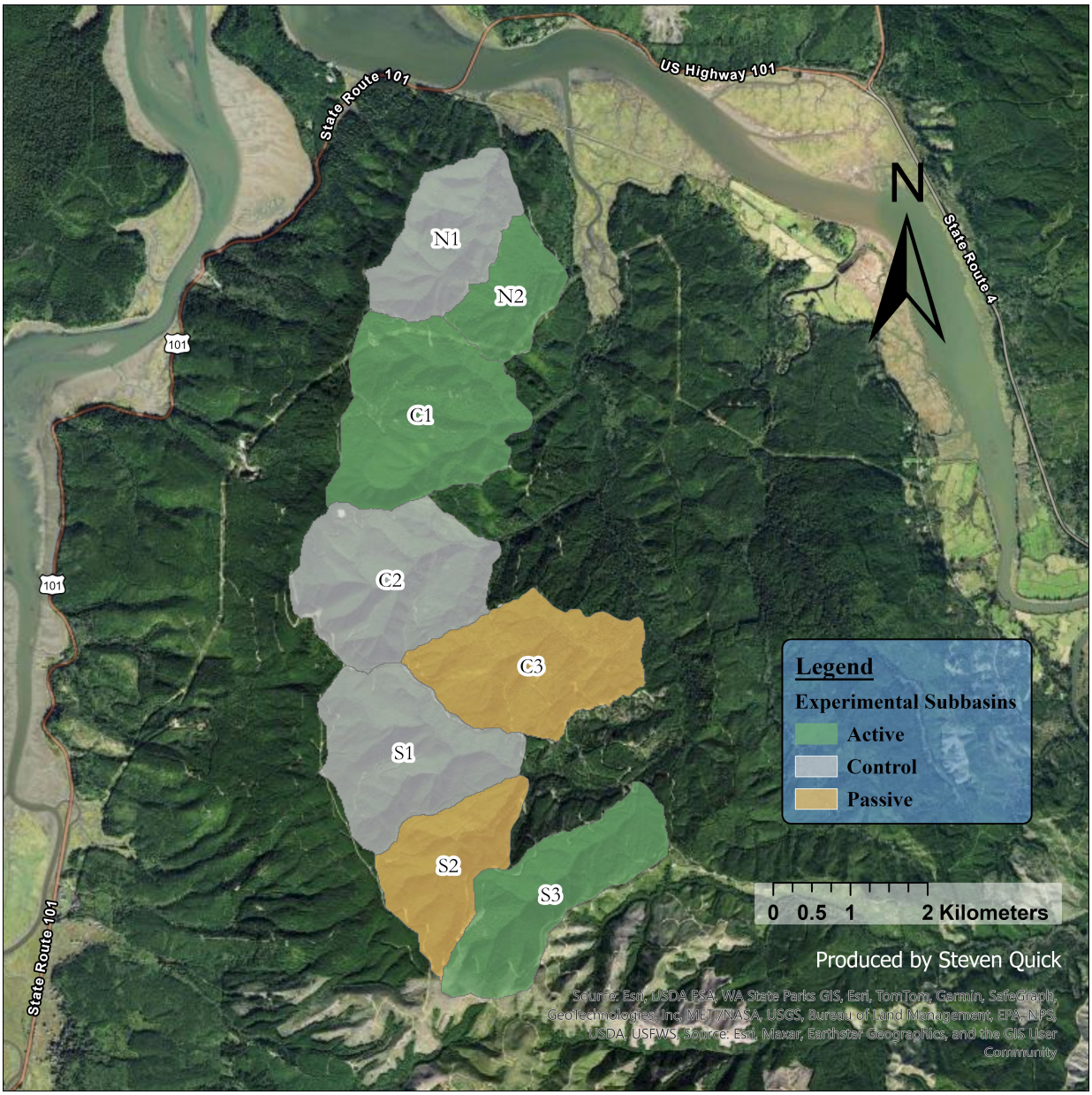

Figure 1. Map of Ellsworth Creek Preserve in Southwest Washington with sub-basins highlighted (polygons). Sub-basins that received treatment are colored in green (N2, C1, S3). Those that had roads removed but no thinning are colored in gray (N1, C2, S1), while a third group of sub-basins colored in yellow (C3, S2) still have roads intact but received no treatment. Passive sub-basins are part of the larger study design but not represented in this project.

2.2. Treatment Applications

Restoration treatments were applied in treated sub-basins in 2009 and 2013. Treatment blocks varied in size from 75 to 221 hectares. Mature stands received commercial thinning, and young stands received pre-commercial thinning. Species removal preference was applied in the following order: western hemlock, Douglas fir, Sitka spruce, western redcedar, and red alder; but unhealthy trees of any species were removed first. Treatments also avoided cutting hardwoods, tree saplings, and seedlings and minimized understory disturbance. See Case et al. [21] for detailed silvicultural prescription details.

2.3. Forest Structure Measurements

Within all plots, measurements in both 2007 and 2020 included overstory, understory, vertical and horizontal structures, forest health, regeneration density, and soil organic layer depth. Protocols were adapted from Cissel et al. [28], and measurements included tree diameter, tree height, and tree basal area (BA). Plots were randomly located within treatment blocks and sometimes were located in treatment areas. That is to say, some of the vegetation plots were thinned according to the treatment protocol. In 2020, repeat measures allowed an assessment of growth and changes in forest structure. All measured plots were located at least 30 m from the border of the associated treatment area. Geo- and topographic data were also collected for each plot, including slope, aspect, elevation, and topographic position. Elevation was derived from digital elevation models. See Case et al. [21] and Cissel et al. [28] for detailed forest structure measurement methods.

2.4. Soil Sample Collection and Analysis

Soil sampling was not conducted during the initial 2007 surveys, but organic litter (OM layer) depth was measured during the 2020 remeasurement survey (as reported in [21]. Organic litter depth was measured five times in each subplot and included all duff and litter less than or equal to 2 cm in diameter. Measurements were made along a 2.5 m slope-corrected transect at 0.5, 1.0, 1.5, 2.0, and 2.5 m from the subplot center, and the orientation of these transects corresponded with the cardinal direction of the subplot (e.g., transects ran north in the North subplot). Using a small trowel, a small hole was dug down to the A-horizon, and the OM layer thickness was subsequently recorded.

While OM layer thickness can be indicative of surface soil C changes, differences in OM bulk density can also result in changes in soil C that would not be reflected in thickness measurements alone. Accordingly, in 2022, we collected additional soil samples to directly measure OM layer C content. Soil core samples were collected to a depth of 10 cm (below the OM layer) from within 1 m of the subplot center using rigid 5 cm PVC soil cores, stored in a labeled brown paper bag, then sealed in a plastic bag for transport. Organic litter depth was subsequently measured in the field for comparison against 2020 depth measurements described above. After samples were dried (105 °C) for at least 48 h and weighed, organic matter was separated, and the remaining material was stratified by fragment size (>2 mm, <2 mm, and <5 mm) using mesh sieves. Organic matter and each fragment size were then weighed again before 5.0 g samples of organic matter were prepared in crucibles to estimate organic matter using loss-on-ignition methods (using a muffle furnace at 5 h at 500 °C). Ash mass was then recorded and compared to initial mass to derive approximate proportions of C. The remaining volume of organic matter was reduced to a similar particle size for elemental analysis for carbon/hydrogen/nitrogen ratios. Sample C and N content was determined using 3–10 mg samples analyzed using a Perkin-Elmer Series II 2400 CHNS/O elemental analyzer (Perkin-Elmer Inc., Waltham, MA, USA).

2.5. Forest Vegetation Simulator

To model changes in stand and soil OM over time, we used the Forest Vegetation Simulator (FVS) developed by the USFS. The base FVS model predicts changes in tree diameter, height, crown ratio, and crown width, as well as mortality and C storage estimates based on standardized national scale allometric biomass estimation equations [29]. Live tree

metrics, including height, age, DBH, live crown ratio, and species, as well as stand metrics, including slope, elevation, and aspect, were formatted for use in FVS and comparisons on the sub-basin-level.

We constructed models using both 2007 and 2020 data. Initial runs constructed from 2007 data were used for comparison with remeasured data from 2020 and 2022 to FVS models (see statistical analysis below), validating the usefulness of the modeling approach produced with initial data from 2007. Once validated, models for forest C pools through 2040 were constructed using the remeasured data from 2020. Control models—"grow-only runs"—were generated by running FVS without any forest management activities to simulate our control plots. These runs were constructed with no management activities selected and were conducted in the Pacific Northwest Coast Variant. In active treatment models, management activities were represented by thinning and pruning operations with the thin-from-below component following the parameters described above for commercial thinning and pre-commercial thinning groups, respectively (Section 2.2, Treatment Applications). All models used a maximum stand density index (SDI) of 600 and a site index (SI_{50}) value of 98. In addition to stand visualization and standard tree list outputs, we enabled carbon and fuel outputs using the carbon reports and fire and fuels extension [29]. Specifically, we compared aboveground total, standing dead, down dead, floor, and total stand C pools for each stand in both treated and control groups. We also loaded summary reports from FVS to retrieve conventionally used metrics in forestry such as BA and Quadratic Mean Diameter (QMD).

2.6. Statistical Analysis

First, we compared empirical measurements of stand variables (TPH and BA) and C content (total aboveground C, stand total C, and OM layer C) in 2020 and 2022 to FVS modeled values (based on 2007 data) using a mixed-model restricted maximum likelihood (REML) approach. The REML methodology is used to analyze linear mixed models and may prevent nuisance parameters from having any effect and prevent false positive associations. Stands in the study were treated as random effects to account for repeat sampling within individual stands. Data type (model vs. empirical) and stand treatment were treated as main effects, stand age was used as a covariate, and data type by stand treatment interactions and age by model type interactions were treated as potential interaction effects. Means comparisons within significant model interaction terms were conducted using Tukey's Honestly Significant Difference tests ($\alpha = 0.05$).

For the comparison of empirical data on soil OM, simple nested Analysis of Variance (ANOVA) was used to examine the differences between treatments in the OM layer, OM bulk density, C content, and total OM C. In these analyses, samples were nested within stands, and the treatment type was used as a main effect.

Values among treatments were compared over time in long-term modeling (2020–2040) using repeated-measures ANOVA, where distinct stand structure (BA, TPH) and carbon (aboveground C, OM C, and total C) pools were treated as response variables; treatment type, year, and treatment by year interactions were treated as main effects; and individual stands nested within years were treated as random effects.

All analyses were conducted in the statistical program JMP Pro 16.2.0 with an α of 0.05 for determination of statistical significance.

3. Results

Forest Vegetation Simulator Models and Comparisons

Our data demonstrated nearly universal underestimation of TPH, BA, and C stocks ($p < 0.05$) in models developed from 2007 compared to empirical data from 2020, driven by poor modeling of tree regeneration. Variation was high for empirical measurements (CV = 26.5%–46.4%), but empirical data in 2020 were significantly different from the FVS models in TPH, BA, aboveground C, and total stand C ($p > 0.05$; Figure 2; Table 1). Values for BA, TPH, aboveground C, and total stand C were all lower in models based on 2007

data than in empirical inventories in 2020 in the active stands (Figure 2; Table 1). For BA ($p < 0.0001$, $R^2 = 0.92$), the factors treatment, run type, and stand age were all significant. The interaction between treatment and run type was not significant, but the interaction between age and run type was significant (Table 1), indicating that there was convergence among modeled and empirical stand BA in older stands but not younger stands (Figure 3). The overall model for TPH ($p = 0.006$, $R^2 = 0.74$) demonstrated significance for factors treatment and run type (Table 1) but not for other variables or interaction effects. Aboveground C results ($p < 0.001$, $R^2 = 0.95$) mirrored results for BA where treatment, run type, age, and age by run type were all significant, and convergence in modeled and empirical data occurred with age (Table 1, Figures 2 and 3). Interactions between treatment and run type were not significant (Table 1). Total stand C mirrored both BA and aboveground C results, and treatment, run type, age, and age by run type interactions were again significant ($p < 0.001$, $R^2 = 0.95$; Table 1, Figure 2). Convergence in run type results again occurred in older stands (Figure 3). Modeled data also reported that tree regeneration should have been lower, and carbon losses in the treated stands following thinning should have been higher than observed ($p < 0.05$). Accordingly, modeling results from 2007 data for control stands were much closer to empirical measurements in 2020 and 2022 than for active management stands.

Table 1. Mixed-model results comparing run type by FVS modeled (2007) data and empirical (2020–2022) results from Ellsworth Creek treatment stands across active and control treatments.

	Effect	df_{den} **	*F*	*p*
BA	Treatment	14.97	14.1182	**0.0019**
	Run.Type	14.97	50.4598	**<0.0001**
	Stand Age	15.23	36.5626	**<0.0001**
	Treatment:Run.Type	14.97	3.9925	0.0642
	Stand Age:Run.Type	15.03	4.7280	**0.0461**
TPH	Treatment	15.01	8.4556	**0.0108**
	Run.Type	16	12.1081	**0.0034**
	Stand Age	15.2	0.0711	0.7933
	Treatment:Run.Type	16	2.4303	0.112
	Stand Age:Run.Type	15.05	2.8498	0.112
Aboveground C	Treatment	14.97	11.5283	**0.004**
	Run.Type	14.97	63.2752	**<0.0001**
	Age	15.36	37.8432	**<0.0001**
	Treatment:Run.Type	15.04	4.1703	0.0592
	Stand Age:Run.Type	16	4.9621	**0.0416**
Total Stand C	Treatment	14.98	11.5921	**0.0039**
	Run.Type	14.97	58.8258	**<0.0001**
	Age	15.37	29.5479	**<0.0001**
	Treatment:Run.Type	14.97	2.5344	0.1323
	Stand Age:Run.Type	15.04	8.2344	**0.0117**
Soil OM	Treatment	2.083	5.9772	0.1294
	Run.Type	7.109	0.7224	0.4231
	Age	0.558	0.9083	0.5971
	Treatment:Run.Type	17.82	10.6954	**0.0043**
	Stand Age:Run.Type	3.681	2.1882	0.2191

Note: FVS modeled based on 2007 data versus empirical data from 2020–2022. ** Numerator is 1 for all *df* values. Only denominator is shown.

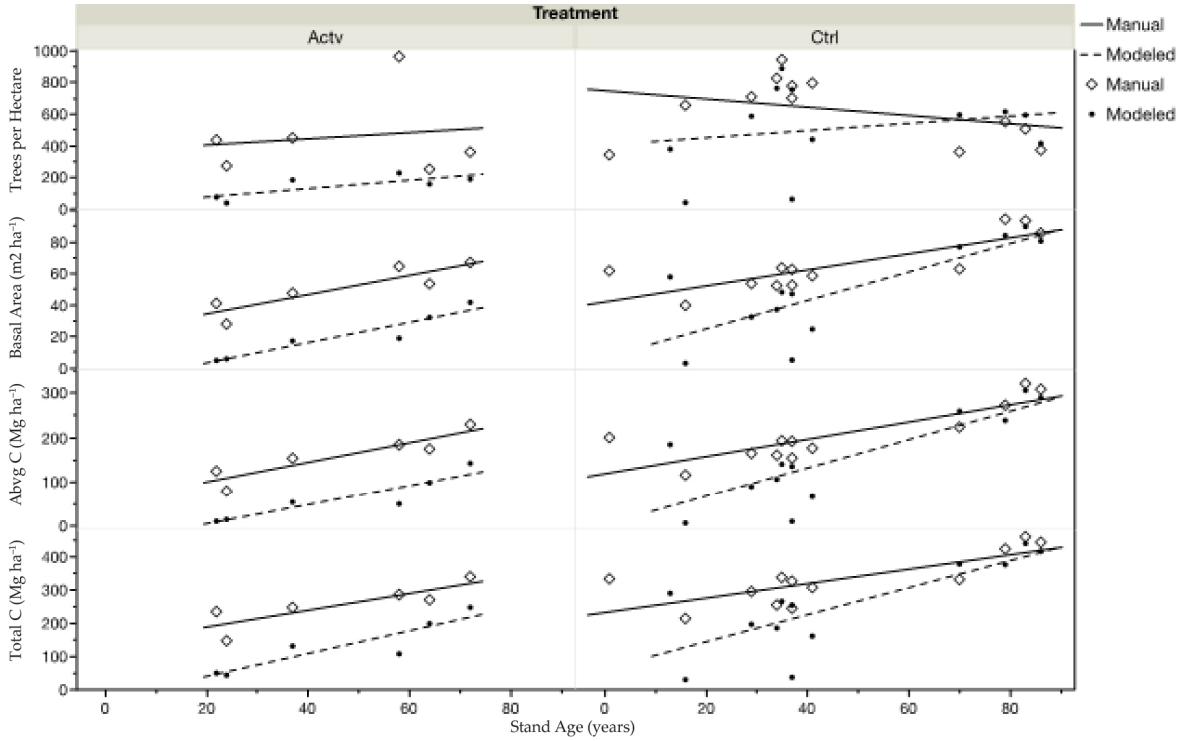

Figure 2. Comparison of empirical measurements (diamonds) and modeled values (points) based on 2007 inventory data versus stand age.

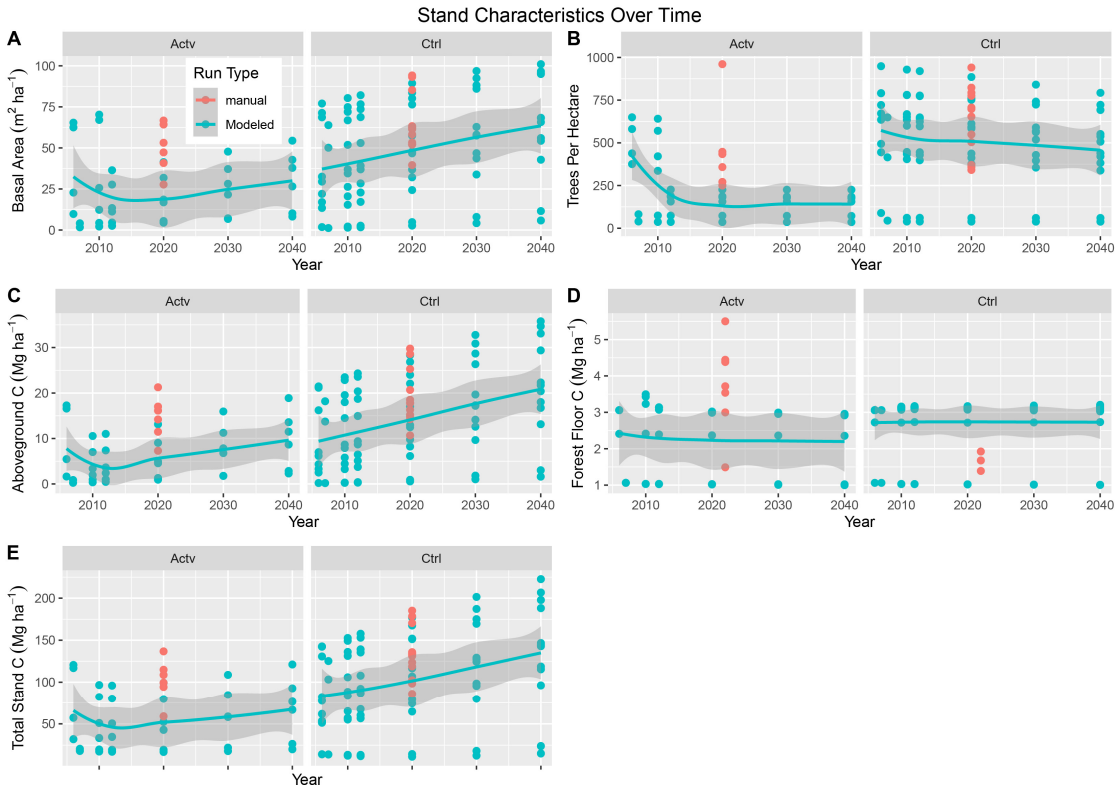

Figure 3. An overall comparison of data collected in 2020 and 2022 to FVS model estimates produced with 2007 inventory data. Panels show basal area (**A**), trees per hectare (**B**), aboveground C (**C**), forest floor OM C (**D**), and total stand C (**E**). Teal points show stand estimates by FVS, and orange points reflect manual measurements in 2020 and 2022.

For forest floor OM C values, an interaction effect between run type and treatment was significant (Table 1), but no other effects were significant. Tukey's HSD tests showed active treatment manual measurements were significantly greater than control treatment manual measurements and all modeled values in 2022 (Figures 2 and 4). Based on manual empirical soil data only, thinning treatments had a significant effect on soil OM C ($p = 0.0272$) where OM C was marginally higher in the active treatment stands (Figure 4). Active stands largely had values between 10 and 20 Mg C ha^{-1}, while control stands tended towards a median value closer to 10 Mg C ha^{-1}. Stand age was significantly related to soil OM C for stands <70 years old, as OM C declined with age in a negative exponential fashion (LOG [soil OM C] = 6.13 − 0.09 × stand age]; $R^2 = 0.91$, $p = 0.003$; Figure 5). When all stands were included, soil OM C trends with stand age were better described by a polynomial function where OM C declined until approximately age 50 and then increased again towards the 70+ year old stands (soil OM C = 16.7 − 0.31 × [stand age] + 0.07 × [stand age]^2; $R^2 = 0.88$, $p = 0.0006$; Figure 5). Stands <50 years old suggested a trend where active treatments were generally higher in soil OM C compared to controls (Figure 5B). For stands greater than 50 years old, control and active treatments showed similar values (Figure 5C). Nevertheless, across all ages, the treatments were very similar in % OM C, and median values were generally between 47% and 49% C (Figure 4A). OM bulk density was also similar across treatments (Figure 4C).

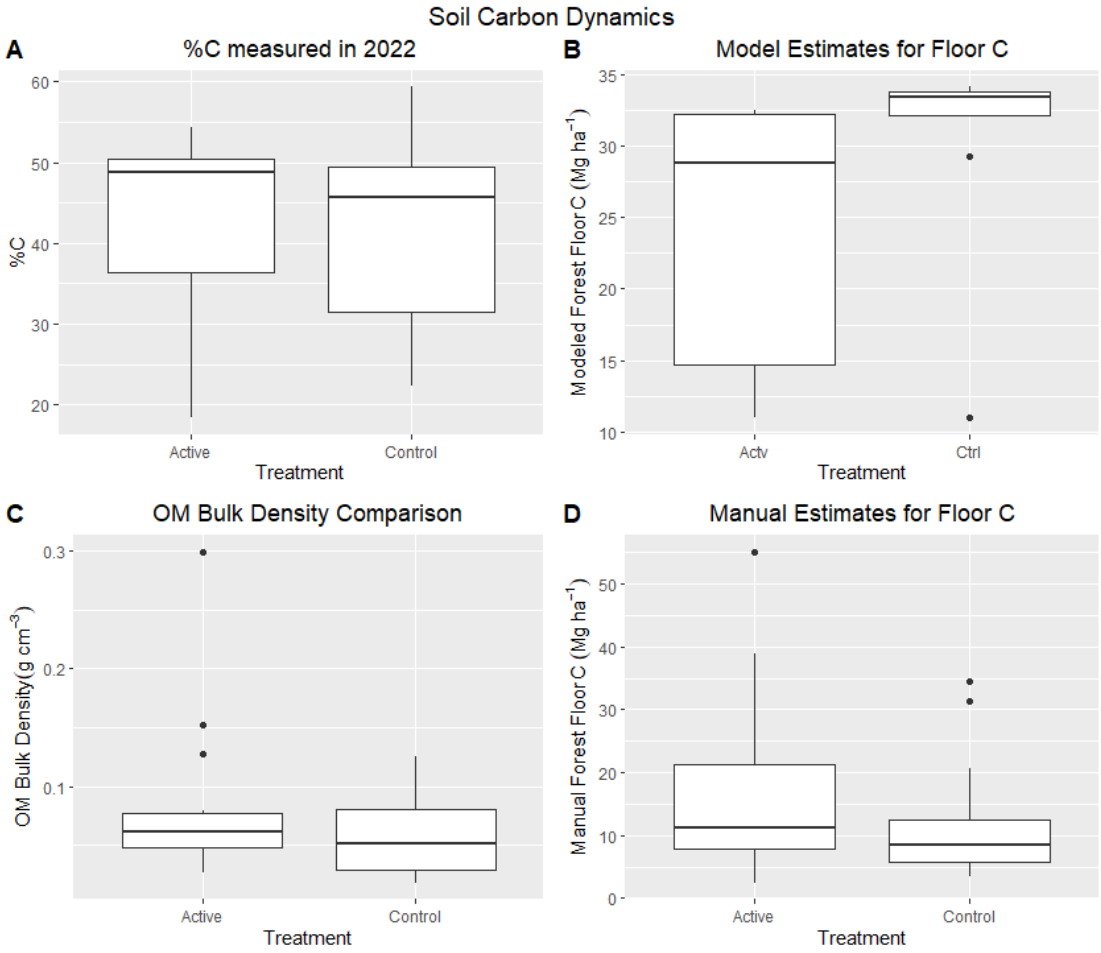

Figure 4. A comparison of forest floor C estimates from empirical versus modeled estimates. Panels show %C and bulk density (**A**,**C**, left side), and modeled and empirical forest floor OM C values (**B**,**D**, right side). Model estimates were produced using 2020 data and overestimated empirical observations (**D**).

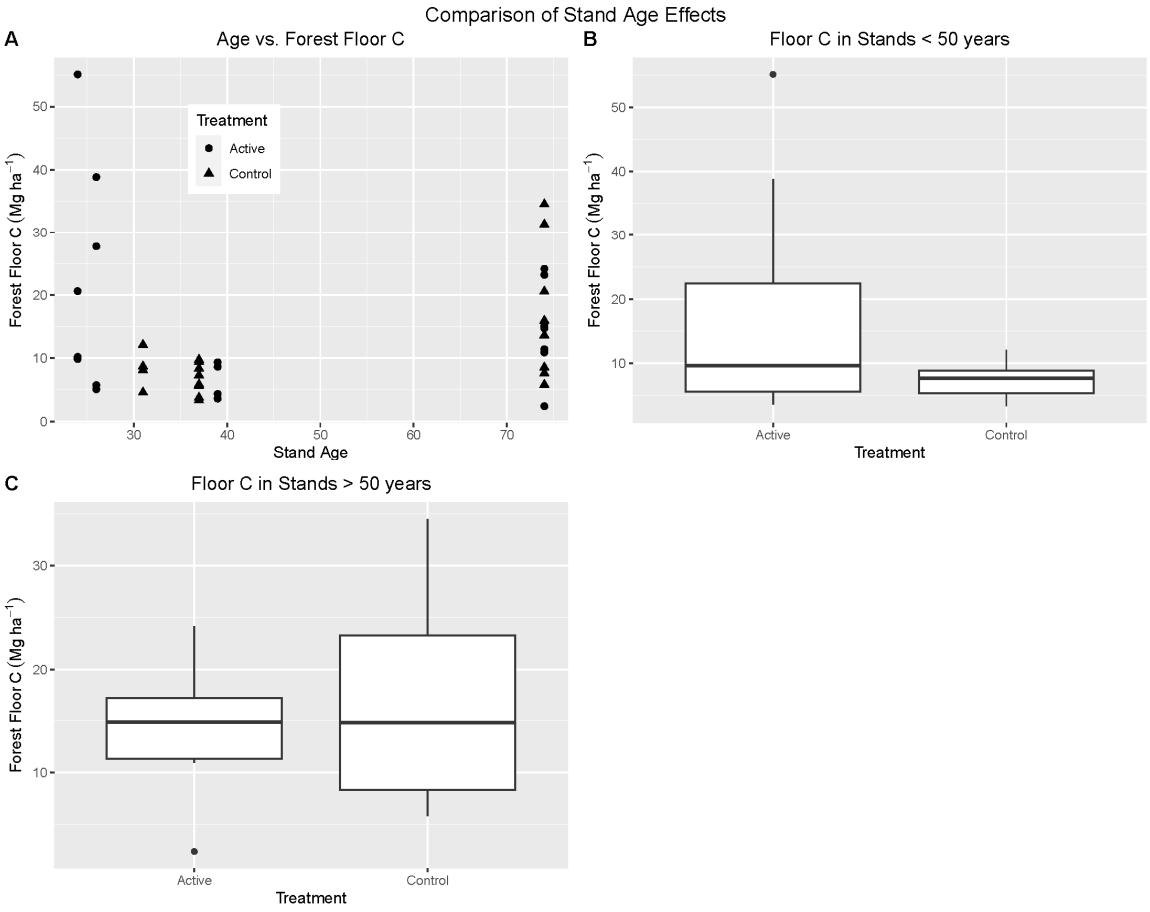

Figure 5. Comparison of soil C variables using empirical measurements from 2022, approximately 14 years after treatments began. Panel (**A**) shows a comparison of stand age effects. Comparisons between treatments are also shown for stands <50 years old (**B**) and greater than 50 years old (**C**).

The FVS Models based on 2020 data suggested that treated plots had reduced BA, TPH, aboveground C, and total C compared to controls (Table 2). Year was also a significant effect for BA, aboveground C, and total C (Table 2), as all variables except forest floor OM C increased with time (Table 2, Figure 6). There was no significant interaction between treatment and year for any response variable ($p > 0.05$). Interestingly, even when the FVS model was run through 2110 (90 years after the 2020 stand survey), results uniformly suggested a significant year and year by treatment interaction effect but no effect of treatment alone ($p > 0.05$). This result was apparently due to a convergence in values between treatments by about 2090 (Figure 7).

Long-term convergence among models suggested overlapping 95% confidence intervals and that the active plot C is likely to represent >80% that of control plots by 2040 and >90% of control plot C by 2100 (Figure 7). Since our early model comparisons suggested significant underestimation of model results, especially in active management stands, these estimates of model convergence are likely conservative, and convergence in C values among treatment types is likely to be sooner.

Table 2. Repeated-measures ANOVA results comparing FVS modeled (2020 data) over time from 2007 to 2040 Ellsworth Creek treatment stands across active and control treatments. Treatment and Year are main effects and Treatment*Year is an interaction.

	Effect	*df*	*F*	*p*
BA	Treatment	1, 50	9.0499	**0.0041**
	Year	1, 50	1.7505	**0.0019**
	Treatment*Year	1, 50	0.0331	0.8564
TPH	Treatment	1, 50	7.8758	**0.0071**
	Year	1, 50	0.5066	0.4799
	Treatment*Year	1, 50	0.0133	0.9088
Aboveground C	Treatment	1, 50	7.6966	**0.0078**
	Year	2, 50	18.7569	**<0.0001**
	Treatment*Year	2, 50	0.0063	0.9371
OM C	Treatment	1, 48	13.6534	**0.0005**
	Year	2, 48	0.0811	0.7770
	Treatment*Year	2, 48	0.0295	0.8643
Total C	Treatment	1, 48	12.4876	**0.0009**
	Year	2, 48	16.5111	**0.0002**
	Treatment*Year	2, 48	0.0123	0.9120

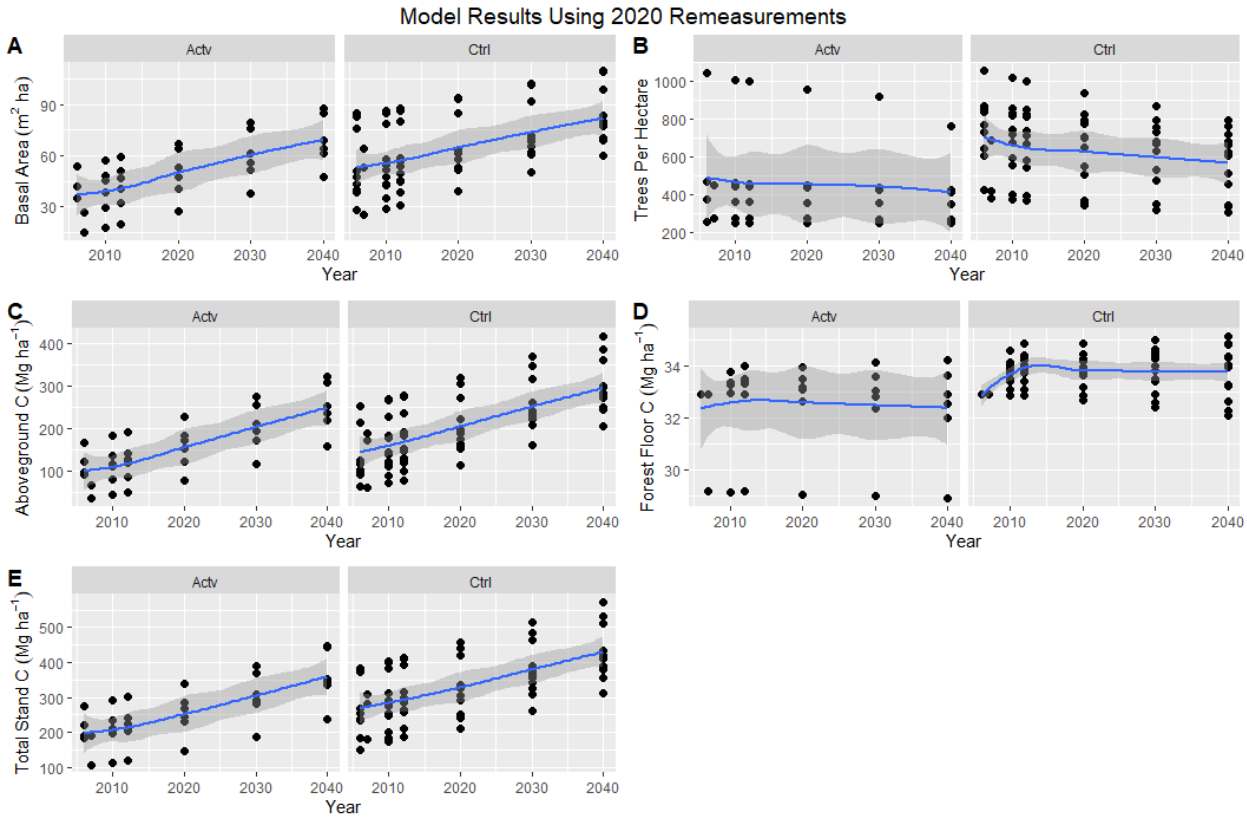

Figure 6. Model results from FVS using data taken in 2020. Panels are divided by active treatment (Actv) and control stands (Ctrl). Panels show basal area (**A**), trees per hectare (**B**), aboveground C (**C**), forest floor C (**D**), and total stand C (**E**). Blue lines represent the mean for each metric.

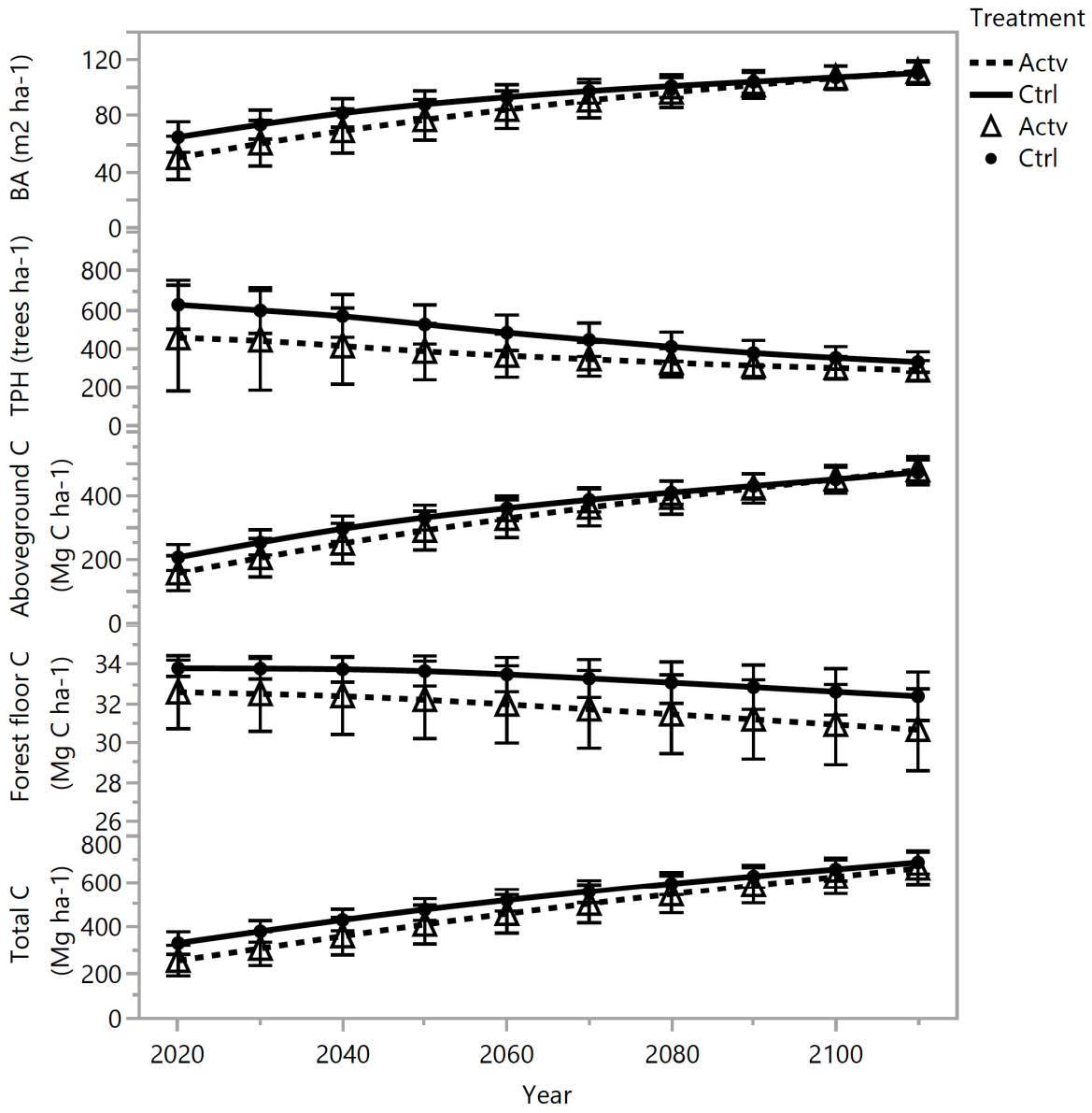

Figure 7. FVS model results from 2020 data modeled through the year 2110. Means are represented along with 95% CI bars. Note the convergence in lines over time as managed stands approach control stands in structure and C content. Each error bar is constructed using a 95% confidence interval of the mean.

4. Discussion

Previous work focusing on aboveground structure and understory species found quick recovery of aboveground canopy cover, tree growth, and sapling density in response to restoration treatments for old-growth restoration at Ellsworth Creek [21]. Nevertheless, modeling efforts in Northwest forests have long demonstrated the carbon consequences of active management, as thinning and gap treatments that remove aboveground carbon and photosynthetic biomass have an intuitively obvious effect on reducing stand C—even over the long term [12]. The C consequences of silvicultural practices for restoration of old-growth structural attributes are not well modeled or understood, but reduced C storage in treated stands is expected in the short term. In our analysis, we found statistical differences between modeled and empirically measured values of TPH, BA, and total aboveground C and total stand C in 2020, where the modeled values tended to be lower, especially for treated stands.

A more detailed analysis of aboveground stand metrics at our site [21] found higher-than-expected regrowth and sapling density following restoration treatments. The data from 2020 reflect this higher-than-expected sapling growth and density; however, the statistical results suggested that models built on existing forest structure (e.g., control plots) may more reliably project carbon stores aboveground, and simulated management projections (active treatments) are more challenging. This might be due to insufficient regeneration establishment models developed for the Pacific Northwest Variant of FVS [30]. Forests in the PNW tend to respond to disturbance with rapid regrowth. Measuring the growth of saplings and seedlings is often separate from tree measurements, and trees smaller than 14.5 cm DBH were not cut according to our treatment methods (also represented in the model) and may have been present in 2007 and then became much larger by 2020. Treatments indeed varied in timing (2009 and 2013) and may affect our empirical data, which can be a source of error, but this effect was not a clear driver in our study.

The relatively light treatments associated with old-growth restoration coupled with rapid tree growth and sapling responses [21] resulted in similar stand C storage over time, even when differences between treatments remained significant through 2040 projections. Our long-range projections suggest that average differences in TPH may converge in the different treatments relatively rapidly, and agreement in BA, total tree C, and total stand C will occur even faster. For example, by 2040, models suggest both active and control stands will average within ~25–50 Mg C ha^{-1} of each other in total stand C, though individual plots may have higher or lower values in control and treatment stands, respectively (Figure 2). By 2107, projections indicate that total stand C may be near within 10% of each other for both treatments, approaching the anticipated ceiling for C storage in PNW forests [31]. Total tree C (Mg ha^{-1}) similarly is projected to range around 50–300 Mg ha^{-1} in active treatments by 2040, and 200–400 Mg C ha^{-1} in control treatments, with both treatments approaching 400–500 Mg ha^{-1} by 2100. Meanwhile, the C stores in trees are likely to be associated with larger trees (stands with larger QMD) and fewer trees (lower TPH in most stands).

Caution should be employed when interpreting these data, and differences among treatments are likely conservative. Regrowth models for FVS are notoriously inaccurate, especially for Western Washington, where forests are characterized by explosive regrowth and individual tree maturation is highly variable. Our analysis did not include any regrowth calibration to the base partial-establishment model in FVS, which is insufficient for modeling regrowth by itself in the Pacific Northwest [30,32]. Generally, FVS underestimated aboveground C in both active and control stands, but especially in active stands (Figure 3). These known errors suggest that our models of future C may overestimate the treatment differences and further suggest that the gap in C storage between active and control stands may be negligible within decades. A caveat is that this is for stands where ecological restoration was the goal, treatments were light and variable, and tree regrowth is rapid due to high rainfall and moderate temperatures. These results are unlikely to apply to more extreme production-oriented cuts, and we note that our results did still indicate less C over time in treated stands—consistent with well-documented effects of timber harvests on C storage.

Earlier work at our site found no difference in soil OM litter depths [21]. Similarly, our results suggest treatments were conducted at the Ellsworth Creek Preserve 10–14 years ago and may have already recovered to pre-treatment soil OM and C levels. We expected thinning treatments to result in reduced C because of reduced litter inputs, but microclimatic changes resulting from canopy reductions have been found to drive recovery of soil C pools in coniferous forests within a couple decades [33]. Although we also expected age to play a role in the accumulation rate and recovery of soil C following treatments, the interaction of treatment by age had a much stronger effect than treatments. Both young and mature control plots represent forests in the stem exclusion phase of succession, but mature control forests possess significantly greater soil C than their younger controlled counterparts. In active stands, higher OM C in young stands was likely an artifact of post-harvest debris and reduced decomposition during dry conditions.

Forest floor OM C was much more variable in our empirical measurements than in model projections (Figure 4), and this is likely due to overly simplistic assumptions in the soil OM content associated with a given stand age in FVS. Soil OM C is notoriously variable, and variation is much likely more predictable when accounting for microsite effects and species composition differences that can result in fast or slow decomposition [32]. Additionally, though, soil OM C was underestimated by models in the treatment stands and overestimated by models in the control stands. Underestimates may have been associated with low initial tree density, underestimated litter contributions to the forest floor during harvests, and overestimated increased decomposition of litter following harvest [34,35]. Additionally, the high moisture and leaf litter quality associated with trees in a high rainfall temperate rainforest could result in faster litter decomposition, and hence lower OM C, in the untreated stands than predicted by FVS. The lack of a reliable regeneration model also reduces the accuracy of modeling new recruitment unless a planting event occurs, and in many stands, regeneration was higher than expected following harvests at our sites [21]. Early in stand development, these results may emphasize the need for better modeling of regeneration and OM inputs associated with harvest treatments.

Nevertheless, averages of soil OM C from both modeling and empirical measurements were within one 95% confidence interval of the empirical measures in both managed and unmanaged stands. Empirical measurements may give higher OM C estimates when high litter inputs associated with harvest activities are not properly accounted for. Our direct measurement of values in 2022 suggested similar % C between treatments, and similar bulk density of the OM layer between treatments, and any differences in soil OM C (e.g., higher in the active treatments) were likely associated with higher OM inputs or reduced decomposition, rather than differences in OM quality or density. Over longer periods of time, realized climate changes could result in drier conditions, further reducing decomposition.

Logging debris following treatments typically results in high OM values, followed by rapid decomposition, and therefore soil C declines [35]. Interestingly, our study design (where active and control treatments were variable in age) resulted in an opportunity to examine the data in the context of stand age where our data align well with traditional interpretation of curves in soil OM content though time following harvest—the "Covington Curve" [36]. Both active and control treatment stands had OM C values that suggested a curve where initial high OM C was followed by a reduction by stand age 40–50, followed by a gradual increase in soil OM C by age 80 (Figure 5A). Again, our results suggested far more variability between plots within treatments than between treatments. Importantly though, our analysis was limited to surface soil OM C, and we did not examine patterns with soil depth. Soil OM leaching and depth profiles in mineral soils may either exaggerate or nullify patterns in soil C found by looking at the OM layer only [36]. Further analysis of soil C at greater sample depths [23,25] would also help inform our understanding.

5. Conclusions

These data from the Ellsworth Creek Preserve suggest that light-prescription ecological forestry treatments aimed at restoring old-growth conditions have resulted in small differences in above-ground stand C but have not resulted in significant differences in forest soil surface OM pools. Our comparison of modeled values and empirical measurements suggest that modeled estimates of C pools were frequently underestimated. Our model projections suggest that convergences in future stand C and OM C content are likely in coming decades and may occur sooner than expected. Small differences in stand C pools among treatments may be explained based on the relatively light harvest activity associated with skip and gap silvicultural prescriptions for old-growth structural development, rapid regrowth by retained trees and saplings, and high soil OM variability based on microsite conditions. Additionally, the role of stand age since complete harvest may have played a more dominant role in the response of soil OM C storage. We expected to see greater reductions in soil C for young managed stands. Indeed, soil OM C was lower in managed stands, but mature stands suffered greater C losses compared to younger counterparts.

The combined effect of age and treatment was significant, indicating that C resilience to disturbance may change with age. Future projections greatly simplify variation, but our comparison of modeled and field data over thirteen years suggests that projections give realistic values within 95% confidence intervals of empirical measurements. Accordingly, the projections of rapid C recovery following small-scale treatments suggest that lost soil OM C associated with harvest disturbance and altered microclimate may be rapidly recovered in subsequent decades.

Author Contributions: Conceptualization, S.A.Q., D.G.F., and M.J.C.; methodology, D.G.F.; validation, S.A.Q. and D.G.F.; formal analysis, D.G.F.; investigation, S.A.Q., D.G.F., and M.J.C.; resources, D.G.F. and M.J.C.; data curation, S.A.Q., D.G.F., and M.J.C.; writing—original draft preparation, S.A.Q.; writing—review and editing, D.G.F. and M.J.C.; visualization, S.A.Q. and D.G.F.; supervision, D.G.F. and M.J.C.; project administration, D.G.F.; funding acquisition, D.G.F. and S.A.Q. All authors have read and agreed to the published version of the manuscript.

Funding: This research received external funding from the Northwest Scientific Association (data collection), Louis Stokes' All Nation's Alliance for Minority Participation (conference travel), and the Ecological Society of America (conference lodging).

Data Availability Statement: Raw data will be made available at OSF following the publication of this manuscript. The data title will be: "Forest Restoration Thinning has Minimal Impacts on Surface Soil Carbon in a Second-Growth Temperate Rainforest: DATA". Available online: https://osf.io/fnxsa/?view_only=4b1564d951de494a84e0dc49799da334 (accessed on 3 October 2024).

Acknowledgments: We recognize that the Ellsworth Creek Preserve is located on the historic Chinook, Lower Chinook, Confederated Tribes of Siletz Indians, and Confederated Tribes of Grand Ronde territories. Gratitude is also due to The Nature Conservancy (land access) and the Evergreen State College (supplies) for supporting this research effort.

Conflicts of Interest: The authors declare no conflicts of interest. The funders had no role in the design of the study; in the collection, analyses, or interpretation of data; in the writing of the manuscript; or in the decision to publish the results.

References

1. Case, M.J.; Johnson, B.G.; Bartowitz, K.J.; Hudiburg, T.W. Forests of the Future: Climate Change Impacts and Implications for Carbon Storage in the Pacific Northwest, USA. *For. Ecol. Manag.* **2021**, *482*, 118886. [CrossRef]
2. Smith, P.; Davis, S.J.; Creutzig, F.; Fuss, S.; Minx, J.; Gabrielle, B.; Kato, E.; Jackson, R.B.; Cowie, A.; Kriegler, E.; et al. Biophysical and Economic Limits to Negative CO2 Emissions. *Nat. Clim. Chang.* **2016**, *6*, 42–50. [CrossRef]
3. McDowell, N.G.; Allen, C.D.; Anderson-Teixeira, K.; Aukema, B.H.; Bond-Lamberty, B.; Chini, L.; Clark, J.S.; Dietze, M.; Grossiord, C.; Hanbury-Brown, A.; et al. Pervasive Shifts in Forest Dynamics in a Changing World. *Science* **2020**, *368*, eaaz9463. [CrossRef]
4. Reilly, M.J.; Zuspan, A.; Halofsky, J.S.; Raymond, C.; McEvoy, A.; Dye, A.W.; Donato, D.C.; Kim, J.B.; Potter, B.E.; Walker, N.; et al. Cascadia Burning: The Historic, but Not Historically Unprecedented, 2020 Wildfires in the Pacific Northwest, USA. *Ecosphere* **2022**, *13*, e4070. [CrossRef]
5. Franklin, J.F.; Spies, T.A.; Pelt, R.V.; Carey, A.B.; Thornburgh, D.A.; Berg, D.R.; Lindenmayer, D.B.; Harmon, M.E.; Keeton, W.S.; Shaw, D.C.; et al. Disturbances and Structural Development of Natural Forest Ecosystems with Silvicultural Implications, Using Douglas-Fir Forests as an Example. *For. Ecol. Manag.* **2002**, *155*, 399–423. [CrossRef]
6. Spies, T.A.; Stine, P.A.; Gravenmier, R.A.; Long, J.W.; Reilly, M.J. *Synthesis of Science to Inform Land Management within the Northwest Forest Plan Area*; U.S. Department of Agriculture, Forest Service, Pacific Northwest Research Station: Portland, OR, USA, 2018.
7. Kardol, P.; Wardle, D.A. How Understanding Aboveground–Belowground Linkages Can Assist Restoration Ecology. *Trends Ecol. Evol.* **2010**, *25*, 670–679. [CrossRef]
8. Williams, N.G.; Powers, M.D. Carbon Storage Implications of Active Management in Mature Pseudotsuga Menziesii Forests of Western Oregon. *For. Ecol. Manag.* **2019**, *432*, 761–775. [CrossRef]
9. Chamberlain, C.; Kane, V.; Case, M. Accelerating the Development of Structural Complexity: Lidar Analysis Supports Restoration as a Tool in Coastal Pacific Northwest Forests. *For. Ecol. Manag.* **2021**, *500*, 119641. [CrossRef]
10. Bauhus, J.; Puettmann, K.; Messier, C. Silviculture for Old-Growth Attributes. *For. Ecol. Manag.* **2009**, *258*, 525–537. [CrossRef]
11. Puettmann, K.J.; Ares, A.; Burton, J.I.; Dodson, E.K. Forest Restoration Using Variable Density Thinning: Lessons from Douglas-Fir Stands in Western Oregon. *Forests* **2016**, *7*, 310. [CrossRef]
12. Harmon, M.E.; Ferrell, W.K.; Franklin, J.F. Effects on Carbon Storage of Conversion of Old-Growth Forests to Young Forests. *Science* **1990**, *247*, 699–702. [CrossRef] [PubMed]

13. Yanai, R.D.; Currie, W.S.; Goodale, C.L. Soil Carbon Dynamics after Forest Harvest: An Ecosystem Paradigm Reconsidered. *Ecosystems* **2003**, *6*, 197–212. [CrossRef]
14. Piene, H.; Cleve, K.V. Weight Loss of Litter and Cellulose Bags in a Thinned White Spruce Forest in Interior Alaska. *Can. J. For. Res.* **1978**, *8*, 42–46. [CrossRef]
15. Jandl, R.; Lindner, M.; Vesterdal, L.; Bauwens, B.; Baritz, R.; Hagedorn, F.; Johnson, D.W.; Minkkinen, K.; Byrne, K.A. How Strongly Can Forest Management Influence Soil Carbon Sequestration? *Geoderma* **2007**, *137*, 253–268. [CrossRef]
16. Law, B.E.; Thornton, P.E.; Irvine, J.; Anthoni, P.M.; Van Tuyl, S. Carbon Storage and Fluxes in Ponderosa Pine Forests at Different Developmental Stages. *Glob. Change Biol.* **2001**, *7*, 755–777. [CrossRef]
17. Larson, A.J.; Franklin, J.F. The Tree Mortality Regime in Temperate Old-Growth Coniferous Forests: The Role of Physical Damage. *Can. J. For. Res.* **2010**, *40*, 2091–2103. [CrossRef]
18. Kane, V.R.; Gersonde, R.F.; Lutz, J.A.; McGaughey, R.J.; Bakker, J.D.; Franklin, J.F. Patch Dynamics and the Development of Structural and Spatial Heterogeneity in Pacific Northwest Forests. *Can. J. For. Res.* **2011**, *41*, 2276–2291. [CrossRef]
19. Ameray, A.; Bergeron, Y.; Valeria, O.; Montoro Girona, M.; Cavard, X. Forest Carbon Management: A Review of Silvicultural Practices and Management Strategies Across Boreal, Temperate and Tropical Forests. *Curr. For. Rep.* **2021**, *7*, 245–266. [CrossRef]
20. Davis, L.; Kollasch, T.; Smith, K.M.; Boston, K. Chapter 26—South Willapa Bay Conservation Area, Washington, United States of America. In *Forest Plans of North America*; Siry, J.P., Bettinger, P., Merry, K., Grebner, D.L., Boston, K., Cieszewski, C., Eds.; Academic Press: San Diego, CA, USA, 2015; pp. 225–233, ISBN 978-0-12-799936-4.
21. Case, M.J.; Ettinger, A.K.; Pradhan, K. Forest Restoration Thinning Accelerates Development of Old-growth Characteristics in the Coastal Pacific Northwest, USA. *Conserv. Sci. Pract.* **2023**, *5*, e13004. [CrossRef]
22. Beese, W.J.; Sandford, J.S.; Harrison, M.L.; Filipescu, C.N. Understory Vegetation Response to Alternative Silvicultural Systems in Coastal British Columbia Montane Forests. *For. Ecol. Manag.* **2022**, *504*, 119817. [CrossRef]
23. James, J.; Harrison, R. The Effect of Harvest on Forest Soil Carbon: A Meta-Analysis. *Forests* **2016**, *7*, 308. [CrossRef]
24. Harrison, R.B.; Footen, P.W.; Strahm, B.D. Deep Soil Horizons: Contribution and Importance to Soil Carbon Pools and in Assessing Whole-Ecosystem Response to Management and Global Change. *For. Sci.* **2011**, *57*, 67–76. [CrossRef]
25. Simard, S.W.; Roach, W.J.; Defrenne, C.E.; Pickles, B.J.; Snyder, E.N.; Robinson, A.; Lavkulich, L.M. Harvest Intensity Effects on Carbon Stocks and Biodiversity Are Dependent on Regional Climate in Douglas-Fir Forests of British Columbia. *Front. For. Glob. Chang.* **2020**, *3*, 88. [CrossRef]
26. Franklin, J.F.; Dyrness, C.T. *Natural Vegetation of Oregon and Washington*; Oregon State University Press: Corvallis, OR, USA, 1988.
27. Oliver, C.D.; Larson, B.C. Forest Stand Dynamics. McGraw-Hill: New York, NY, USA, 1996; ISBN 978-0-471-13833-4.
28. Cissel, J.; Anderson, P.; Olson, D.; Puettmann, K.; Berryman, S.; Chan, S.; Thompson, C. *BLM Density Management and Riparian Buffer Study: Establishment Report and Study Plan*; U.S. Geological Survey: Reston, VA, USA, 2006.
29. Hoover, C.M.; Rebain, S.A. *Forest Carbon Estimation Using the Forest Vegetation Simulator: Seven Things You Need to Know*; U.S. Department of Agriculture, Forest Service, Northern Research Station: Newtown Square, PA, USA, 2011; p. NRS-GTR-77.
30. Vandendriesche, D. *Integrated Management of Carbon Sequestration and Biomass Utilization Opportunities in a Changing Climate: Proceedings of the 2009 National Silviculture Workshop; 2009 June 15-18; Boise, ID*; USDA Forest Service Proceedings; U.S. Department of Agriculture, Forest Service, Northern Research Station: Newtown Square, PA, USA, 2010; Volume RMRS-P-61, pp. 289–320.
31. Smithwick, E.A.H.; Harmon, M.E.; Remillard, S.M.; Acker, S.A.; Franklin, J.F. Potential Upper Bounds of Carbon Stores in Forests of the Pacific Northwest. *Ecol. Appl.* **2024**, *12*, 1303–1317. [CrossRef]
32. Binkley, D.; Giardina, C. Why Do Tree Species Affect Soils? The Warp and Woof of Tree-Soil Interactions. In *Plant-Induced Soil Changes: Processes and Feedbacks*; Van Breemen, N., Ed.; Developments in Biogeochemistry; Springer: Dordrecht, The Netherlands, 1998; pp. 89–106, ISBN 978-94-017-2691-7.
33. Sun, O.J.; Campbell, J.; Law, B.E.; Wolf, V. Dynamics of Carbon Stocks in Soils and Detritus across Chronosequences of Different Forest Types in the Pacific Northwest, USA. *Glob. Change Biol.* **2004**, *10*, 1470–1481. [CrossRef]
34. O'Neill, K.P.; Kasischke, E.S.; Richter, D.D. Seasonal and Decadal Patterns of Soil Carbon Uptake and Emission along an Age Sequence of Burned Black Spruce Stands in Interior Alaska. *J. Geophys. Res. Atmos.* **2003**, *108*, FFR 11-1–FFR 11-15. [CrossRef]
35. Covington, W.W. Changes in Forest Floor Organic Matter and Nutrient Content Following Clear Cutting in Northern Hardwoods. *Ecology* **1981**, *62*, 41–48. [CrossRef]
36. Jobbágy, E.G.; Jackson, R.B. The Vertical Distribution of Soil Organic Carbon and Its Relation to Climate and Vegetation. *Ecol. Appl.* **2000**, *10*, 423–436. [CrossRef]

JOURNAL OF THE AMERICAN WATER RESOURCES ASSOCIATION
Vol. 44, No. 6 AMERICAN WATER RESOURCES ASSOCIATION December 2008

GUIDELINES FOR RIPARIAN VEGETATIVE SHADE RESTORATION BASED UPON A THEORETICAL SHADED-STREAM MODEL[1]

David R. DeWalle[2]

ABSTRACT: Guidelines for riparian vegetative shade restoration were developed using a theoretical model of total daily radiation received by a shaded stream. The model assumed stream shading by nontransmitting, vertical or overhanging, solid vegetation planes in infinitely long reaches. Radiation components considered in the model were direct beam shortwave on the stream centerline, diffuse atmospheric shortwave, shortwave reflected by vegetation, atmospheric longwave, and longwave emitted by vegetation. Potential or extraterrestrial shortwave irradiation theory was used to compute beam shortwave radiation received at the stream centerline, and view factor theory was used to compute diffuse radiation exchange among stream, vegetation, and atmospheric planes. Model shade effects under clear skies were dominated by reductions in receipt of direct beam shortwave radiation. Model shade effects with cloudy skies were dominated by the "view factor effect" or the decreases in diffuse shortwave and longwave radiation from the atmosphere balanced against increases in longwave radiation from vegetation. Model shade effects on shortwave radiation reflected by vegetation were found to be negligible. The model was used to determine the vegetation height (*H*) to stream width (*W*) ratios needed to achieve 50, 75, and 90 % shade restoration for mid-latitude conditions on clear and cloudy days. Ratios of vegetation height to stream width, for dense nontransmitting vegetation, generally ranged from 1.4 to 2.3 for 75% shade restoration at a mid-latitude site (40°N). The model was used to show *H/W* needed for E-W *vs*. N-S stream azimuths, varying stream latitudes between 30° and 50°N, channels with overhanging vegetation, channels undergoing width changes, as well as the limits to shade restoration on very wide channels.

(KEY TERMS: restoration; stream temperature; riparian ecology; best management practices; modeling; radiation view factors; vegetation overhang angles; stream azimuth; extraterrestrial solar radiation.)

DeWalle, David R., 2008. Guidelines for Riparian Vegetative Shade Restoration Based Upon a Theoretical Shaded-Stream Model. *Journal of the American Water Resources Association* (JAWRA) 44(6):1373-1387. DOI: 10.1111/j.1752-1688.2008.00230.x

INTRODUCTION

Restoration of riparian vegetative shade to improve water temperature regimes and help rehabilitate aquatic ecosystems is becoming a common watershed management practice (Broadmeadow and Nisbet, 2004; Kauffman *et al.*, 1997; Poole and Berman, 2001; Roni *et al.*, 2002; Rutherford *et al.*, 1997a; Watanabe *et al.*, 2005). Many streams have lost riparian vegetation due to human disturbances (agriculture, forestry, urbanization, mining, etc.) or natural

[1]Paper No. JAWRA-07-0124-P of the *Journal of the American Water Resources Association* (JAWRA). Received August 31, 2007; accepted February 12, 2008. **Discussions are open until June 1, 2009**.

[2]Professor Emeritus of Forest Hydrology, School of Forest Resources, and Penn State Institutes for Energy and the Environment, 107 Land and Water Research Bldg., The Pennsylvania State University, University Park, Pennsylvania 16802 (E-mail/DeWalle: drdewalle@psu.edu).

disasters (high winds, fire, flooding, etc.) which has resulted in increased maximum daily stream temperatures and loss or modification of aquatic ecosystems (Bartholow, 2000; Borman and Larson, 2003; Brown, 1970; LeBlanc *et al.*, 1997; Lynch *et al.*, 1984; Moore *et al.*, 2005; Scarsbrook and Halliday, 1999; Swift and Messer, 1971; Wilkerson *et al.*, 2006; Zwieniecki and Newton, 1999). Shifts in aquatic macro- and microflora and fauna due to changing thermal regimes in streams caused by changes in shading have been reported in many regions (Whitledge *et al.*, 2006; Parkyn *et al.*, 2003; Sweeney, 1993; Harding *et al.*, 2006). Spring-fed headwater streams in karst terrain found in states like Pennsylvania have been partially converted from cold-water to warm-water fisheries by loss of shade (Grant, 2005), which provided further local incentive for this paper.

A major question that arises in re-establishing riparian shade is what amount and type of shade is necessary to significantly affect the heat balance of the stream. Other related questions are whether smaller headwater streams can be significantly shaded by short grass and shrub vegetation rather than taller trees, the benefits of using overhanging vegetation, effects of stream width changes during shade restoration, and the effectiveness of shade restoration on larger streams and rivers.

Small headwater channels with shade from relatively tall, dense trees, receive most of their radiation as longwave radiation from vegetation and a varying component of transmitted shortwave radiation. In these situations, emphasis can be placed on specification of the buffer zone width, height, leaf area index, tree crown diameter, and/or density to be maintained or cultivated. Forested buffer zone widths ranging from about 9-30 m width are generally considered adequate to maintain thermal regimes in such small streams (Beschta *et al.*, 1987; Sridhar *et al.*, 2004; Lanini *et al.*, 2004; Wilkerson *et al.*, 2006; Zwieniecki and Newton, 1999). An alternative approach for transmitted radiation is specification of the crown cover above the channel (Tate *et al.*, 2005) or the fraction of incoming shortwave radiation transmitted by vegetation (Amaranthus *et al.*, 1989; Davies-Colley and Payne, 1998). For example, forest streams may only naturally receive 10-20% of above-canopy solar radiation during summer when maximum temperatures occur, but receipt of only 30-50% of incoming solar after restoration is often considered desirable or acceptable (Davies-Colley and Quinn, 1998; Broadmeadow and Nisbet, 2004; Rutherford *et al.*, 1997a).

Transmission of shortwave radiation through vegetation is a complex process that depends upon an attenuation coefficient, the plant or leaf area index, arrangement and clumping of plant parts and the path length for radiation transmission within vegetation. Applicability of simple exponential Beer's Law models to transmission of shortwave radiation has been tested (Aubin *et al.*, 2000; Baldocchi *et al.*, 1984; Federer, 1971; Link *et al.*, 2004) and found primarily suited to relatively homogeneous vegetation layers. Transmission in more heterogeneous or discontinuous vegetation can be analyzed using more data-intensive simulation models (Li *et al.*, 1995) or hemispherical photography of the plant canopy along channels (Hardy *et al.*, 2004).

At the other extreme, where riparian vegetation is completely absent or very sparse, shading may be initially limited to that caused by stream banks and local topography. In this situation, the ultimate height and overhang of vegetation in relation to stream width and stream azimuth, which control shadow lengths and receipt of direct beam shortwave radiation, become more important variables. Ratios of vegetation height to stream width are proposed in this paper as a useful way to characterize shade. The greater importance of shade for smaller headwater channels, where the lower water depths can lead to more-rapid and greater heating of the stream, than for deeper, higher-order channels where heating is less rapid is well known (Poole and Berman, 2001; Chen *et al.*, 1998b; Rutherford *et al.*, 1997b). Experimental development of shade restoration guidelines is difficult due to the large number of controlling variables, and modeling is probably the best way to infer such guidelines.

Models vary in treatment of shortwave and longwave fluxes and effects of riparian shade. Models generally include a reduction in the receipt of shortwave radiation by shaded streams (Meier *et al.*, 2003; Sinokrot and Stefan, 1993) or separate reduction procedures for direct beam shortwave radiation with consideration of transmission by vegetation and diffuse shortwave radiation from the atmosphere (Bartholow, 2002; Chen *et al.*, 1998a; LeBlanc *et al.*, 1997; Quigley, 1981; Rutherford *et al.*, 1997b; Sridhar *et al.*, 2004; Welty *et al.*, 2002; Tung *et al.*, 2007). Topographic shading is considered separately from vegetative shading in some applications where transmission by vegetation is considered (Bartholow, 2002; Chen *et al.*, 1998a; Rutherford *et al.*, 1997b). Diffuse atmospheric shortwave radiation received by shaded streams is generally reduced by the view factor from the stream to atmosphere and in some applications view factors are also used to compute atmospheric longwave radiation (Bartholow, 2000; DeWalle, 1974; Quigley, 1981; Rutherford *et al.*, 1997b; Chen *et al.*, 1998a; LeBlanc *et al.*, 1997; O'Driscoll and DeWalle, 2006; Tung *et al.*, 2007). Longwave radiation exchange corrections with view factors become important when the radiating temperatures and emissivities of riparian vegetation are significantly different from that of the atmosphere. Shortwave radiation reflected to the stream by

riparian vegetation has not generally been considered; DeWalle (1974) found negligible amounts of reflected shortwave radiation received by rivers in large valleys. View factors can be computed from measurements along shaded channels (Rutherford *et al.*, 1997b; Welty *et al.*, 2002) or by heat transfer theory (Holman, 1972) assuming simple geometric shapes for shaded stream cross-sections (DeWalle, 1974). Overhanging vegetation effects have been implicitly considered in a few models where crown diameter of trees is allowed to overlap the channel width (Chen *et al.*, 1998a; Quigley, 1981). As vegetative shading will affect direct beam and diffuse shortwave differently, shading effectiveness should also vary between clear and cloudy days. Overall, application of models to specific locations requires considerable site-specific data inputs.

Shade restoration in this paper is defined as the process of converting the incoming radiation regime of exposed streams, typically dominated by direct beam shortwave radiation and atmospheric diffuse shortwave and atmospheric longwave radiation, into the incoming radiation regime typical of heavily shaded streams dominated by longwave radiation from vegetation. Due to the lack of general guidelines for shade restoration for channels that initially have little to no shade, the major objective of this paper was to determine an index of shading needed to reduce all-wave radiation received by exposed streams to 50, 75, and 90% of that for fully shaded streams for various stream azimuths and latitudes, based upon vegetation height to stream width ratios. Other sub-objectives were to: (1) quantify the net impact of increased shading on direct beam solar radiation relative to other shortwave and longwave radiation fluxes to the stream, (2) estimate the relative importance of increased shade on shortwave radiation reflected to small streams by riparian vegetation, and (3) determine the impact of overhanging vegetation on stream radiation receipt in terms of an overhang angle.

SHADED STREAM MODEL

A shaded stream model was developed assuming an infinitely long, horizontal stream plane which was shaded by two adjoining, parallel, nontransmitting vegetation planes of equal height (Figure 1). Shading by both vertical and overhanging vegetation planes was considered. Direct beam shortwave radiation receipt on the stream centerline was computed using potential or extraterrestrial solar irradiation theory (Lee, 1978) for entire days. Diffuse shortwave and longwave radiation receipt by the stream plane was computed using radiation exchange view factor theory (Holman, 1972), which assumes isotropic diffuse radiation exchange.

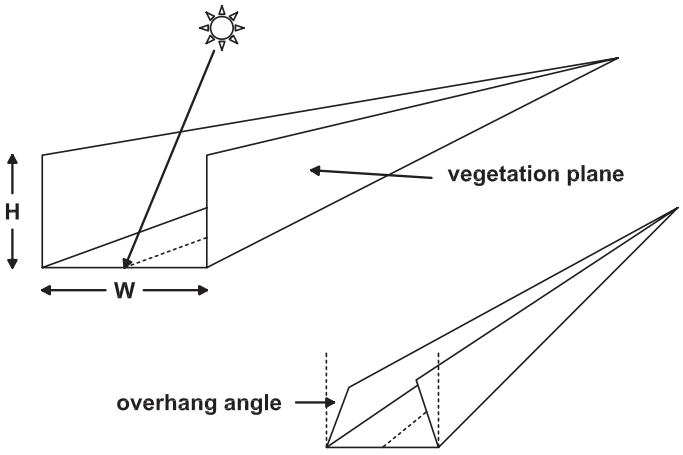

FIGURE 1. Model of an Infinitely Long Shaded Stream Section With and Without Vegetation Overhang Used in the Theoretical Analysis.

Shortwave Radiation

Shortwave radiation reaching a shaded stream surface was modeled as the sum of a direct beam solar ($K\downarrow_{\text{beam}}$) and two diffuse shortwave radiation components; one diffuse component representing shortwave from the atmosphere ($K\downarrow_{\text{atm diffuse}}$) and the other diffuse reflected by riparian vegetation ($K\downarrow_{\text{refl diffuse}}$) as

$$K\downarrow_{\text{stream}} = [\text{FP} \cdot K\downarrow_{\text{beam}}] + [F_{\text{s-a}} \cdot K\downarrow_{\text{atm diffuse}}] + [2F_{\text{s-v}} \cdot K\downarrow_{\text{refl diffuse}}], \quad (1)$$

where $K\downarrow_{\text{stream}}$ is daily total incoming shortwave radiation at the stream surface, FP is the ratio of daily potential or extraterrestrial solar irradiance on the centerline of a shaded plane to that on an unobstructed plane at the top of the atmosphere, $K\downarrow_{\text{beam}}$ is the incoming daily shortwave beam radiation reaching an unobstructed horizontal surface, $F_{\text{s-a}}$ is the view factor from stream plane to atmosphere plane, $K\downarrow_{\text{atm diffuse}}$ is the incoming daily shortwave atmospheric diffuse radiation reaching an unobstructed horizontal surface, $F_{\text{s-v}}$ is the view factor from stream plane to vegetation plane on one bank, and $K\downarrow_{\text{refl diffuse}}$ is the incoming daily shortwave diffuse radiation received and reflected by vegetation planes. FP can be determined by theoretical analysis of beam irradiation, ignoring atmospheric attenuation, at the stream center-line for a given *H/W* and stream azimuth, latitude and time of year (summer solstice assumed). The necessary view factors $F_{\text{s-a}}$ and $F_{\text{s-v}}$

were derived from heat transfer theory and shaded stream reach geometry. The incoming radiation totals $K\downarrow_{\text{beam}}$, $K\downarrow_{\text{atm diffuse}}$, and $K\downarrow_{\text{refl diffuse}}$ can be measured, extrapolated from published data, as in this analysis, or computed using theoretical relationships (Niemelä *et al.*, 2001; Iqbal, 1983).

Longwave Radiation

Longwave radiation received by shaded streams derives from atmospheric longwave emissions reaching the stream plane and longwave radiation emitted by vegetation along both banks as

$$L\downarrow_{\text{stream}} = [F_{\text{s-a}} \cdot L\downarrow_{\text{atmos}}] + [2F_{\text{s-v}} \cdot L\downarrow_{\text{veg}}], \quad (2)$$

where $L\downarrow_{\text{stream}}$ is the daytime total longwave radiation received by the stream surface, $L\downarrow_{\text{atmos}}$ is the daytime longwave radiation received from the atmosphere on an unobstructed surface, and $L\downarrow_{\text{veg}}$ is the daytime longwave radiation emitted by riparian vegetation. Longwave radiation fluxes from vegetation or the atmosphere can also be measured, extrapolated from published data or computed using the Stefan-Boltzmann law where

$$L\downarrow = \varepsilon \sigma T^4, \quad (3)$$

where $L\downarrow$ is the longwave flux density in W/m^2, ε is the emissivity of the radiator (atmosphere or vegetation), σ is the Stefan-Boltzmann constant or 5.67×10^{-8} W/m^2/K^4, and T is the absolute temperature (°K) of the radiator. Emissivity of clear sky varies mainly with water vapor content, whereas emissivity for cloudy sky is increased by cloud cover (see Duarte *et al.*, 2006; Crawford and Duchon, 1999). Emissivity for vegetation generally exceeds 0.95 (Oke, 1987). Given the low longwave reflectivity of vegetation and soil (<5%), reflection of longwave radiation to streams was ignored in this analysis.

METHODS

Fraction of Potential Solar Irradiation

Equations describing the solar altitude and solar azimuth angles for any latitude, time of year, and time of day (List, 1968) were used to establish times of sunrise and sunset on the shaded stream (Figure 1). Height of the vegetation (H), stream width (W), and stream azimuth were varied to simulate a range of conditions. Once the times of sunrise and sunset on the stream plane were established, the potential solar irradiation of the unshaded or shaded stream plane during a day was computed as (Frank and Lee, 1966)

$$I = (I_o/r^2)[(t_2 - t_1) \cdot \sin \text{lat} \cdot \sin d + 3.8197 \cdot \cos \text{lat} \cdot \cos d \cdot (\sin \omega t_2 - \sin \omega t_1)], \quad (4)$$

where I_o is the solar constant (1360 W/m^2), r is the radius vector which corrects for varying earth-sun distance, t_2 is the sunset time, t_1 is the sunrise time, lat is latitude, d is solar declination which varies with time of year, and ω is the daily angular velocity of the earth's rotation (2π radians per 24 hours).

The stream centerline was used as the point of reference for FP computations and stream azimuths were varied from N-S to E-W. Vegetative shade altitudes, or angle between the stream centerline and the top of the vegetation plane in the direction of the sun, were computed for incremental 0.1 hour time steps from sunrise to sunset on an unobstructed horizontal plane. Sunrise occurred on the stream centerline whenever the solar altitude exceeded the shade altitude and sunset on the stream occurred whenever solar altitude fell below shade altitude. Double sunrise and sunset times can occur particularly for E-W stream azimuths, where the stream centerline would be shaded at noon but illuminated for a period in the morning when the sun was in the East and for a period in the afternoon when the sun was from the West. Calculations were conducted for the summer solstice (June 21, solar declination = +23.5°) when the sun is at its maximum elevation during the year for a given latitude; shading would be greater at other times of year. Emphasis was given to computations for 40°N latitude, which generally represents conditions in the mid-latitudes of the United States (U.S.), but results for 30°N and 50°N latitudes are also shown.

Knowing the appropriate sunrise and sunset times for the unobstructed and shaded stream plane and values of r and d from ephemeris tables (List, 1968; Frank and Lee, 1966), the fraction of potential or extraterrestrial beam radiation received by the stream was computed as

$$\text{FP} = I_{\text{stream}}/I_{\text{horizontal}} \quad (5)$$

using Equation (4) for shaded (I_{stream}) and exposed ($I_{\text{horizontal}}$) stream conditions, respectively. FP was then be used to represent the fraction of beam shortwave radiation reaching the stream plane over a

given day using Equation (1). Double sunrise and sunsets required two integrations to obtain FP and I_{stream} for a given day.

Effects of varying vegetation overhang angle on FP were computed from simple geometry within the shaded stream reach. Overhang angle was defined as the angle between the vertical and a line from the stream edge to the bottom edge of overhanging foliage (Figure 1). Effects of overhang angle were given as a family of curves (Figure 4), each for a different *H/W* without overhang, showing how the effective *H/W* ratios increase with increasing overhang angle. Overhang angle also affects the view factor from the stream to vegetation for a given *H/W* as described below.

View Factors

View factors were used to approximate exchange of diffuse radiation between plane surfaces in the stream-atmosphere-vegetation system. The view factor between two infinitely long parallel planes of width = W separated by distance *H* was computed (Hottel, 1931) and used to represent the view factor from the stream to the atmosphere as

$$F_{s-a} = [1 + (H/W)^2]^{1/2} - H/W \quad (6)$$

As the sum of view factors from a plane surface to all surfaces in the hemispherical view above the plane must add to unity, $1 - F_{s-a}$ represents the view factor from the stream to the vegetation along both banks ($2F_{s-v}$). Alternatively, the view factor between two infinitely long planes sharing a common edge with a 90° included angle can be computed (Siegel and Howell, 2001) and used to represent the view factor from the stream plane to vegetation along one bank as

$$F_{s-v-90} = 1/2\,\{1 + H/W - [1 + (H/W)^2]^{1/2}\} \quad (7)$$

The view factor from an infinitely long stream plane to an overhanging infinitely long vegetation plane with an included angle <90° (α) can be similarly computed (Schröder and Hanrahan, 1993) as

$$F_{s-v-<90} = 1/2\,\{A + 1 - [A^2 + 1 - 2A\cos\alpha]^{1/2}\}, \quad (8)$$

where $A = H/(W \sin \alpha)$ and $0 \geq F_{s-v-<90} \leq 1$. In Equations (6-8), the term *W* is analogous to the width of the stream plane and *H* to the vertical height of the vegetation plane. Equations (7) and (8) can also be used to compute view factors from stream to vegetation planes of unequal heights on opposing banks, although only symmetrically shaded stream sections are considered here.

Modeling Radiation Received by Streams

Radiation received by shaded streams using Equations (1) and (2) was computed for mid-latitude conditions (40°N) using representative radiation data from Pennsylvania (Table 1). Emphasis is placed upon clear-sky and the summer solstice conditions when maximum solar radiation and maximum stream heating are likely to occur, although results for cloudy conditions in summer are also given. Potential or extraterrestrial solar irradiation on a horizontal surface at the top of the atmosphere for the summer solstice (42.81 MJ/m^2/day at 40-42°N latitude) was used as a starting point (Frank and Lee, 1966). Clear-sky global radiation (direct beam plus diffuse shortwave) on this date of 29.54 MJ/m^2 was next computed using a June clear sky (<10% cloud cover) clearness index of 0.69 for northcentral Pennsylvania (NASA Surface Meteorology and Solar Energy Tables). The clearness index is the fraction of radiation at the top of the atmosphere which reaches the earth's surface as global radiation during clear-sky days (days with <10% cloud cover). Global radiation was apportioned to 80% solar beam ($K\downarrow_{beam}$ = 23.63 MJ/m^2) and 20% diffuse shortwave from the atmosphere ($K\downarrow_{atm}$ = 5.91 MJ/m^2) based upon analysis of the beam *vs*. diffuse fractions of clear-sky radiation days at the NOAA SURFRAD network Penn State station during June-July 2002-2006. Representative clear-sky, daytime, incoming longwave flux from the atmosphere ($L\downarrow_{atmos}$ = 16.4 MJ/m^2) was also based upon measurements at the Penn State SURFRAD site based upon a 14-hour daytime period.

TABLE 1. Daytime Radiation Totals for Clear and Cloudy Days Used to Model Effects of Riparian Vegetative Shade for Mid-Latitude (40°N) Conditions.

Radiation Component	Clear Day, MJ/m^2	Cloudy Day, MJ/m^2
Direct beam shortwave ($K\downarrow_{beam}$)	23.63	3.4
Diffuse atmospheric incoming shortwave ($K\downarrow_{atm\ diffuse}$)	5.91	13.7
Shortwave received by unobstructed vertical planes[1] ($K\downarrow_{vert}$)	3.27 E- and W-facing 1.52 N-facing 2.25 S-facing	2.18 1.02 1.48
Atmospheric incoming longwave radiation ($L\downarrow_{atmos}$)	16.4	19.7
Longwave radiation emitted by vegetation[2] ($L\downarrow_{veg}$)	20.66	20.66

[1]Used to compute $K\downarrow_{veg}$, source DOE NREL website for Williamsport PA, see text.
[2]Approximately 18°C average vegetation radiating temperature.

Blackbody radiating temperatures and fluxes of longwave radiation from riparian vegetation during clear days are not known. As a first approximation, longwave emitted from vegetation ($L\downarrow_{veg}$) was assumed equal to the June average outgoing radiation flux from the ground surface of unirrigated grass turf and row crops measured at the Penn State SURFRAD site ($L\downarrow_{veg} = 20.66$ MJ/m^2). Based upon Equation (3), this flux is approximately equal to a blackbody radiating temperature of 18°C for vegetation, which is probably a conservative estimate for clear days. Sunlit edges could radiate at much higher temperatures during parts of the day; for example, with E-W stream azimuths the South-facing vegetation could receive solar radiation at near normal incidence and heat at times to much higher temperatures than vegetation on the opposite bank which was facing North. Mean air temperatures during clear days in summer at the Penn State SURFRAD site averaged about 22°C and model results using a vegetation temperature of about 25°C (22.5 MJ/m^2) are also shown.

Shortwave radiation reflected from vegetation planes along streams also presented special problems, as no measurements of reflected radiation from vegetation along streams were available. Estimated clear-day shortwave radiation received on unobstructed vertical planes ($K\downarrow_{vert}$) facing N, E, S, and W at Williamsport, Pennsylvania for June (DOE National Renewable Energy Laboratory website) was used to approximate shortwave received by vertical vegetation planes. Fluxes for North- and South-facing vertical planes were associated with an E-W stream azimuth, while fluxes for East- and West-facing vertical planes, which were equal, were associated with a N-S stream azimuth (Table 1). These fluxes for unobstructed vertical planes were assumed to be entirely diffuse radiation and were corrected for the reduction in amount of radiation that could reach the vegetation from the atmosphere as shading increased using the view factor from the vegetation to atmosphere (F_{v-a}) and then multiplied by an assumed albedo for vegetation of 0.2 to estimate $K\downarrow_{refl\ diffuse}$. The view factor from vegetation to atmosphere, F_{v-a},was derived from other view factors previously discussed, since by symmetry in the shaded stream section, $F_{v-a} = F_{v-s}$ and by reciprocity $F_{v-s} = F_{s-v}$ W/H (Holman, 1972). Thus, the reflected shortwave radiation from vegetation for use in Equation (1) was

$$K\downarrow_{refl\ diffuse} = 0.2F_{s-v} \cdot W/H \cdot K\downarrow_{vert} \quad (9)$$

Substitution of Equation (9) into Equation (1), converts the third term in Equation (1) to

$$2F_{s-v} \cdot K\downarrow_{refl\ diffuse} = (2)(0.2)F_{s-v}^2 \cdot W/H \cdot K\downarrow_{vert}, \quad (10)$$

where the product $2F_{s-v}{}^2 \cdot W/H$ becomes the effective view factor from stream to vegetation along both banks controlling receipt of reflected shortwave radiation to the stream.

Cloudy days were also modeled where it was assumed that incoming shortwave to an unobstructed plane was only 0.4 of potential, with 80% being diffuse shortwave and 20% being direct beam shortwave, which was representative of partial to heavy cloud cover days in Pennsylvania. For cloudy-day modeling, shortwave radiation reaching vertical vegetative planes was reduced to two-thirds of that for clear days (based upon clear to average day ratios given on DOE NREL website for Williamsport), incoming atmospheric longwave was increased to 19.7 MJ/m^2 for the daytime period (based upon data at the Penn State SURFRAD site) and longwave emitted from vegetation was not changed.

RESULTS

Fraction of Potential Solar for Shaded Streams

Effects of stream shade on the daily fraction of direct beam solar radiation reaching the stream centerline are summarized in Figure 2 for E-W, N-S, and intermediate stream azimuths as a function of H/W for latitude of 40°N on the summer solstice.

Increasing shading or H/W produces a gradual curvilinear reduction in receipt of direct beam solar radiation as expected, but for E-W streams the curves shows a more complex pattern due to occurrence of double sunrises and sunsets. For E-W streams a threshold or inflection point exists where the fraction

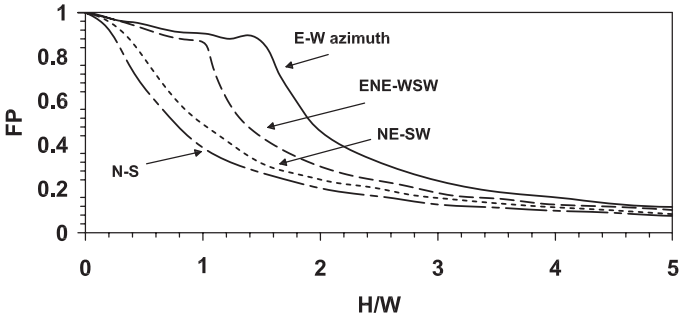

FIGURE 2. Fraction of Potential Extraterrestrial Solar Irradiation (FP) Received on a Shaded Stream Centerline on the Summer Solstice and a Latitude of 40°N as a Function of Stream Azimuth and the Ratio of Vegetation Height (H) to Stream Width (W). Vegetation overhang angle = 0°.

of beam radiation received begins to drop rapidly for increasing shade angles or *H/W* ratios, which represents the point where the maximum shade angle [arctan *H/*(*W*/2)] begins to exceed the maximum solar altitude for that day. This threshold also marks the initiation of double sunrise and sunsets on the stream centerline as vegetation height (*H*) increases relative to stream width (*W*). For dense shade (e.g., *H/W* = 5) FP is reduced to values less than 0.1, equivalent to 10% of beam solar radiation received.

Importance of stream azimuth in controlling effectiveness of riparian shading from shortwave radiation has been documented by several investigators. Ice (2004) described the varying shading effect of vegetation buffers through interactions with stream azimuth. Modeling studies have also shown that E-W azimuth streams can experience double sunrise and sunsets under certain shading conditions (University of Washington 2001).

Latitude can have a major influence on the direct beam radiation reaching the stream for E-W streams (Figure 3a), but has a smaller influence on the direct beam receipt for N-S streams (Figure 3b). Generally for a given *H/W*, the fraction of potential solar beam radiation received is greatest for 30°N latitude and least for 50°N latitude. The threshold for onset of double sunrises and sunsets exists at *H/W* = 1 for latitude of 50°N, and for a latitude of 30° the threshold occurs at *H/W* = 4. No similar threshold exists for N-S streams where the fraction of direct beam solar received for a given *H/W* is only slightly reduced with increasing latitude over the range of 30-50°N latitude.

Vegetation overhang can reduce the fraction of direct beam solar radiation that reaches the stream beyond that due to shading by vegetation without overhang (see Figure 4). An effective *H/W* ratio can be defined which accounts for shading by overhanging vegetation to compute changes in FP using Figures 1 and 2 for beam shortwave radiation received. For example, shading by vegetation with *H/W* = 1 with a 0° overhang angle can be increased to an effective *H/W* = 4 with just a 20° overhang angle. The effect of overhang angle can be great where *H/W* is initially larger, but has a very limited effect where *H/W* is initially lower (Figure 4). For example, for an initial *H/W* = 0.2 with 0° overhang, a 64° overhang angle is needed to achieve an effective *H/W* = 1; however, if the initial *H/W* = 0.6 with 0° overhang, only a 18° overhang angle is needed to achieve an effective *H/W* = 1.

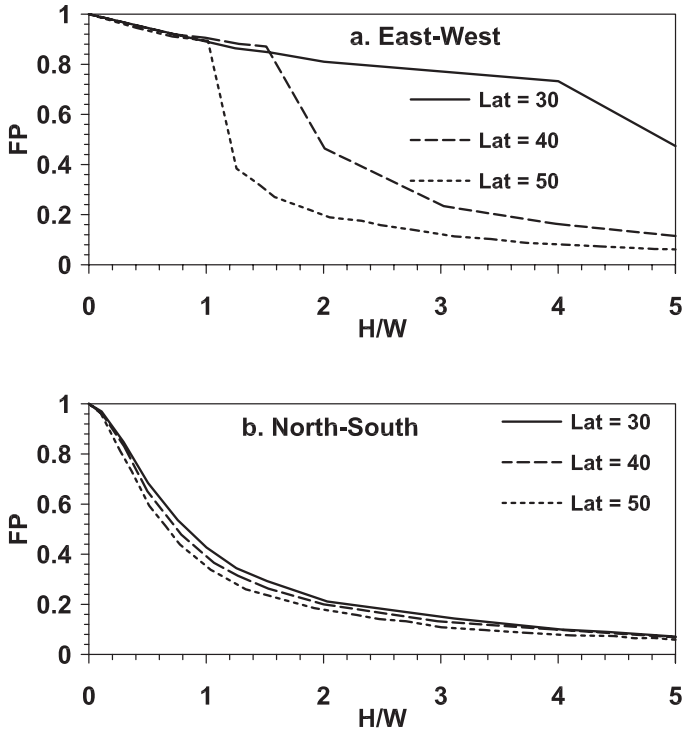

FIGURE 3. Effect of Latitude (30-50°N) on the Relationship Between Fraction of Potential Solar Irradiation (FP) Received on the Stream Centerline and the Ratio of Vegetation Height (*H*) to Stream Width (*W*). Upper graph (a) shows curves for E-W stream azimuths and the lower graph (b) shows N-S stream azimuths. Vegetation overhang angle = 0°, summer solstice.

View Factors for Shaded Streams

Radiation exchange view factors vary with the ratio of vegetation height to stream width and the amount of vegetation overhang. View factors from the stream to atmosphere without vegetation overhang vary from 100% view of the atmosphere at *H/W* = 0 to about 10% of the view at *H/W* = 6 (Figure 5). One minus this view factor gives the view factor from the stream to the vegetation along both banks used to compute longwave radiation receipt. The composite view factor expression used in Equation (10) to compute diffuse shortwave reflected by vegetation to the

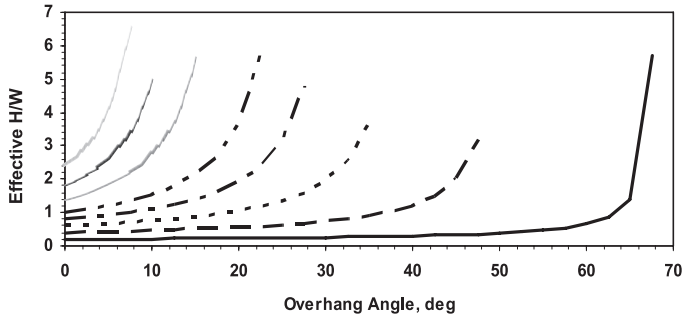

FIGURE 4. Overhang Angle Effects on the Effective Ratio of Vegetation Height (*H*) to Stream Width (*W*) to be Used to Determine FP for Direct Beam Shortwave Radiation Shading. Each Line Shows the Variation in Effective *H/W* With Overhang Angle, Beginning With a 0° Overhang Angle or Vertical Vegetation Plane.

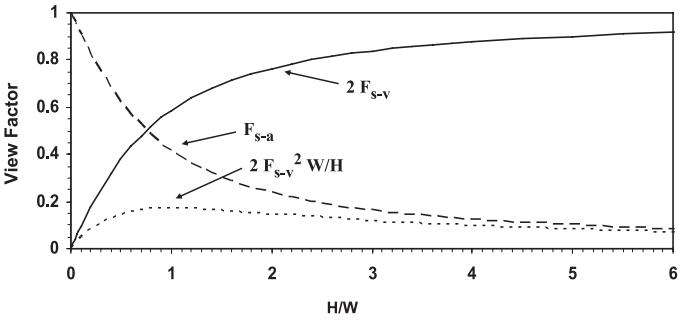

FIGURE 5. View Factors Used to Model Radiation Received by a Shaded Stream as a Function of Vegetation Height to Stream Width Ratio: F_{s-a} = View Factor From Stream Plane to Atmosphere, $2F_{s-v}$ = View Factor From Stream Plane to Vegetation Planes Along Both Banks, $2F_{s-v}{}^2W/H$ = Composite View Factor Derived to Compute Diffuse Reflected Shortwave Radiation From Both Vegetative Planes to the Stream. Vegetation overhang angle = 0°.

stream ($2{\cdot}F_{s-v}^2 \cdot W/H$) is also shown in Figure 5. As H/W and hence shading increases, this view factor for reflected shortwave initially increases because the increasing view from stream to vegetation dominates, reaches a peak of 18% at $H/W = 1$, and then decreases because the view factor from vegetation to atmosphere begins to dominate.

Vegetation overhang reduces the view from the stream to the atmosphere and increases the view to vegetation along the banks (Figure 6), which increases the importance of longwave emitted and shortwave reflected to the stream by vegetation. For example, the view factor from the stream to vegetation on both banks with $H/W = 1$ and zero overhang is about 0.6, but this view factor increases to about 0.72 with just a 10° overhang angle and to about 0.9 with 20° overhang angle. Note that a maximum view factor from the stream to vegetation along both banks of 1.00 is achieved relatively easily at small $H/W < 1$ with only 30° overhang angles. Long overhanging branches from trees and shrubs or stems from grasses which do not reach a very great height above the stream plane (H) may still be effective in altering the reflected shortwave and emitted longwave radiation received. Overhanging planes are also assumed to be nontransmitting and thus are solid planes in the model.

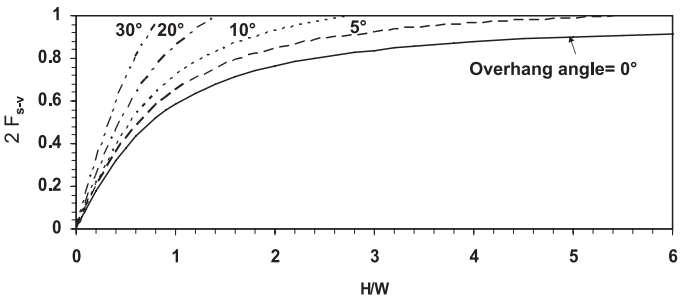

FIGURE 6. Overhanging Vegetation Effects on Radiation Exchange View Factor From Shaded Stream Plane to Vegetation Planes on Both Banks as a Function of Vegetation Height (H) to Stream Width Ratio (W) for Several Different Vegetation Overhang Angles.

Modeled Radiation Received by Shaded Streams

Modeled shortwave and longwave radiation components received by shaded streams based upon Equations (1) and (2) are shown in Figure 7 for a N-S stream azimuth and Figure 8 for an E-W azimuth, respectively. Results are based upon clear-sky mid-latitude conditions on the summer solstice without overhanging vegetation. Figure 7 shows total daytime radiation received on a N-S stream varied from about 46 MJ/m^2 with no shade to about 25 MJ/m^2 with $H/W = 5$. The reductions in total radiation received are largely caused by reductions of shortwave beam, with reduction in shortwave atmospheric and longwave atmospheric radiation being largely offset by increases in longwave radiation received from vegetation. Shortwave reflected to the stream by vegetation, based upon modeling assumptions, was negligible, but rose slightly and then declined as shading increased. At $H/W = 5$, which simulates heavy shade, radiation received was reduced by about 45% and dominated by longwave radiation (80% of the total) received from vegetation.

In Figure 8, analogous radiation components for an E-W stream azimuth are given for clear-sky, mid-latitude conditions. Patterns of changes of radiation components with increased shading on E-W streams are similar to those for a N-S stream except for the shortwave beam radiation, which differs according to FP with azimuth as shown in Figure 2,

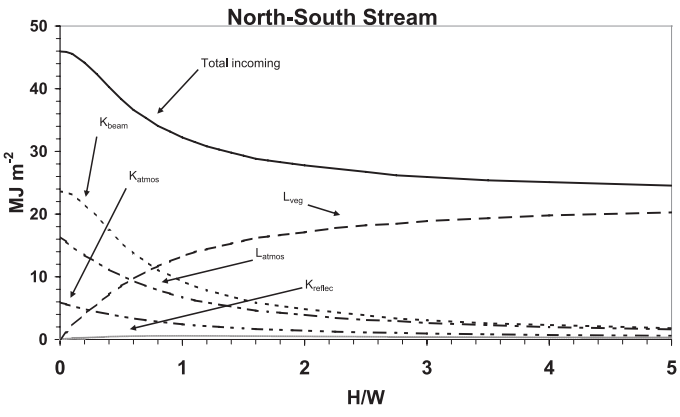

FIGURE 7. Modeled Daytime Components of Radiation Received by Shaded N-S Streams for Clear-Sky, Mid-Latitude (40°N) Conditions at Various Vegetation Height (H) to Stream Width (W) Ratios. Vegetation overhang angle = 0°.

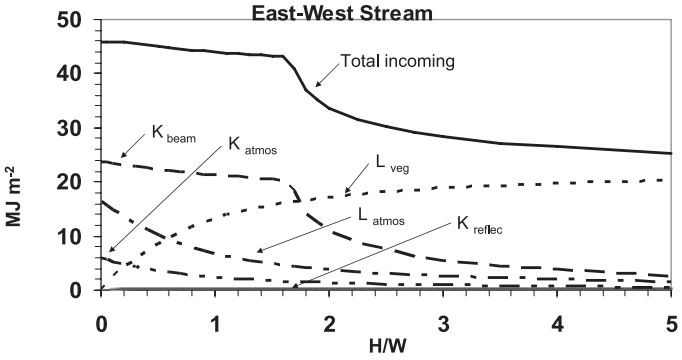

FIGURE 8. Modeled Daytime Totals of Radiation Received by Shaded E-W Streams for Clear-Sky, Mid-Latitude (40°N) Conditions at Various Vegetation Height (*H*) to Stream Width (*W*) Ratios. Vegetation overhang angle = 0°.

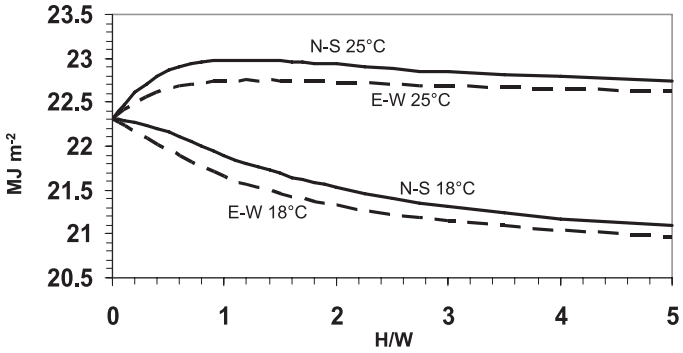

FIGURE 9. Modeled Variation in the Sum of Diffuse Shortwave and Longwave Radiation Components Received by a Shaded Stream With Varying Vegetation Height (*H*) to Stream Width (*W*) Ratios for Clear-Sky, Mid-Latitude (40°N) Conditions. Results are given for both N-S and E-W stream azimuths and for two assumed vegetation radiating temperatures (18°C and 25°C). Vegetation overhang angle = 0°.

and very slight differences in reflected shortwave radiation due to differences in shortwave received by vertical vegetation planes. Regardless of stream azimuth, vegetative shade effects on FP and receipt of shortwave beam radiation were most important during clear days.

The role of changes in diffuse shortwave and longwave radiation (total minus shortwave direct beam radiation) contributions to the stream with shade increases on clear days is shown in Figure 9. The changes in the sum of all diffuse fluxes with increased shading are negative and quite small, less than 1 MJ/m^2, thus it is clear that most changes in total radiation received are due to changes in shortwave beam radiation. Small differences in the sum of diffuse shortwave and longwave radiation fluxes with azimuth are due to minor differences in the amount of shortwave reflected from vegetation in the model. Increasing the assumed vegetation temperature from about 18°C to about 25°C, also shown in Figure 9, caused a minor peak at $H/W = 1$, but again the changes in the sum of diffuse components remained small and the overall effect of increased shading on diffuse shortwave and longwave radiation was generally negative. Even though the total diffuse flux does not change appreciably with increased shading, diffuse shortwave plus longwave radiation equals about 85% of the total received at $H/W = 5$ or heavy shade conditions and represents the minimum amount of radiation achievable by shade restoration programs.

Cloudy-day results showed that varying H/W could also be effective in reducing the radiant energy received by streams, but results varied little between N-S and E-W stream azimuths (Figure 10). Regardless of azimuth, maximum radiant energy received by the stream for cloudy days declined curvilinearly from a maximum of 37 MJ/m^2 at a $H/W = 0.0$ to a minimum of about 22 MJ/m^2 at $H/W = 5$. Radiation received without shading was dominated by diffuse atmospheric shortwave and atmospheric longwave radiation, while with heavy shade radiation received was dominated by longwave radiation emitted by vegetation. Under cloudy conditions, shade effects on view factors from the stream to atmosphere and vegetation played a dominant role.

APPLICATIONS

Shade Height Requirements

Modeled total radiation loads on shaded streams in Figures 7, 8, and 10 were used to estimate H/W needed for shade restoration in mid-latitude sites (40°N) in the U.S. with zero overhang (Table 2).

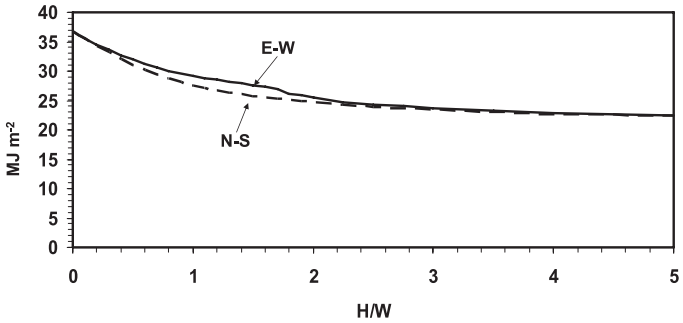

FIGURE 10. Modeled Variation in the Sum of Total Radiation Received by a Shaded Stream Under Cloudy-Sky, Mid-Latitude (40°N) Conditions as a Function of Vegetation Height (*H*) to Stream Width (*W*) Ratios for Both E-W and N-S Stream Azimuths. Vegetation overhang angle = 0°.

Ratios for three levels of shade restoration are given, 50, 75, and 90%, which might be relevant to those planning a shade restoration program. Based upon radiation totals in Figure 7 for N-S streams, restoration to 50, 75, and 90% of heavy shade can be achieved by vegetation height to stream width ratios of 0.7, 1.4 and 2.5, respectively. Restoration for E-W streams would require much greater *H/W* ratios of 1.8, 2.3 and 3.3, respectively (Figure 8). For example, if 50% shade restoration is desired, a 4-m wide stream would require vegetation height of about 2.8 m for a N-S stream azimuth, but about 7.2 m vegetation height for equivalent shading for an E-W stream azimuth. Shade heights of 2.8 m are possible with tall grass or shrub vegetation for N-S, but for E-W streams young, pole-sized woody vegetation would likely be needed. Blann *et al.* (2002) found that grasses and forbs could be as effective as taller woody vegetation in shading streams in Minnesota based upon modeling results. Whitledge *et al.* (2006) noted that potential for shade restoration was greater for narrower and N-S azimuth streams in the Missouri Ozarks based upon modeling results. Ratios needed for other stream azimuths would be intermediate to these values and in rough proportion to changes in FP with azimuth shown in Figure 2.

Stream bank height above the water surface is implicitly included in the vegetation height used in these examples. Entrenched streams may be partially shaded by banks and actual vegetation height from restoration efforts can be added to bank heights for purposes of this computation. Exposed stream banks will have a somewhat different albedo than vegetation, but as reflected shortwave is not a major component in shade computations, this effect should be negligible. Shading by topography can also be effective and the same *H/W* ratios in Figures 2 and 3 can be used to include topographic effects on direct beam radiation receipt by streams. The assumption of zero vegetation transmission in this analysis permits shading by stream banks and topography to be added with little error.

TABLE 2. Predicted Vegetation Height/Stream Width Ratios Needed to Achieve 50, 75, and 90% Shade Restoration for Clear and Cloudy Days for Mid-Latitude Conditions (40°N) Overhang Angle = 0°.

	Vegetation Height to Stream Width Ratios for Shade Restoration		
Sky Conditions/ Stream Azimuth	**50% Restoration**	**75% Restoration**	**90% Restoration**
Clear days/north-south	0.7	1.4	2.5
Clear days/east-west	1.8	2.3	3.3
Cloudy days/all azimuths	0.8	1.6	2.7

Cloudy day modeling results (Figure 10) were also used to infer impacts of shade restoration (Table 2). On cloudy days for all stream azimuths, model results suggest that 50, 75, and 90% of shade restoration could be achieved with *H/W* of 0.8, 1.6, and 2.7, respectively. Estimates for N-S and E-W streams differed only slightly and average ratios were used. These *H/W* ratios for cloudy days, where a larger fraction of diffuse shortwave radiation is received, are intermediate between clear-day estimates for N-S and E-W stream azimuths.

Grant (2005) studied the temperature increases in six stream reaches in Pennsylvania during summer in relation to FP and view factors to the atmosphere using a similar modeling strategy as used here based upon extrapolation of relationships for larger rivers from DeWalle (1974). He found that temperature increases were moderated by riparian vegetation where the view factor from stream to atmosphere (F_{s-a})was <0.40 and where the fraction of shortwave beam radiation reaching the stream centerline (FP) was <0.75.

Vegetation Overhang Effects

Vegetation overhang increases the effective *H/W* of vegetation and can be an important consideration in shade restoration programs for small streams, as shown in Figure 4. For example, 6-m high vegetation along a 4-m wide E-W azimuth stream would only give a ratio of vegetation height to stream width of 1.5, which is below the ratio of 2.3 needed to produce 75% shade restoration (Table 2). However, if this vegetation also had an overhang angle of 10° over the stream, then according to Figure 4, the effective *H/W* for direct beam shortwave would be increased to about *H/W* = 2.8, which is adequate to produce 75% shade restoration, as long as net changes in other radiation fluxes (e.g., reduced diffuse atmospheric shortwave and atmospheric longwave *vs*. increased longwave from vegetation) did not offset the change. Vegetation overhang of 10° with *H/W* = 1.5 essentially gives an increase in view factor from the stream to vegetation along both banks from 0.68 to about of 0.84 according to Figure 6; however, the sum of diffuse shortwave and longwave radiation received with this increased view was still only slightly less than that without overhang as was found in the model without overhang. Thus, impacts of overhanging vegetation on shading guidelines can be determined largely by analyzing effects on shortwave beam radiation using Figures 2 and 4 for clear sky conditions.

Analysis suggests that preference should be given to plant species that have overhanging foliage and

branches to benefit the most from shade restoration programs. Rapidly growing overhanging grass and shrub vegetation can be used to provide quick shade, while slower growing woody vegetation becomes fully established. Planting riparian vegetation very close to the banks to get the most overhang could be very important in increasing the effective height of shorter grass and shrub vegetation for a given stream width. Planting near stream banks does increase the risk of loss of plant material due to bank collapse over time and the effect of channel width changes is considered below. Vegetation overhang in this analysis also assumes no transmission by foliage, thus only dense overhanging vegetation should be considered when using these guidelines.

Impacts of Stream Width Changes

Use of Figures 7, 8, and 10 and Table 2 implies that changes in width of channels over time can also cause significant changes in shading needs. For example, 90% shade restoration on a 1-m wide stream with N-S azimuth would require a $H/W = 2.5$ on clear days and $H/W = 2.7$ on cloudy days or a vegetation height range of 2.5-2.7 m. If the channel width increased to 2 m during shade restoration, the required vegetation height range needed for 90% shade restoration would double to a range of 5-5.4 m. If shade height were fixed, then such channel widening would effectively reduce the level of shade restoration that was obtained. Of course, channel narrowing during a shade restoration program could render the existing vegetation more effective than originally planned.

Restoration on Wide Streams

Given the natural limits on vegetation height that can be achieved with mature trees, Table 2 for 40°N latitude implies that there are some practical limits on the maximum stream width that can be appreciably affected by shade restoration programs. Assuming that if 30 m is the maximum vegetation height that can be achieved, then 50% shade restoration could only be achieved for E-W streams up to about 17-m wide ($H/W = 1.8$ needed) or N-S streams up to 43-m wide ($H/W = 0.7$ needed). Maximum stream widths that could be restored for other stream azimuths would fall within this range. In addition, as the time required for these maximum vegetation heights to be reached is significant, shade restoration programs on such wide streams would be a very long-term investment. There are many other good reasons for restoration of riparian vegetation along very wide streams, but lowering water temperatures by shading is probably not one of them.

Shading on wide streams would be somewhat more effective at higher latitudes and less effective at lower latitudes, at least for E-W stream azimuths. Based upon Figure 3, the maximum E-W stream width for 50% restoration by 30-m tall vegetation would be about 25-m at 50°N latitude compared to about 17-m width at 40°N latitude.

Latitude Effects

Effects of latitude on shade restoration requirements can be easily demonstrated using Figures 3a and 3b by considering only shortwave beam radiation reaching the stream, which is justified based upon modeling results. The vegetation height to stream width ratio (H/W) needed for 50% shade restoration (FP = 0.5) in Figure 3a for E-W stream azimuths is about 1.2, 1.9, and 4.8 for 50°, 40°, and 30°N latitudes, respectively. In Figure 3b for N-S streams, the H/W ratios needed to achieve 50% restoration with varying latitudes are about 0.66, 0.74, and 0.82 for 50°, 40°, and 30°N latitudes, respectively. Shading would be obviously much more effective at higher latitudes than lesser latitudes for E-W streams, but relatively unimportant for N-S streams.

Assumptions and Limitations

Analysis of stream shade involved several key assumptions that affect the application of results. Analysis was based upon the premise that daylight totals of radiation received by streams from sunrise to sunset provide a useful index to riparian vegetation shading. Results thus apply to idealized long channel reaches which are longer than the distance traveled by a slug of water during the daylight period. Analysis was also based upon daily direct beam shortwave radiation received on the stream centerline rather than radiation integrated over the entire width of the channel. Ultimately the effectiveness of radiation received in heating a stream will depend upon how discharge is distributed across the channel (e.g., whether the bulk of the flow occurs along one bank or near mid-stream). In this analysis, for the long straight channel reaches modeled, the stream centerline was simply used as the reference point. Impacts of shade on stream temperature regimes can depend upon many other factors such as water velocity, water depth, wind speed, humidity, air temperature, channel bed conductivity (Johnson, 2004), groundwater inputs (Story *et al.*, 2003; Mellina *et al.*, 2002), and vegetation characteristics including transmission and longitudinal distribution of

vegetation along the channel (Burton and Likens, 1973; Scarsbrook and Halliday, 1999; Rutherford *et al.*, 2004), that cannot be easily generalized. Computation of shade restoration impacts on stream temperature would require case-specific calculations using one of the several available models including radiation components given in Equations (1) and (2).

Analysis also treated vegetation as nontransmitting planes, which means shading guidelines should only be applied to dense or wide vegetative riparian buffer zones or very dense overhanging vegetation. Transmission of solar radiation by vegetation would increase the amount of radiation reaching the stream and increase the *H/W* ratio shade restoration guidelines shown in this analysis as well as blur differences in shading guidelines due to stream azimuth. However, shade restoration guidelines also represent summer solstice conditions which would equate to greater shading at other times during the growing season, somewhat compensating for the nontransmitting assumption in this analysis. A definition of buffer zone characteristics needed for "nontransmitting" vegetation is not prescribed here, but reference can be made to the buffer widths typically recommended for restoring or maintaining shade; widths ranging from about 9-30 m width are generally considered adequate to maintain thermal regimes in small streams (Beschta *et al.*, 1987; Sridhar *et al.*, 2004; Wilkerson *et al.*, 2006; Zwieniecki and Newton, 1999). Other accommodations for effects of radiation transmission by vegetation would be to only use the larger *H/W* for 90% shade restoration given in Table 2 or to estimate transmission using Beer's law and apply the resulting increase in FP to Figure 2.

An estimate of increase in FP due to transmission of shortwave radiation by vegetation can be made based upon the Beer's Law in the form (Jarvis et al. 1976):

$$\Delta FP = e^{-K\ LAI} \qquad (Eq.II)$$

Where LAI is the leaf area index of the plant community and K is an extinction coefficient. LAI can be measured, but impacts of clumping and non-foliar components can be problematical (Bréda 2003). The attenuation coefficient (K) of plant stands varies with many factors including solar altitude and path length of radiation through the vegetation (Sridhar et al. 2004, Pomeroy and Dion 1996), which makes applications to buffer zones of finite dimensions (width, height, density) and varying stream-buffer geometries problematical. Regardless, as a rough approximation, if LAI = 5, representing dense vegetation and K = 0.47 representing mean broad-leaved forest (Bréda 2003), then $\Delta FP = 0.095$. Pro-rating ΔFP by the fraction of the day when the stream is actually shaded (e.g. multiplying by 1−FP) is also needed. For example, given FP = 0.5 (H/W = 1) in Figure 2 for a NE-SW stream azimuth at 40°N latitude without transmission, this level of transmission increases FP received by 0.0475 (=ΔFP(1−FP)) and increases the solar beam radiation reaching the stream to FP = 0.5475 (H/W = 0.9). Viewed alternatively, shade requirements in Figure 2 would have to be increased from about H/W = 1.0 at FP = 0.5 without transmission to about H/W = 1.1 at FP = 0.4525 with consideration of transmission, to get the same shade restoration.

CONCLUSIONS

Vegetative shade effects on receipt of daily total shortwave beam radiation were found to dominate model results for clear weather conditions on the summer solstice. Increases in longwave radiation from vegetation due to increased shading were essentially offset by decreases in atmospheric diffuse shortwave and atmospheric longwave radiation based upon assumptions used in the model for clear weather. Consideration of view factors from the stream to vegetation and atmosphere and exchange of diffuse shortwave and longwave radiation were more important for cloudy weather conditions. Model results also indicated that shortwave radiation reflected by vegetation to the stream would be small and could be ignored. Measurements of all diffuse and direct and shortwave and longwave radiation fluxes received by shaded streams appear to be lacking, but are needed to support future modeling efforts.

Ratios of vegetation height to stream width for dense, nontransmitting riparian buffers are given as general guidelines for use by ecosystem managers to help plan shade restoration programs. For example, shade height to stream width ratios needed to reduce all-wave radiation received on the stream centerline to within 75% of that on a fully shaded stream ranged between 1.4 to 2.3 for mid-latitudes (40°N) depending on cloud conditions and stream azimuth. Ratios needed to achieve shade restoration will be greater for E-W than for N-S stream azimuths with clear sky, but stream azimuth would be relatively unimportant with cloudy weather. On small streams, shade restoration is possible with grass and shrub vegetation for N-S azimuths for some configurations, but taller woody vegetation may be needed for E-W azimuths depending upon stream width. Regardless, dense vegetation overhanging the stream can greatly enhance shading and measurements of overhang angles can be used to

estimate this enhancement. Changing stream widths during shade restoration programs can also cause important shifts in ratios needed for restoration. Shade effects on E-W streams were especially effective for streams at higher latitudes. On larger streams, opportunities for shade restoration, with or without overhang, are limited to widths less than about 17 m for E-W azimuths and widths less than about 43 m for N-S streams for clear-day, mid-latitude conditions.

ACKNOWLEDGMENTS

Support for this research given by the School of Forest Resources and Penn State Institutes of Energy and the Environment at Penn State University are gratefully acknowledged.

LITERATURE CITED

Amaranthus, M., J. Jubas, and D. Arthur. 1989. Stream Shading, Summer Streamflow and Maximum Water Temperature Following Intense Wildfire in Headwater Streams. USDA, Forest Service, Gen. Tech. Rpt. PSW-109, Washington, DC.

Aubin, I., M. Beaudet, and C. Messier, 2000. Light Extinction Coefficients Specific to the Understory Vegetation of the Southern Boreal Forest, Quebec. Canadian Journal of Forest Research 30:168-177.

Baldocchi, D.B., D.R. Matt, B.A. Hutchison, and R.T. McMillen, 1984. Solar Radiation Within an oak-Hickory Forest: An Evaluation of the Extinction Coefficients for Several Radiation Components During Fully-Leafed and Leafless Periods. Agricultural and Forest Meteorology 32:307-322.

Bartholow, J.M., 2000. Estimating Cumulative Effects of Clearcutting on Stream Temperatures. Rivers 7(4):284-297.

Bartholow, J., 2002. Stream Segment Temperature Model (SSTEMP) Version 2.0, Revised August 2002. U. S. Geological Survey, Ft. Collins, Colorado, 29 pp.

Beschta, R.L., R.E. Bilby, R.E. Brown, G.W. Brown, L.B. Holtby, and T.D. Hofstra, 1987. Stream Temperatures and Aquatic Habitat: Fisheries and Forestry Interactions. *In:* Proceedings, Streamside Management: Forestry and Fishery Interaction, E.O. Salo and T.W. Cundy (Editors). Institute of Forest Resource, University of Washington, Seattle, pp. 191-232.

Blann, K., J.F. Nerbonne, and B. Vondracek, 2002. Relationship of Riparian Buffer Type to Water Temperature in the Driftless Area Ecoregion of Minnesota. North American Journal of Fisheries Management 22:441-451.

Borman, M.M. and L.L. Larson, 2003. A Case Study of River Temperature Response to Agricultural Land use and Environmental Thermal Patterns. Journal of Soil and Water Conservation 58(1):8-12.

Bréda, N.J.J., 2003. Ground-Based Measurements of Leaf Area Index: A Review of Methods, Instruments and Current Inventories. Journal of Experimental Botany 54(392):2403-2417.

Broadmeadow, S. and T.R. Nisbet, 2004. The Effects of Riparian Forest Management on the Freshwater Environment: A Literature Review of Best Management Practices. Hydrology and Earth System Sciences 8(3):286-305.

Brown, G.W., 1970. Predicting the Effect of Clearcutting on Stream Temperatures. Journal of Soil and Water Conservation 25:11-13.

Burton, T.M. and G.E. Likens, 1973. The Effect of Strip-Cutting on Stream Temperatures in the Hubbard Brook Experimental Forest, New Hampshire. BioScience 23(7):433-435.

Chen, Y.D., R.F. Carsel, S.C. McCutcheon, and W.L. Nutter, 1998a. Stream Temperature Simulation of Forested Riparian Areas: I. Watershed Scale Model Development. Journal of Environmental Engineering 124(4):304-315.

Chen, Y.D., S.C. McCutcheon, D.J. Norton, and W.L. Nutter, 1998b. Stream Temperature Simulation of Forested Riparian Areas: II Model Applications. Journal of Environmental Engineering 124(4):316-328.

Crawford, T.M. and C.E. Duchon, 1999. An Improved Parameterization for Estimating Effective Atmospheric Emissivity for use in Calculating Daytime Downwelling Longwave Radiation. Journal of Applied Meteorology 38(4):474-480.

Davies-Colley, R.J. and G.W. Payne, 1998. Measuring Stream Shade. Journal of North American Benthological Society 17:2.

Davies-Colley, R.J. and J.M. Quinn, 1998. Stream Lighting in Five Regions of North Island, New Zealand: Control by Channel Size and Riparian Vegetation. New Zealand Journal of Marine and Freshwater Research 32:591-605.

DeWalle, D.R., 1974. Effect of Partial Vegetation and Topographic Shade on Radiant Energy Exchange of Streams-With Applications to Thermal Loading Problems. Res. Publ. No. 82. Instit. Res Land and Water Resour., The Pennsylvania State University, University Park, PA, 105 pp.

DOE National Renewable Energy Laboratory Website. http://rredc.nrel.gov/solar/old_data/nsrdb/bluebook/data/14778.SBF, *accessed* on July 22, 2008.

Duarte, H.F., N.L. Dias, and S.R. Maggiotto, 2006. Assessing Daytime Downward Longwave Radiation Estimates for Clear and Cloudy Skies in Southern Brazil. Agricultural and Forest Meteorology 139(3-4):171-181.

Federer, C.A., 1971. Solar Radiation Absorption by a Leafless Hardwood Forest. Agricultural Meteorology 9:3-20.

Frank, E.C. and R. Lee, 1966. Potential Solar Beam Irradiation on Slopes. USDA, Forest Service, Research Paper RM-18, Washington, DC, 116 pp.

Grant, C.J., 2005. Relationships Between Riparian Buffers and Summer Stream Temperatures. M. S. Thesis, The Pennsylvania State University, University Park, Pennsylvania, 105 pp.

Harding, J.S., K. Claassen, and N. Evers, 2006. Can Forest Fragments Reset Physical and Water Quality Conditions in Agricultural Catchments and act as Refugia for Forest Stream Invertebrates? Hydrobiologia 568:391-402.

Hardy, J.P., R. Melloh, G. Koenig, D. Marks, A. Winstral, J.W. Pomeroy, and T. Link, 2004. Solar Radiation Transmission Through Conifer Canopies. Agricultural and Forest Meteorology 126:257-270.

Holman, J.P., 1972. Heat Transfer (Third Edition). McGraw-Hill Book Co., New York, 462 pp.

Hottel, H.C., 1931. Radiant Heat Transmission Between Surfaces Separated by non-Absorbing Media. Transactions. American Society of Mechanical Engineers 53:265-273, FSP-53-196.

Ice, G., 2004. How Direct Solar Radiation and Shade Influences Temperature in Forest Streams and Relaxation of Changes in Stream Temperature. National Council for Air and Stream Improvement, Misc. Doc., Research Triangle Park, 34 pp.

Iqbal, M., 1983. An Introduction to Solar Radiation. Academic Press, Toronto.

Jarvis, P.G., G.B. James, and J.J. Landsberg 1976. Chapter 7. Coniferous Forest. *In*: Vegetation and the Atmosphere, Vol. 2, Case Studies, J.L. Monteith (Editor). Academic Press, London, pp. 171-240.

Johnson, S.L., 2004. Factors Influencing Stream Temperatures in Small Streams: Substrate Effects and a Shading Experiment. Canadian Journal of Fisheries and Aquatic Sciences 61:913-923.

Kauffman, J.B., R.L. Beschta, N. Otting, and D. Lytjen, 1997. An Ecological Perspective of Riparian and Stream Restoration in the Western United States. Fisheries 22(5):12-24.

Lanini, J., V. Sridhar, A.L. Sansone, J. LaMarche, and D.P. Lettenmaier, 2004. Reply to Discussion by J. D. Fox Jr., Prediction of Stream Temperature in Forested Watersheds. Journal of American Water Resources Association 40(6):1661-1662.

LeBlanc, R.T., R.D. Brown, and J.E. FitzGibbon, 1997. Modeling the Effects of Land use Change on the Water Temperature in Unregulated Urban Streams. Journal of Environmental Management 49:445-469.

Lee, R., 1978. Forest Microclimatology. Columbia University Press, New York, 276 pp.

Li, X., A.H. Strahler, and C.E. Woodcock, 1995. A Hybrid Geometric Optical-Radiative Transfer Approach for Modeling Albedo and Directional Reflectance of Discontinuous Canopies. IEEE Transactions on Geoscience and Remote Sensing 33:466-480.

Link, T.E., D. Marks, and J.P. Hardy, 2004. A Deterministic Model to Characterize Canopy Radiative Transfer Properties. Hydrological Processes 18:3583-3594.

List, R.J., 1968. Smithsonian Meteorological Tables (Sixth Revised Edition). Smithsonian Institution, Misc. Collections, Volume 114, Washington, D.C., 527 pp.

Lynch, J.A., G.B. Rishel, and E.S. Corbett, 1984. Thermal Alteration of Streams Draining Clearcut Watersheds: Quantification and Biological Implications. Hydrobiologia 111(3):161-169.

Meier, W., C. Bonjour, A. Wüest, and P. Reichert, 2003. Modeling the Effect of Water Diversion on the Temperature of Mountain Streams. Journal of Environmental Engineering 129(8):755-764.

Mellina, E., R.D. Moore, S.G. Hinch, J.S. Macdonald, and G. Pearson, 2002. Stream Temperature Responses to Clearcut Logging in British Columbia: The Moderating Influences of Groundwater and Headwater Lakes. Canadian Journal of Fisheries and Aquatic Sciences 59:1886-1900.

Moore, R.D., D.L. Spittlehouse, and A. Story, 2005. Riparian Microclimate and Stream Temperature Response to Forest Harvesting: A Review. Journal of American Water Resources Association 41(4):813-834.

NASA Surface Meteorology and Solar Energy Website. http://earth-www.larc.nasa.gov/cgi-bin/cgiwrap/solar/grid.cgi?email=grid@larc.nasa.gov, *accessed* July 22, 2008.

Niemelä, S., R. Räisänen, and H. Savijärvi, 2001. Comparison of Surface Radiative Flux Parameterizations Part II. Shortwave Radiation. Atmospheric Research 58(2):141-154.

NOAA SURFRAD Website. http://www.srrb.noaa.gov/surfrad/sitepage.html, *accessed* July 22, 2008.

O'Driscoll, M.A. and D.R. DeWalle, 2006. Stream-air Temperature Relations to Classify Stream-Ground Water Interactions. Journal of Hydrology 329(1-2):140-153.

Oke, T.R., 1987. Boundary Layer Climates (Second Edition). Methuen, London, 435 pp.

Parkyn, S.M., R.J. Davies-Colley, N.J. Halliday, K.J. Costley, and G.F. Croker, 2003. Planted Riparian Buffer Zones in New Zealand: Do They Live up to Expectations? Restoration Ecology 11(4):436-447.

Pomeroy, J.W. and K. Dion, 1996. Winter Radiation Extinction and Reflection in a Boreal Pine Canopy: Measurements and Modeling. Hydrological Processes 10:1591-1608.

Poole, G.C. and C.H. Berman, 2001. An Ecological Perspective on in-Stream Temperature: Natural Heat Dynamics and Mechanisms of Human Caused Thermal Degradation. Environmental Management 27(6):782-802.

Quigley, T.M., 1981. Estimating Contribution of Overstory Vegetation to Stream Surface Shade. Wildlife Society Bulletin 9(1):22-27.

Roni, P., T.J. Beechie, R.E. Bilby, F.E. Leonetti, M.M. Pollock, and G.R. Pess, 2002. A Review of Stream Restoration Techniques and a Hierarchical Strategy for Prioritizing Restoration in Pacific Northwest Watersheds. North American Journal of Fisheries Management 22:1-20.

Rutherford, J.C., S. Blackett, C. Blackett, L. Saito, and R.J. Davies-Colley, 1997b. Predicting the Effects of Shade on Water Temperature in Small Streams. New Zealand Journal of Marine and Freshwater Research 31:707-721.

Rutherford, J.C., R.J. Davies-Colley, J.M. Quinn, M.J. Stroud, and A.B. Cooper 1997a. Stream Shade: Towards a Restoration Strategy. National Institute of Water and Atmospheric Research Ltd., Hamilton, New Zealand, NIWA Client Report DOC303, 159 pp.

Rutherford, J.C., N.A. Marsh, P.M. Davies, and S.E. Bunn, 2004. Effects of Patchy Shade on Stream Water Temperature: How Quickly do Small Streams Heat and Cool. Marine and Freshwater Research 55:737-748.

Scarsbrook, M.R. and J. Halliday, 1999. Transition From Pasture to Native Forest Land-use Along Stream Continua: Effects on Stream Ecosystems and Implications for Restoration. New Zealand Journal of Marine and Freshwater Research 33:292-310.

Schröder, P. and P. Hanrahan, 1993. On the Form Factor Between two Polygons. Computer Graphics, Assoc. Computing Machinery, Proc., Ann. Conf. Series. SIGGRAPH 93:163-164.

Siegel, R. and J.R. Howell, 2001. Thermal Radiation Heat Transfer (Forth Edition). Taylor and Francis, New York, 864 pp.

Sinokrot, B.A. and H.G. Stefan, 1993. Stream Temperature Dynamics: Measurements and Modeling. Water Resources Research 29(7):2299-2312.

Sridhar, V., A.L. Sansone, J. LaMarche, T. Dubin, and D.P. Lettenmaier, 2004. Prediction of Stream Temperature in Forested Watersheds. Journal of American Water Resources Association 40(1):197-213.

Story, A., R.D. Moore, and J.S. Macdonald, 2003. Stream Temperatures in two Shaded Reaches Below Cutblocks and Logging Roads: Downstream Cooling Linked to Subsurface Hydrology. Canadian Journal of Forest Research 33:1383-1396.

Sweeney, B.W., 1993. Effects of Streamside Vegetation on Macroinvertebrate Communities of White Clay Creek in Eastern North-America. Proceedings of the Academy of Natural Sciences of Philadelphia 144:291-340.

Swift, Jr., L.W. and J.B. Messer, 1971. Forest Cuttings Raise Temperatures of Small Streams in the Southern Appalachians. Journal of Soil and Water Conservation 26(3):111-116.

Tate, K.W., D.F. Lile, D.L. Lancaster, M.L. Porath, J.A. Morrison, and Y. Sado, 2005. Statistical Analysis of Monitoring Data Aids in Prediction of Stream Temperature. California Agriculture 59(3):161-167.

Tung, C.-P., Y.-C.E. Yang, T.-Y. Lee, and M.-H. Li, 2007. Modification of a Stream Temperature Model With Beer's Law and Application to GaoShan Creek in Taiwan. Ecological Modelling 200:217-224.

University of Washington, 2001. Fact Sheet #08: The Impact of Riparian Forest Management on Shade Production. University of Washington, College of Forest Resources, Seattle, WA, 5 pp. http://www.ruraltech.org/pubs/fact_sheets/fs008/index.asp, *accessed* August 27, 2007.

Watanabe, M., R.M. Adams, J. Wu, J.P. Belte, M.M. Cox, S.L. Johnson, W.J. Liss, W.G. Boggess, and J.L. Ebersole, 2005. Toward Efficient Riparian Restoration: Integrating Economic, Physical and Biological Models. Journal of Environmental Management 75(2):93-104.

Welty, J.J., T. Beechie, K. Sullivan, D.M. Hyink, R.E. Bilby, C. Andrus, and G. Pess, 2002. Riparian Aquatic Interaction Simulator (RAIS): a Model of Riparian Forest Dynamics for the Generation of Large Woody Debris and Shade. Forest Ecology and Management 162:299-318.

Whitledge, G.W., C.F. Rabeni, G. Annis, and S.P. Sowa, 2006. Riparian Shading and Groundwater Enhance Growth Potential for Smallmouth Bass in Ozark Streams. Ecological Application 16(4):1461-1473.

Wilkerson, E., J.M. Hagan, D. Siegel, and A.A. Whitman, 2006. The Effectiveness of Different Buffer Widths for Protecting Headwater Stream Temperature in Maine. Forest Science 52(3):221-231.

Zwieniecki, M.A. and M. Newton, 1999. Influence of Streamside Cover and Stream Features on Temperature Trends in Forested Streams of Western Oregon. Western Journal of Applied Forestry 14(2):106-113.